DNA repair and chromatin

DNA-Reparatur und Chromatin

Vom Fachbereich Biologie der Technischen Universität Darmstadt zur Erlangung des akademischen Grades eines Doctor rerum naturalium genehmigte Dissertation
von Diplom-Biologin Britta Muster aus Bad Homburg
Darmstadt 2014 — D 17

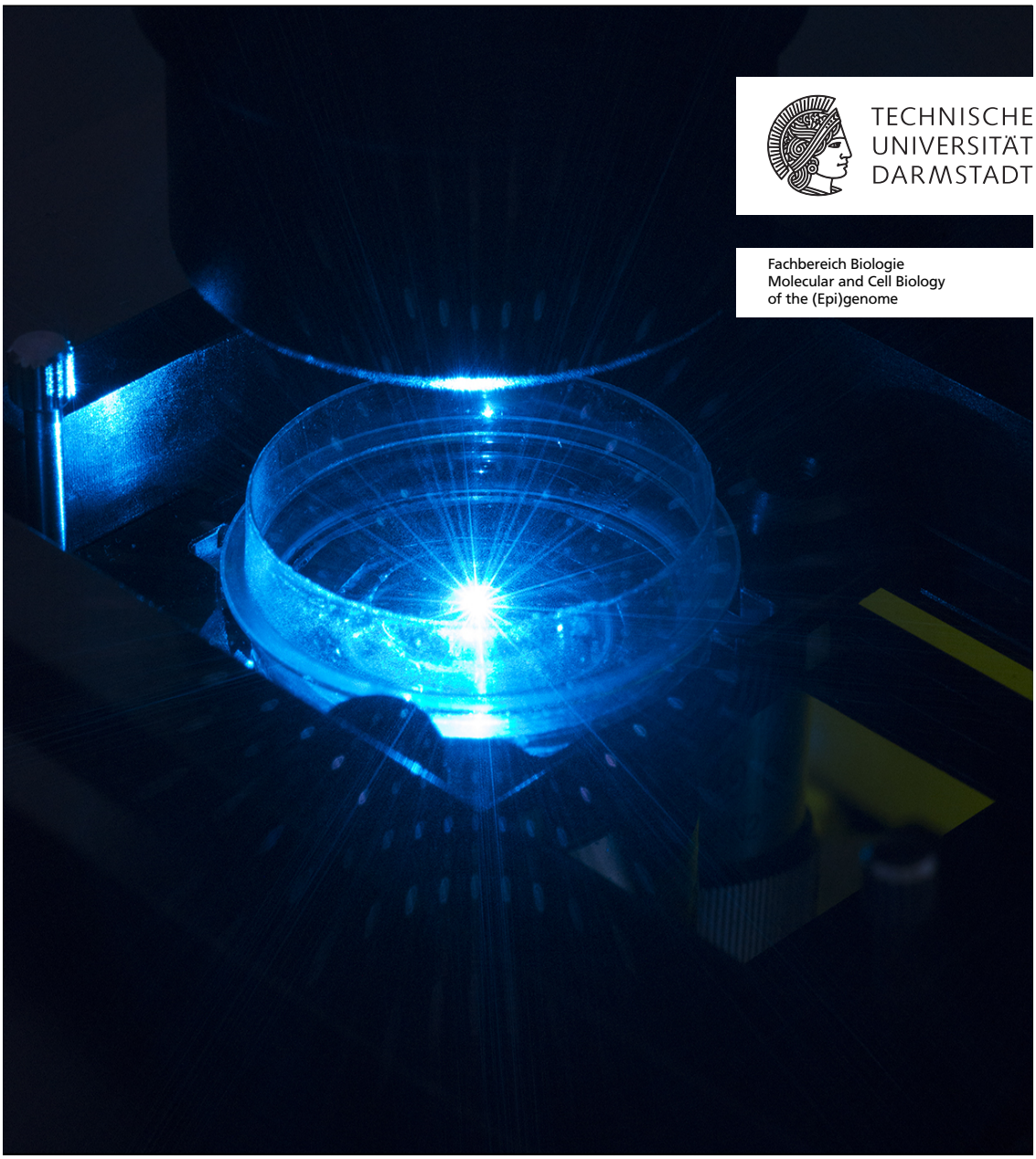

TECHNISCHE UNIVERSITÄT DARMSTADT

Fachbereich Biologie
Molecular and Cell Biology
of the (Epi)genome

DNA repair and chromatin
DNA-Reparatur und Chromatin

Vom Fachbereich Biologie der Technischen Universität Darmstadt zur Erlangung des akademischen Grades eines Doctor rerum naturalium genehmigte Dissertation von Diplom-Biologin Britta Muster aus Bad Homburg

1. Referentin: Prof. Dr. M. Cristina Cardoso
2. Referent: Prof. Dr. Paul Layer

Tag der Einreichung: 21.03.2014
Tag der mündlichen Prüfung: 23.05.2014

Darmstadt 2014 — D 17

Summary

Laser microirradiation can be used to induce DNA damage with high spatial and temporal resolution, representing a powerful tool to analyze DNA repair in living cells. However, most lasers induce a mixture of DNA damage leading to the activation of multiple DNA repair pathways, making it impossible to study the kinetics of individual repair processes or the interaction of repair factors. To overcome this, we established conditions to discriminate specific repair pathways using lasers commonly available in confocal microscopes. We used cells expressing fluorescently tagged proteins specific for different repair processes and monitored their accumulation after microirradiation with lasers of different wavelengths (405, 488, 561, 633 nm). In addition, we validated DNA damage using a series of DNA damage markers (CPDs, TUNEL, γH2AX-foci). Our data showed that irradiation with a 405 nm laser led to activation of all tested repair pathways. Irradiation with 488 or 561 nm lasers led to selective activation of short-patch base excision repair. These conditions discriminated against processive long-patch base excision repair, nucleotide excision repair as well as double strand break repair pathways.

We applied this microirradiation strategy to study differences between eu- and heterochromatin upon DNA damage. Highly compacted heterochromatic regions in human and mouse cells were fluorescently marked and microirradiated. We demonstrated recruitment of repair factors inside these dense heterochromatic regions and showed that conditions leading to processive DNA synthesis resulted in local decondensation with about two fold increase in heterochromatin area. Using pulse labeling with thymidine analogs added immediately before microirradiation, we measured processive DNA synthesis repair directly inside heterochromatic regions. These data are not in agreement with the proposal that repair of heterochromatic DNA damage takes place at the periphery of the domain but show that processive DNA synthesis repair can take place inside heterochromatic regions.

We furthermore took advantage of the discriminating microirradiation strategy to study the newly described post-replicative DNA repair pathway ribonucleotide excision repair. This pathway was proposed to degrade millions of ribonucleotides misincorporated by DNA polymerases during replication. The excision of ribonucleotide is carried out by the nuclease RNase H2. We showed that RNase H2 is not only recruited to sites of DNA replication, but also to sites of processive DNA repair, suggesting that pathway activation takes place not only after replication but also after repair. Mutations in RNase H2 are linked to the autoimmune disease Aicardi-Goutieres syndrome. To shed more light into the pathology of these mutations, we demonstrated that recruitment efficiency and kinetics of exchange at repair and replication sites were diminished by mutations affecting complex formation, PCNA binding and catalysis.

Zusammenfassung

Die vorliegende Arbeit beschäftigt sich mit der Induktion und Reparatur von DNA-Schäden. Eine wirkungsvolle Methode um dies in lebenden Zellen zu erforschen, ist die Laser-Mikrobestrahlung. Sie ermöglicht es, DNA-Schäden mit sehr hoher räumlicher und zeitlicher Auflösung zu erzeugen. Die meisten Laser induzieren jedoch eine Mixtur unterschiedlichster DNA-Schäden und führen somit zu einer Aktivierung multipler DNA-Reparaturwege. Dies macht eine Untersuchung der Kinetik einzelner Reparaturwege unmöglich. Zur Lösung dieses Problems, etablierten wir eine neuartige Methode, indem wir mittels an verschiedenen konfokalen Mikroskopen vorhandenen Lasern Bedingungen erzeugten, die eine Aktivierung von definierten Reparaturwegen ermöglichen. Zur Erreichung dieses Ziels, exprimierten wir fluoreszenzmarkierte Proteine, die spezifisch für die unterschiedlichen Reparaturwegen in Säugetierzellen sind, und quantifizierten ihre Akkumulation nach Mikrobestrahlung mit Lasern verschiedener Wellenlängen (405, 488, 561, 633 nm). Als zusätzliche Validation wiesen wir die Produktion von unterschiedlichen DNA-Schäden mit einer Reihe spezifischer Marker (CPDs, TUNEL, γH2AX-foci) nach. Unsere Daten zeigten, dass nach Mikrobestrahlung mit einer Wellenlänge von 405 nm alle untersuchten Reparaturwege aktiviert wurden. Im Gegensatz hierzu führte die Mikrobestrahlung mit 488 oder 561 nm Wellenlängen zu einer selektiven Aktivierung der nicht prozessiven "short-patch" Basenexzisionsreparatur. Unter diesen Bedienungen ist es demnach möglich, nicht prozessive DNA-Reparaturwege von prozessiven wie "long-patch" Basenexzisionsreparatur, Nukleotidexzisionsreparatur und Doppelstrangbruch-Reparaturwegen, zu unterscheiden.

Wir nutzten die neu von uns entwickelte Mikrobestrahlungsstrategie, um Unterschiede in der Induktion und Reparatur von DNA-Schäden zwischen Eu- und Heterochromatinregionen zu untersuchen. Hoch kompaktiertes Heterochromatin wurde hierzu zunächst markiert und anschließend mikrobestrahlt. Wir konnten damit nachweisen, dass DNA-Reparaturfaktoren unterschiedlicher Reparaturwege innerhalb der Heterochromatinregionen rekrutiert werden und, dass Bedingungen die zu einer prozessiven DNA-Synthese führen in einer 2-fachen Erweiterung der Heterochromatinregion resultieren. Als zusätzlichen Nachweis applizierten wir zu den Zellen halogenierte Nucleotide unmittelbar vor Mikrobestrahlung und wiesen, durch die Inkorporation der modifizierten Nucleotide, prozessive DNA-Reparatur direkt innerhalb der Heterochromatinregionen nach. Diese Daten widersprechen der Hypothese, dass heterochromatische DNA-Schäden an der Peripherie der Region repariert werden, sondern zeigen dass DNA-Synthese direkt innerhalb Heterochromatinregionen stattfinden kann.

Darüber hinaus konnten wir unsere Mikrobestrahlungsstrategie einsetzen, um den kürzlich beschriebenen postreplikativen DNA-Reparaturweg Ribonukleotidexzisionsreparatur näher zu untersuchen. Es wird angenommen, dass dieser Reparaturweg die Millionen Ribonukleotide, die von DNA-Polymerasen während der DNA-Replikation misinkorporiert wurden, degradiert. Die Nuklease RNase H2 führt dabei den initialen Exzisionsschritt durch. Wir zeigten, dass RNase H2 nicht nur zu DNA-Replikations-Stellen, sondern auch zu Stellen mit prozessiver DNA-Reparatursynthese rekrutiert wird, was eine Aktivierung der Ribonukleotidexzisionsreparatur nicht nur nach DNA-Replikation sondern auch nach DNA-Reparatur nahelegt. Mutationen

in RNase H2 führen zu der Autoimmunkrankheit „Aicardi-Goutieres-Syndrome“. Unsere Forschung konnte zeigen, dass Mutationen die Komplex Formierung, PCNA Bindung oder Katalyse beeinflussen zu einer Veränderung des Bindungs- und Mobilitätsverhalten an Replikations- und Reparaturstellen führen und konnten somit beitragen den zugrundeliegenden Krankheitsmechanismus besser zu verstehen.

List of Figures

List of Tables

Contents

1 General introduction

1.1 DNA damage and repair

DNA is the storage of genetic information in each living cell, its integrity and stability are essential for life. Any damage, if not repaired correctly, can lead to mutations resulting in cancer or cell death.

There are at least three different causes for DNA damage in mammalian cells: environmental factors, (by)products of normal cellular metabolism and spontaneously disintegration of chemical bonds in DNA (Hoeijmakers, 2001).

Environmental factors include ultraviolet (UV) component of sunlight or genotoxic chemicals such as compounds in cigarette smoke. An example for (by)products of normal cellular metabolism are reactive oxygen species (ROS) derived from cellular respiration, which are constantly challenging the genome integrity. The spontaneous disintegration of chemical bonds in DNA comprises the hydrolysis of nucleotide residues, which leaves abasic site (AP site) or the deamination of cytosine, adenine, guanine or 5-methylcytosine which converts these bases to the miscoding uracil, hypoxanthine, xanthine and thymine, respectively (Lindahl, 1993). Altogether, it has been estimated that an individual cell suffers up to 10^5 spontaneous DNA lesions per day (Hoeijmakers, 2009).

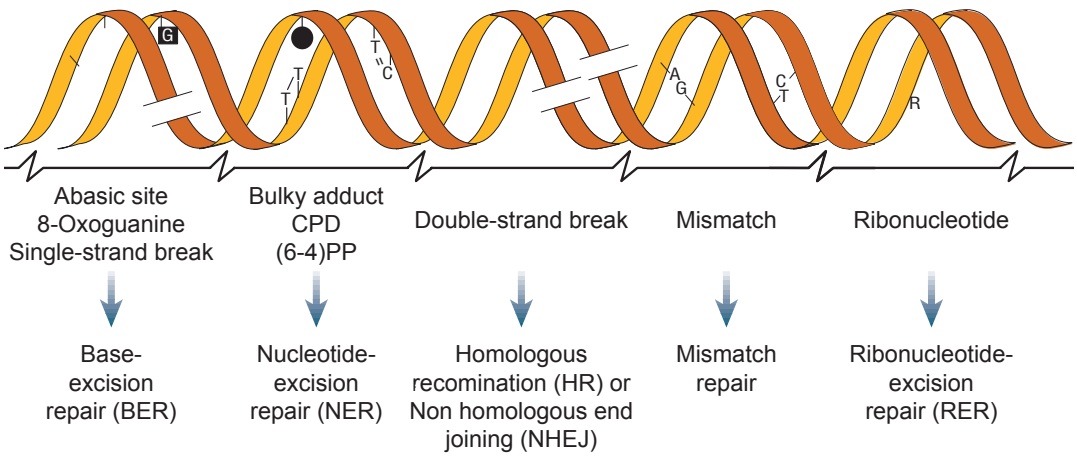

Figure 1.1: DNA damage and repair mechanisms. Examples of DNA lesions and most relevant DNA repair mechanism responsible for the repair of these lesions (modified after (Hoeijmakers, 2001)).

Several DNA repair pathways have evolved to cope with this: base-excision repair (BER), nucleotide-excison repair (NER), homologous recombination (HR) and non-homologous end joining (NHEJ), each specific for a subset of DNA lesions (Hoeijmakers, 2001, Lindahl and Wood, 1999). Errors during DNA replication poses another kind of damage to the cell. They are typically repaired via post-replicative DNA repair pathways such as mismatch repair and ribonucleotide excision repair (RER) (Figure 1.1), which is

describe in detail in the next chapter. In this chapter focuses on BER, NER, HR and NHEJ.

Simple DNA lesions such as base damage (e.g. 8-Oxoguanine), AP sites and single strand breaks can be repaired via the BER pathway (Figure 1.2 A). BER is initiated by DNA glycosylases, which recognize damaged bases and excise them. So far there are 11 glycosylases known specific to different but also partially overlapping base damage. The formed AP site is cleaved by AP endonuclease APEX creating a single stranded break in the DNA backbone. In case of short-patch BER this gap is filled by polymerase β and the nick is sealed by Ligase 3. Only one nucleotide gets replaced in this pathway. XRCC1 serves as a loading platform for this non-processive DNA synthesis reaction. In long-patch BER, polymerization is accomplished by polymerase δ or ϵ. They synthesize up to 10 nucleotides, displacing the old strand and forming a DNA flap. Flap structure-specific endonuclease 1 (Fen1) removes this flap and Ligase 1 seals the nick. As loading platform for this reaction serves the processivity factor 'proliferating cell nuclear antigen' (PCNA), which is also involved in other processive DNA repair pathways as well as in DNA replication (Klungland and Lindahl, 1997, Robertson et al., 2009).
The pathway determination between short- or long-patch BER is still poorly understood, but it has been hypothesized that lesion type and/or local ATP concentration could play a role (Fortini and Dogliotti, 2007, Petermann et al., 2003, Robertson et al., 2009).

NER removes helix-distorting DNA damage (Figure 1.2 B). These include bulky adducts and pyrimidine dimers like cyclobutane pyrimidine dimers (CPD) and 6–4 pyrimidine-pyrimidone photoproducts ((6-4)PPs). Damage recognition in global genomic NER (GG-NER) is accomplished by the DNA binding protein XPC and two additional subunits (HR23B and centurion) (Araki et al., 2001) where unpaired bases serves as trigger. XPA performs an additional function in this damage recognition. Even though its exact role is still not clear, contribution of XPA is absolutely required for NER (Nouspikel, 2009). Opening of double stranded DNA is achieved by helicase XPB, a subunit of transcription factor II human (TFIIH) complex, forming a denaturation bubble around the lesion (Bradsher et al., 2000). The next step is incision of the damaged strand at both ends of the formed bubble. The cut on the 3' side of the lesion is performed by the endonuclease XPG (O'Donovan et al., 1994) and on the 5' side by the XPF-ERCC1 heterodimer (Matsunaga et al., 1995). The excised fragment is about 25 – 30 nucleotides in size, depending on the lesion type. The resulting gap is filled by DNA polymerases δ or ϵ. In the last step DNA ligase I seals the remaining nick (Nouspikel, 2009). As in long-patch BER the loading platform for DNA synthesis is PCNA.
Besides the above described GG-NER there is also a transcription coupled NER (TR-NER). In TR-NER the lesion recognition occurs through an arrest of the elongating RNA polymerase II (RNAPII) when it encounters DNA damage. CSA and CSB are two important RNAPII cofactors in this process, which if mutated can cause Cockayne syndrome (CS). All subsequent steps are equal to GG-NER (Tornaletti, 2009).

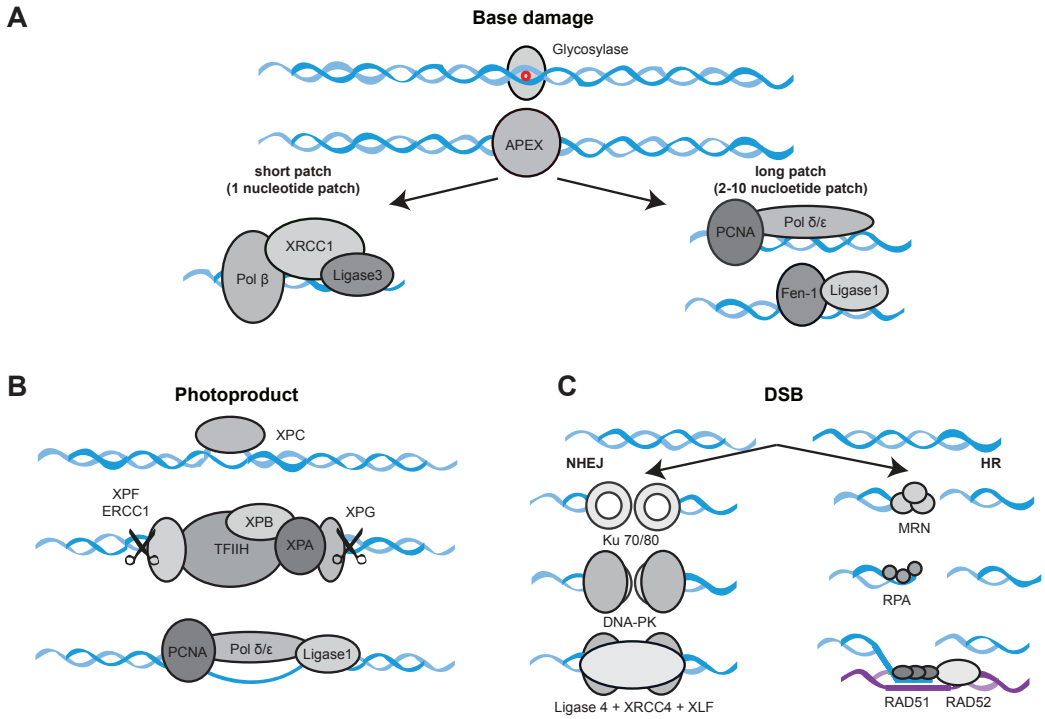

Figure 1.2: DNA repair pathways. Schematic overview of **(A)** base-excision repair, **(B)** nucleotide-excision repair and **(C)** double strand break repair pathways non-homologous end joining (left) and homologous recombination (right) and corresponding key repair factors.

The lesions repaired by BER or NER affect only one DNA strand. Double strand breaks a more problematic situation, as both strands are affected. The two main pathways repairing these damage are HR and NHEJ (Goodarzi and Jeggo, 2013, Pardo et al., 2009) (Figure 1.2 C).

HR depends on an undamaged homologous sequence to repair double strand breaks and only functions in late S/G2 phase when a sister chromatid is available (Johnson and Jasin, 2000).

The initial step of HR is resection of DNA ends from double strand breaks, where the MRN (MRE11-RAD50-NBS1) complex plays a major role. The single-stranded DNA overhangs generated by this process are coated with replication protein A (RPA). Together with Rad51 nucleoprotein the DNA overhangs form filaments, which invade the undamaged homologous DNA strand. The resulting DNA heteroduplex is called a displacement-loop (D-loop). The 3' end of the D-loop is extended by DNA polymerases to restore the missing sequence, forming a cross-shaped structure known as 'Holliday junction'. The newly synthesized DNA strand dissociates and anneals to the initial DNA strand. After DNA ligation the intact double strand is restored (Ghodgaonkar et al., 2013, Kass and Jasin, 2010, Pardo et al., 2009).

The second major double strand break repair pathway is NHEJ. Unlike HR it functions throughout the whole cell cycle and involves direct ligation of DNA ends with minimal processing at the site of DNA end joining. NHEJ is initiated by binding of the heterodimer Ku70-Ku80 (Ku) to the DNA double strand break. Ku binding protects the DNA ends from nucleolytic degradation and recruits DNA-PK catalytic subunit (DNA-PKcs) forming a DNA-PK holoenzyme. Its autophosphorylation licences end processing by a variety of factors, which

are necessary when incompatible double strand break ends are present. The final ligation step is carried out by a complex consisting of DNA ligase IV, XRCC4 and XRCC4-Like Factor (XLF) (Ghodgaonkar et al., 2013, Kass and Jasin, 2010, Pardo et al., 2009).

The importance of accurate DNA repair is reflected by the broad spectrum of defects displayed by individuals carrying mutations in DNA repair genes. Those include defects in the nervous-, immune-, and reproductive-systems, as well as a predisposition to cancer and premature aging (Jackson and Bartek, 2009). Therefor it is of pivotal importance to learn more about the processes and kinetics of these pathways.

1.2 DNA replication and post replicative repair

Every cycling cell needs to duplicate its genome before it divides. In eukaryotes, the entire genome is replicated during S phase. It is extremely important that the replication process is precise since mistakes can result in mutations or loss of genetic information, which may lead to cell death or cancer. Errors are repaired immediately via post replicative DNA repair pathways.

The replication of the genome is catalyzed by DNA dependent DNA polymerases and requires in addition numerous other proteins. At least two different DNA polymerases, a DNA primase, a DNA helicase, a single strand DNA binding protein complex (replication protein A, RPA), DNA topoisomerases, a clamp loading complex (replication factor C), and a DNA polymerase clamp or PCNA are necessary for replication (Chagin et al., 2010) (Figure 1.3).

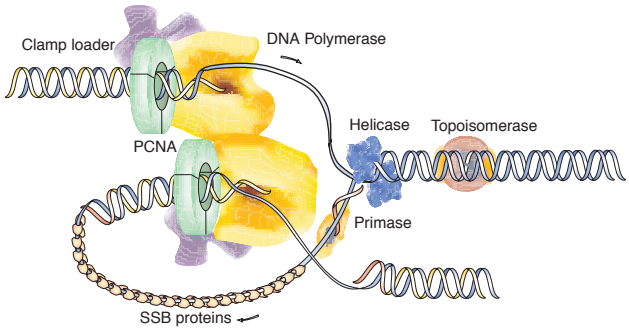

Figure 1.3: Schematic outline of the molecular components of DNA replication. PCNA: proliferating cell nuclear antigen (also termed DNA polymerase clamp or processivity factor). SSB; single strand DNA binding proteins (modified after Chagin et al., 2010).

Each of the two original antiparallel DNA strands serves as a template for the synthesis reaction. Since DNA polymerases can only synthesize new DNA in a 5′ to 3′ direction, a continuous synthesis is only possible on one strand (leading-strand). On the other strand (lagging strand) DNA is duplicated in a discontinuous manner, generating short DNA patches called Okazaki fragments (Okazaki et al., 1968, Perumal et al., 2010). In eukaryotes Okazaki fragments have a length of 180 - 200 bp.

To initialize the synthesis reaction, DNA polymerases require a primer. DNA Primase synthesizes RNA primers to initiate both leading and lagging strand synthesis. On the lagging stand this results in multiple RNA

primers, which have to be eliminated as RNA is more susceptible to strand cleavage than DNA due to its reactive 2' hydroxyl on the ribose ring.

Several nucleases have been proposed as candidates that process these RNA primers in Okazaki fragments including RNase H, flap endonuclease 1 (FEN1) and Dna2 (Bae et al., 2001, Turchi et al., 1994, Waga et al., 1994). RNase H are endonucleases, which cleave RNA in DNA-RNA hybrids, making them perfect candidates for removing RNA primers in double stranded DNA. But at least in yeast, deletion of RNase H causes no obvious phenotype, suggesting that this could not be the primary pathway for RNA primer removal (Zheng and Shen, 2011). The main pathway seems to be the formation of a 5' single-stranded flap structure while the replicating DNA polymerase encounters and displaces the RNA primer from the previous Okazaki fragment. This flap structure is subsequently degraded either by Fen1 or by a combination of Fen1 and Dna2 (Zheng and Shen, 2011).

As mention above, errors in replication can have tremendous effects for single cells or even for the whole organism. The replicative DNA polymerases synthesize DNA with high fidelity and harbor an intrinsic proofreading function. Despite this high accuracy, DNA polymerases make mistakes such as wrong base pairings and incorporation of ribonucleotides instead of deoxyribonucleotides. These errors are repaired via post-replicative DNA repair pathways.

Mispaired base pairs occur with a frequency of 1 per 10^7 nucleotides (Kunz et al., 2009). If left unrepaired, this mismatch would lead to a permanent mutation in the next cell cycle. The pathway, which processes these damage is the mismatch repair (MMR). It excises mismatched nucleotides and resynthesizes the DNA strand harboring the mismatched nucleotides. This pathway is initialized and coordinated by proteins from the MutS and MutL family (Kunz et al., 2009).

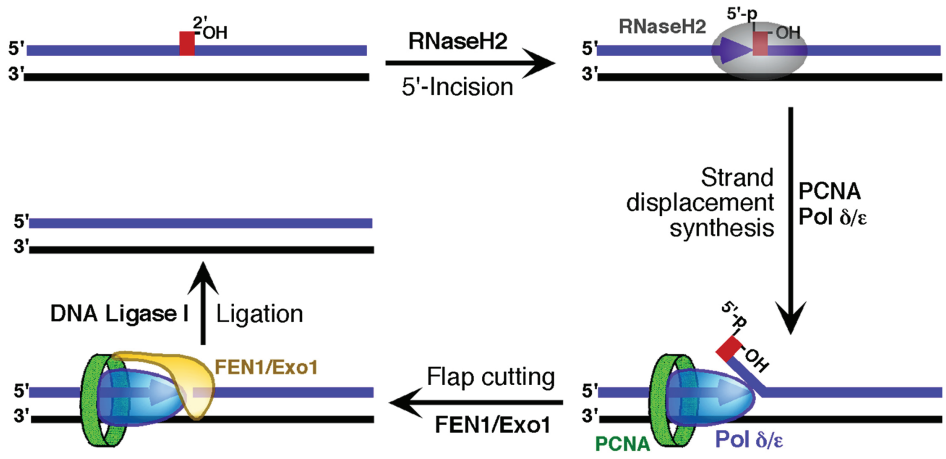

Figure 1.4: Model for ribonucleotide excision repair. Schematic outline of ribonucleotide excision repair proposed by Sparks et al. (2012). Recognition and incision of single ribonucleotides inside DNA is carried out by RNase H2 (Graphic from Sparks et al. (2012)).

In addition, DNA polymerases incorporate approximately one ribonucleotide instead of a deoxyribonucleotide every 7000 basepairs, which makes them the most frequent alterations in genomic DNA (Reijns et al., 2012). The consequence of ribonucleotide incorporation is a DNA backbone more susceptible to strand cleavage. Just recently a DNA repair pathway named ribonucleotide excision repair (RER) was proposed to cope with misincorporated ribonucleotides (Sparks et al., 2012). The recognition of the single ribonucleotide inside of DNA is carried out by the nuclease RNase H2 (Figure 1.4). As in other DNA repair proteins, mutations in RNase H2 have been shown to be associated with human hereditary disease (Crow et al., 2006). The role of RNase H2 in RER and its role in pathology will be discussed in detail in chapter 3.3.

1.3 DNA damage and repair in the context of chromatin

To understand DNA damage and repair, one must consider that DNA is not "naked" inside an eukaryotic cell. Chromatin inside the nucleus consists not only of DNA but also of several proteins, which leads to an organization and a compaction of several levels. The first level of chromatin compaction is the nucleosome. It consists of the core histone proteins H2A, H2B, H3 and H4, which are each present twice and form an octamer around, which DNA is wrapped. This chromatin fiber is further compacted through interaction with linker histone H1 (Jenuwein, 2001). Several higher order organization levels (Woodcock and Ghosh, 2010) have been proposed, leading to increased organization and compaction.

Chromatin can be separated into two major fractions: euchromatin and heterochromatin (Figure 1.5). While euchromatin is less condensed, gene rich and more easily transcribed, heterochromatin on the other hand is highly condensed, gene poor and transcriptionally silent (Tamaru, 2010). Heterochromatin can be further divided into two different subtypes: constitutive heterochromatin and facultative heterochromatin. Constitutive heterochromatin remains condensed throughout an organism's lifespan. One well know example for this type of chromatin are chromocenters representing clustered constitutive heterochromatin and contain pericentric heterochromatin. These prominent structures can be found among others in mouse cells. Facultative heterochromatin is assembled when genes need to be silenced during development. A classic example for facultative heterochromatin is the mammalian inactive X (Xi), which is the randomly inactivated X chromosome in females for dose compensation (Craig, 2005).

Each chromatin type is defined by distinct DNA modifications as well as histone modifications and variants (Figure 1.6). Histones feature a flexible and charged NH2-terminus that protrudes from the nucleosome, the so called "histone tail". Several covalent modifications (e.g. acetylation, phoshorylation, methylation) can be attached to this tail. A typical histone modification in euchromatin is acetylation enrichment while heterochromatin is characterized by a hypoacetylation of histones. Histone modifications provide binding sites for several effector proteins. Well known binding sites are for example acetylated lysine for proteins with

bromodomains or methylation marks for chromodomains (Jenuwein, 2001). Heterochromatin protein 1 (HP1) for instance binds via its chromodomain specifically to methylated H3 at lysine 9 (Bannister et al., 2001) and mediates gene silencing and stabilizes heterochromatin structure (Eissenberg and Elgin, 2000). Besides modifications on the histone tails, also the histones themselves can vary. Various histone variants have been described so far. They differ from the canonical in their primary sequence and can fulfill specialized functions (Bonisch and Hake, 2012, Wolffe and Pruss, 1996). The H2A variant H2AX for instance gets phosphorylated after DNA double strand breaks and supports the DNA damage response (Rogakou et al., 1999). Another H2A variant, macroH2A, is preferentially concentrated at the inactive X chromosome of female mammals (Costanzi and Pehrson, 1998) and plays a role in its inactivation process.

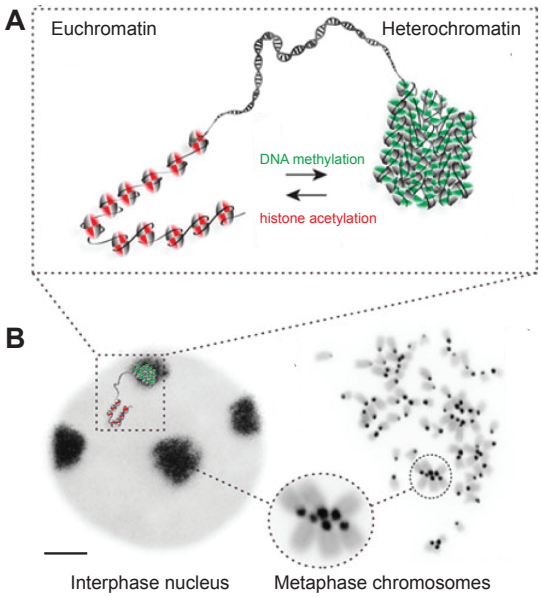

Figure 1.5: Eu- and heterochromatin. **(A)** Simplified graphic of molecular features assigned to eu- and heterochromatic chromatin states. **(B)** Chromocenters are condensed pericentric heterochromatin regions clustered together from multiple chromosomes during interphase. Depicted are fluorescence in situ hybridization stained mouse metaphase chromosomes and interphase cells with probes against pericentric heterochromatin (black) and DNA counterstaining (gray). Scale bar = 2 μm. (modified after (Jost et al., 2012)).

Additional to the histones, also the DNA itself can be modified. The most common modification in mammals is the methylation of cytosine bases at position 5 (5mC), which is occurring predominantly at CpG sites (mCpG) (Leonhardt and Cardoso, 2000). These modified CpGs are mostly found in heterochromatic regions (Razin and Cedar, 1977). DNA methyltransferases are responsible for establishing and maintaining this methylated state (Law and Jacobsen, 2010), which can be read by members of the methyl-CpG binding domain (MBD) protein family via their MBD domain (Zou et al., 2012). So far five proteins from this family are known, the founding member MeCP2 and MBD1-4 (Bird and Wolffe, 1999).

MeCP2 has been shown to concentrate at pericentric heterochromatin in a DNA methylation dependent manner via its MBD domain (Nan et al., 1996). Likewise, MBD1 and MBD2 localize preferentially at het-

erochromatin (Hendrich and Bird, 1998). They have been shown to repress gene transcription and have a role in heterochromatin formation and compaction (Brero et al., 2005, Fujita et al., 2003, Ichimura et al., 2005).

MBD3 is the only family member, which was reported not to bind to 5mC (Hendrich and Bird, 1998) but to 5-hydroxymethyl cytosine (5hmC) (Yildirim et al., 2011). In contrast to the above mentioned MBD proteins, MBD3 is not involved in chromatin compaction or repression of gene transcription, on the contrary even a potential activation function in gene transcription was proposed (Gunther et al., 2013).

MBD4 is a DNA glycosylase and preferentially removes thymidine or uracil mismatched to guanine within methylated or hemimethylated CpG sites (Hendrich and Bird, 1998). These bases often arise in DNA due to the hydrolytic deamination of 5mC and cytosine to thymidine and uracil, respectively, but uracil can also arise due to misincorporation as mentioned in the previous chapter (Sjolund et al., 2013).

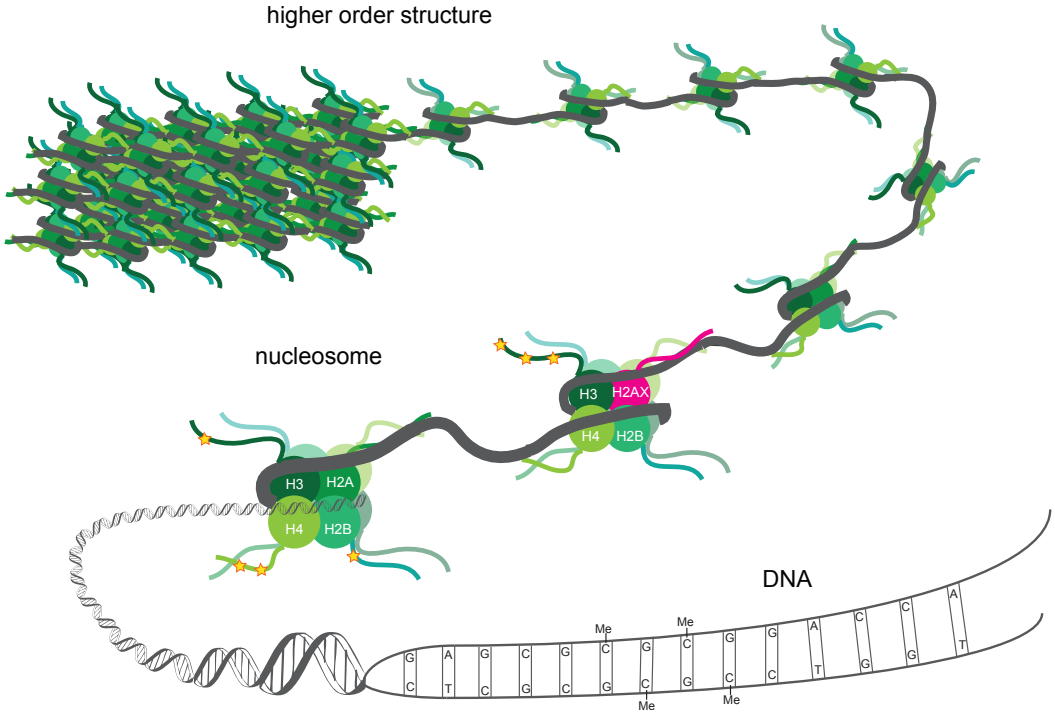

Figure 1.6: Schematic outline of chromatin modifications. Methylation (Me) of cytosine is the most common DNA modification in mammals. On the histone level, modifications (indicated as stars) can be attached to 'histone tails', which are the flexible and charged NH2-terminus of histones. Additionally to the canonical core histone proteins H2A, H2B, H3 and H4 several histone variants exists, which can serve as substitutes (e.g. H2AX instead of H2A, indicated in pink). The combination of these modifications can lead to different higher order structures.

Chromatin packing has an influence on DNA damage induction, response and repair. Transcribed euchromatic regions seem to be more sensitive to DNA damage induction. For example double strand breaks after ionizing radiation occur in lower frequency in highly condensed heterochromatic regions than in euchromatin (Falk et al., 2008, Obe et al., 2002). On the other hand DNA damage in euchromatin is preferentially or faster repaired (Falk et al., 2008, Friedberg, 1996, Goodarzi et al., 2008, Mullenders et al., 1991). Appar-

ently heterochromatin poses a barrier for DNA damage induction and repair (David, 2013, Goodarzi et al., 2010). Matching with this, repair processes in heterochromatic regions are accompanied by a local decondensation (David, 2013) and even relocation of damaged DNA out of heterochromatic regions was reported for DNA repair (Chiolo et al., 2011, Jakob et al., 2011). The role of chromatin in different kinds of DNA repair will be further discussed in chapter 3.2.

1.4 How to study DNA damage and repair in the context of a living cell

The different DNA repair pathways were studied in detail *in vitro* on naked DNA and in yeast. The situation in higher eukaryotes is less clear. Effects of different chromatin states as well as the kinetics inside a functional cell are in need of further investigation. To accomplish this, several experimental setups inducing DNA damage inside a living eukaryotic cell have been established (Figure 1.7).

Short-wave UV light induces bulky adducts and thymidine dimers, which are removed via the NER pathway and is therefor commonly used to study NER. To irradiate a confined area of individual cell nuclei, a polycarbonate filter with pores can be used (Mone et al., 2001). This allows local induction of UV damage and the study of DNA repair in its nuclear localization context.
Another widely used irradiation method is ionizing radiation. This includes X-rays as well as γ-rays. This type of irradiation is widely used to study DSB repair. It results in the formation of ionizing radiation-induced focis, which are used to study factor recruitment and modifications at damaged sites (Kong et al., 2009). One outstanding discovery of this technique is the earlier mentioned phosphoylation of H2AX (γ-H2AX) after DNA double strand break induction (Rogakou et al., 1999). Damage caused by ionizing radiation is complex and can include a variety of other DNA lesions in addition to DSB. Drawbacks of this technique include the inability to target damage to a particular site within the nucleus and the inability to study DNA damage and repair in real time (Goodhead, 1994, Ward, 1995).
To avoid multiple DNA damage and induce exclusively DSBs, endonucleases were also used (Jasin, 1996). They only cleave their specific restriction sites, creating DSBs, which are limited to the number of restriction sides inside the genome. Endonuclease I-PpoI for instance cleaves around 10% of their 200-300 genomic sites in human cells, thus creates 30 DSBs per cell (Berkovich et al., 2007). Taking this approach one step further, cell lines were created containing a single restriction site for specific endonucleases (e.g. I-SceI) (Pierce et al., 2001, Rodrigue et al., 2006). This makes it now possible to study not only single DSBs but DSBs in a defined region of the nucleus. However, real time kinetics and damage induction at a pre-defined location are not possible with this approach.

Laser microirradiation and targeted ion microbeam irradiation are the methods of choice when high spatial resolution in predefined locations and a high temporal resolution in a range from seconds to even milliseconds is desired.

In ion microbeam irradiation a defined number of ions can be used to generate localized DNA damage in pre-selected regions. Damage induction and repair in these restricted regions of the nuclei can be imaged in living cells already during irradiation (Heiss et al., 2006, Jakob et al., 2005). The physical nature of damage generation is similar to sparsely ionizing radiation (Jakob et al., 2009) and a wide variety of DNA damage can be formed. Unfortunately, this approach requires an ion accelerator, which is not present at most locations.

The use of a focused laser beam on the other hand requires only a laser. Laser microirradiation wavelengths in the range of UV-C to near-infrared can be used, generating different compositions of DNA damage (Ferrando-May et al., 2013). UV-C lasers predominantly induce UV-photoproducts, matching with the direct absorption of DNA bases at 260 nm (Voet et al., 1963). Longer wavelengths are poorly absorbed by DNA. At these wavelengths endogenous sensitizers lead to formation of reactive oxygen species (ROS), which subsequently result in various types of DNA damage. The biggest benefit of laser microirradiation is the possibility to use lasers already installed on standard confocal microscopes, making this method widely accessible. In chapter 3.1 the DNA damage profile and pathway activation resulting from laser microirradiation with standard confocal microscopes are discussed in greater detail.

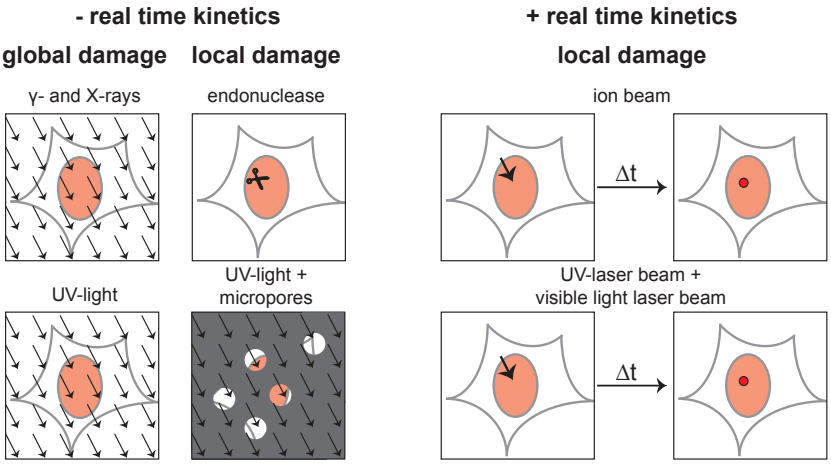

Figure 1.7: Methods for DNA damage induction. Examples for DNA damaging methods in living cells. Left side: global and local damaging methods that do not allow measurement of real time kinetics, right side: damaging methods allowing local damage induction and real time kinetic measurements.

2 Aims of the work

The aim of this work was to study specific DNA repair pathways in the context of living cells. The most promising method to obtain this kind of data is laser microirradiation. This technique allows induction of DNA damage at a pre-selected spot inside the nucleus and the study of DNA repair pathways in real time with fluorescently tagged DNA repair factors.

The first milestone was to establish microirradiation conditions on conventional confocal microscopes, which lead to induction of defined DNA damage and recruitment of DNA repair factors specific for different DNA repair pathways.

Combining high spatial resolution of laser microirradiation with the discriminating conditions established in the first part of this work made it possible to target specific chromatin types. Hence the second goal was to investigate the effect of different DNA damage on chromatin and repair processes inside different chromatin regions.

Finally we applied the above mentioned methodology to elucidate the role of RNase H2 in the recently described post-replicative ribonucleotide excision repair pathway. Mutations in this protein have been found to be the cause of the rare hereditary genetic disorder Aicardi-Goutières-Syndrom.

After establishing a role for RNase H2 in DNA repair using laser microirradiation, we further examined effects of Aicardi-Goutières-Syndrom causing mutations on binding and RNase H2 mobility at sites of DNA repair and replication. These results will be essential for the understanding of the underlying pathogenesis.

3 Results

3.1 Discrimination of DNA repair pathways by laser microirradiation

Britta Muster[1], **Alexander Rapp**[1], **M. Cristina Cardoso**[1]

[1] Cell Biology and Epigenetics, TU Darmstadt, Darmstadt, Germany

Cellular DNA is constantly exposed to endogenous as well as exogenous genotoxic factors, leading to base damage, photoproducts/adducts or DNA single and double strand breaks. If left unrepaired, these lesions can lead to mutations and subsequently cancer and/or cell death. To cope with these different sorts of DNA damage, several DNA repair pathways have evolved. Subtle modifications of DNA, such as base damage, are repaired via base excision repair (BER) whereas the repair of helix-distorting DNA damage, like e.g. photoproducts, are accomplished via the nucleotide excision repair pathway (NER) (Hoeijmakers, 2009). The two main DNA double strand breaks (DSB) repair pathways function by homologous recombination (HR) and non-homologous end joining (NHEJ) (Goodarzi and Jeggo, 2013)).

To explore these distinct DNA repair processes, *in vitro* biochemistry and yeast genetics as well as mutants or knock out cell systems have been extensively used and revealed detailed insights into their molecular mechanisms. The shortcoming of the above mentioned approaches is that DNA repair is not studied in its natural context, the chromatin inside living cells. A technique, which promises to overcome these limitations is laser microirradiation. With the use of a focused laser beam, it is possible to induce DNA damage with a high spatial resolution and tight temporal control inside of living cells.

This method can be applied to a large variety of cells in order to study the kinetics of DNA repair *in situ* (Mortusewicz et al., 2008). Using genetically encoded fluorescently-tagged versions of different DNA repair factors one has the further advantage to study their as/dissociation at sites of induced DNA damage in real time with a very high temporal resolution (Mortusewicz et al., 2008).

The first applications of microirradiation were performed with UVC laser light (257 nm) and showed a localized induction of DNA photoproducts (Cremer et al., 1980). Subsequently, laser microirradiation was also successfully employed within the UVA range ∼360 nm. For induction of DNA double strand breaks, cells were often pre-sensitizes with either halogenated thymidine analogs (BrdU, IdU), DNA intercalating dyes (Hoechst) or both (Lukas et al., 2003, 2004, Rogakou et al., 1999, Tashiro et al., 2000). However, these sensitizers potentially induce DNA damage by themselves and have considerable consequences on different aspects of the cell, e.g. cell cycle (Dinant et al., 2007). To bypass this problem, microirradiation was also performed without sensitizers and it was demonstrated that microirradiation alone (365 nm) leads to DNA damage, including DNA double strand breaks (Lan et al., 2004).

Nevertheless, using this technique to image the earliest time points in the range of seconds or even milliseconds directly after DNA damage requires coupling the UVA laser into a (confocal) microscope (Lan et al., 2004, Lukas et al., 2004) and often require specialized UV optics. In contrast continuous wave 405 nm lasers are nowadays available in most confocal microscope systems and are compatible with standard optics. This wavelength was also shown to induce DNA damage after pre-sensitization of the cells, leading to the activation of different DNA repair pathways (Dinant et al., 2007, Mortusewicz and Leonhardt, 2007, Mortusewicz et al., 2006, 2005). However, as with UVA lasers, also 405 nm laser microirradiation conditions lead to the induction of mixed DNA damage that result in the activation of various DNA repair pathways (David, 2013).

This makes it impossible to study individual DNA repair pathways separately.

To overcome this challenge, other lasers were tested. It was shown that using a 1050 nm pulsed laser is favors the induction of DSBs over cyclobutane pyrimidine dimers (CPD) when compared to a 775 nm pulsed laser (Trautlein et al., 2010). Furthermore, microirradiation with a 266 nm laser predominantly forms photolesions such as CPDs and 6-4 photoproducts (6-4PP) and only induced DSBs after high intensity irradiation (Dinant et al., 2007). Taken together these studies show that it is possible to discriminate between specific DNA damage. Nevertheless, these distinguishments are based on non-linear absorption and require special laser and/or lenses (UV transmitting) not commonly available in most laboratories (Ferrando-May et al., 2013).

Our aim was consequently to achieve discrimination between specific DNA damage and repair pathways using lasers commonly available on most confocal microscopes. We tested four different wavelengths (405, 488, 561 and 633 nm) with and without sensitizers on a spinning disk confocal microscope as well as on a laser scanning confocal microscope with laser powers ranging from 1 mJoule to 66 mJoule in the objective plane. After using different DNA damage markers to validate the type of induced DNA damage, we analyzed the activation of the different DNA repair pathways with the help of fluorescently tagged DNA repair factors specific to the different repair pathways. We were able to establish conditions to discriminate between the non-processive short-patch base excision repair and processive DNA repair pathways using the 488 and 561 nm lasers respectively.

Materials and Methods

Cell culture and transfection

HeLa Kyoto (Landry et al., 2013) cells were grown at 37 °C 5% CO2 in DMEM supplemented with 10% FCS and 1 μM/ml gentamycin. Stable transfected cherry-PCNA (Rottach et al., 2008) HeLa Kyoto cells were cultivated in the presence of blasticidin (2.5 μg/ml). Cells grown on cover slide dishes or in 8-well chambered coverslips (Sarstedt) were transfected with fluorescence-tagged proteins using polyethylenimin as described elsewhere (Casas-Delucchi et al., 2012). For discrimination of different DNA repair pathways the following fluorescence tagged proteins were used: cherry-PCNA (Mortusewicz et al., 2011, Sporbert et al., 2005), GFP-Ligase4 (Mortusewicz et al., 2006), Ku70-GFP (Rodgers et al., 2002), XPC-GFP (gift from Wim Vermeulen), XPG-GFP (gift from Wim Vermeulen), mRFP-XPA (gift from Wim Vermeulen), GFP-Ligase3 (Mortusewicz et al., 2006, 2005) GFP-p66 (subunit of polymerase delta) (Pohler et al., 2005), GFP-Fen1 (Ingrid Grunewald), GFP-Rad51, GFP-XRCC1, mRFP-APEX, NBS1-GFP.

GFP-Rad51, GFP-XRCC1 and mRFP-APEX constructs were generated by cloning the corresponding human cDNA into either pEGFP-C1 or pmRFP-C1 backbone (Clontech) vectors. For PCR amplification following primers were used (with indicated restriction sites):

XRCC1 forward: 5'AA ACCGGT ATGCCGGAGATCCGCCTCC3' (HpaI),

XRCC1 revers: 5' AA GCTAGC GGCTTGCGGCACCACCCC3' (NheI),

APEX1 forward: 5' AA ACCGGT ATGCCGAAGCGTGGGAAAAAGG3' (HpaI),
APEX1 reverse: 5' AA GCTAGC CAGTGCTAGGTATAGGGTGATAGG3' (NheI),
Rad51 forward: 5' AA GTCGAC GTAATGGCAATGCAGATGC3' (SalI),
Rad51 reverse: 5' AA GGATCC AAGTCTTTGGCATCTCCCACTC3' (BamHI)
NBS1-GFP construct was generated by Dr. Paulius Grigaravicius. NBS1 was cloned from NBS1 cDNA vector into pEGFP-C3 by SacII and BamHI restriction sites (unpublished data).
All constructs were verified by sequencing.

Microscopy and microirradiation

Imaging and microirradiation experiments were performed using an UltraVIEW VoX spinning disc confocal system (PerkinElmer) in a closed live cell microscopy chamber (ACU, Perkin Elmer) at 37 °C with 5% CO_2 and 60% humidity, mounted on a Nikon TI microscope (Nikon). Images were taken with a CFI Apochromat 60x/1.45 NA oil immersion objective. GFP and cherry or mRFP were imaged with 488 and 561 nm laser excitation and 527 ± 55 and 612 ± 70 nm (full width at half maximum) emission filters, respectively.
For standard microirradiation, a preselected spot (1 μm diameter) within the nucleus was microirradiated for 1.2 seconds with one of the following laser lines 405, 488, 561 or 633 nm laser set to 100%, resulting in 1, 3, 8 and 5 mJoule respectively. Additionally lower energy microirradiations were performed using 200 or 800 milliseconds resulting in 0.1 and 0.6 mJoule for the 405 nm laser, 0.5 and 2 mJoule for the 488 nm laser and 1 and 5 mJoule for the 561 nm laser. For these energies additional exogenous sensitizers e.g. the thymidine analog Bromdesoxyuridin (BrdU) or the DNA intercalating agent Ethidiumbromid (EtBr) were used. BrdU was added at a final concentration of 10 μM over night and EtBr in a final concentration of 200 nM directly before microirradiation. Higher energy microirradiation with the 488 nm laser was done for 6.8 seconds resulting in 17 mJoule and with the 561 nm laser for 10 seconds resulting in 66 mJoule. Energy output of the different lasers was measured with a laser power meter (OPHIR) directly after the objective with beam park setting. For validation on another microscope system, a Leica SP5 II confocal laser-scanning microscope was used. Energy levels for each wavelength were adjusted to be in the same order as for the standard experiments on the spinning disk microscope.
Before and after microirradiation, confocal image series of one mid nucleus z-section were recorded in 15 seconds intervals.

***In situ* quantification of protein accumulation**

For evaluation of the accumulation kinetics at least four cells were analyzed. Images were first corrected for cell movement and subsequently mean intensity of the irradiated region was divided by mean intensity of the whole nucleus (both corrected for background) using ImageJ software. Maximal accumulation represents the highest ratio from each experiment. Half-times for XRCC1 accumulation were calculated from time of bleach till maximal accumulation with one phase association (single exponential function:

$Y = Y_0 + (Plateau - Y_0) \cdot (1 - e^{(-K \cdot x)})$ using Prism 5 (GraphPad Software, Inc.).

Immunofluorescence staining with DNA damage and repair markers

HeLa Kyoto cells were microirradiated with the different wavelengths, fixed directly after irradiation and stained for different DNA damage markers or marker proteins. DAPI was used as a DNA counterstain.

For γH2AX and XRCC1 staining, cells were fixed with 3.7% formaldehyde room temperature for 15 min, permeabilized for 20 min in 0.5% Triton-X 100 in PBS, blocked for 30 min with 2% BSA in PBS and subsequently stained with primary antibody anti-phopho-Histon H2AX (upstate, JBW301) diluted 1:200 or anti-XRCC1 (Biozol (abcam)) diluted 1:100 in 1% BSA in PBS for 1 h at RT. Secondary antibody (anti mouse IgG Cy5, Jackson ImmunoResearch Laboratories) was diluted 1:400 in 1% BSA in PBS and also incubated for 1 h at RT.

For detection of Cyclobutane pyrimidine dimers (CPDs), cells were fixed for 10 min at -20 °C with ethanol and treated with 2 N HCl for 10 min on ice. After blocking for 30 min with 2% BSA in PBS, mouse anti-CPD (Kamyia) was diluted 1:200 in 1% BSA in PBS and incubated for 1 h at RT. Secondary fluorescence tagged antibody (anti mouse IgG Alexa 488; 1:400 in 1% BSA in PBS, Invitrogen) was also incubated for 1 h at RT.

For TUNEL staining cells were fixed with 1% formaldehyde for 15 min, permeabilized 20 min with 0.5% Triton-X 100 and treated for 10 min at -20 °C with MeOH/Acetat (3:1). Terminal transferase incubation was performed according to the manufacturers protocol (transferase in 1x Tdt buffer plus CoCl2 and Biotin-16-dTUP (1 mM)) plus additional ATP (1 mM) for 2 h at 37 °C. After blocking for 30 min with 2% BSA in PBS, Streptdavidin Alexa 488 was diluted 1:200 in 1% BSA in PBS and incubated for 30 min at RT.

For PCNA staining cells were fixed with -20 °C MetOH for 10 min, blocked for 30 min with 2% BSA in PBS and subsequently stained with mouse anti-PCNA (Dako, clone PC10) diluted 1:100 in 1% BSA in PBS and incubated for 1 h at RT. Incubation with secondary anti-mouse Cy5 (1:400) was also performed for 1 h at RT.

Results and Discussion

Microirradiation with 405 but not with 488 and 561 nm lasers induces pyrimidine dimers and DNA strand breaks

Microirradiation with 405 nm continuous wave (cw) lasers was previously shown to induce a mixture of DNA damage, ranging from pyrimidine dimers to double strand breaks (Dinant et al., 2007). Since damage induction is dependent on the applied energy (Lan et al., 2005, Solarczyk et al., 2012), we wanted to validate what kind of damage is induced with an energy of 1 mJoule for the 405 nm laser. Additionally, also longer wavelengths of cw lasers were tested (488 and 561 nm with 3 mJoule and 8 mJoule respectively).

To directly assess the induction of pyrimidine dimers, we stained cells directly after microirradiation with an anti cyclobutan pyrimidin dimer (CPD) antibody. We detected the induction of CPDs exclusively after microirradiation with the 405 nm laser, but not after microirriadiation with 488 or 561 nm lasers (Fig 3.1 A).

Another type of known DNA damage induced by microirradiation with 405 nm lasers are DNA double strand breaks (Dinant et al., 2007, Mortusewicz and Leonhardt, 2007, Mortusewicz et al., 2006). To verify this type of damage, we used Terminal deoxynucleotidyl transferase dUTP Nick End Labeling (TUNEL) to stain open DNA ends. This method labels enzymatically free 3'OH DNA ends characteristic for double strand breaks. A TUNEL positive signal was detected after microirradiation with the 405 nm laser, but not when cells were irradiated with longer wavelengths (Fig 3.1 B). An alternative marker for DSBs is the phosphorylated form of H2AX (γH2AX), which appears within few minutes after DSB induction (Rogakou et al., 1999). Thus, we further validated the induction of DSBs using immunofluorescence with a γH2AX specific antibody. Again this marker was exclusively detected after microirradiation with the 405 nm laser, but not with the 488 or 561 laser line (Fig 3.1 C).

Although others reported induction of DSBs by 488 nm lasers this only occurred at very high energy level of 17mJoule (Solarczyk et al., 2012), which is more than 5 times higher than the energy we applied. When we increased our laser energy to this level, we were also able to detect formation of γH2AX foci, indicating formation of DSBs even with this wavelength (Figure 3.3 A). Prompted by this observation, we also increased the energy level for the 561 nm laser up to 66 mJoule. Again the formation of γH2AX foci was detectable (Figure 3.3 A). Additionally, we were interested if with these very high energies we could also detect the formation of CDPs. Indeed, CPD induction can be observed after microirradiation with these high energies for both lasers tested. The level of induced CPDs is greater after microirradiation with 561 nm compared to microirradiation with 488 nm (Figure 3.3 A). DNA damage induction is therefor largely dependent on the applied energy and differences between setups must be taken into account when comparing data sets from different studies.

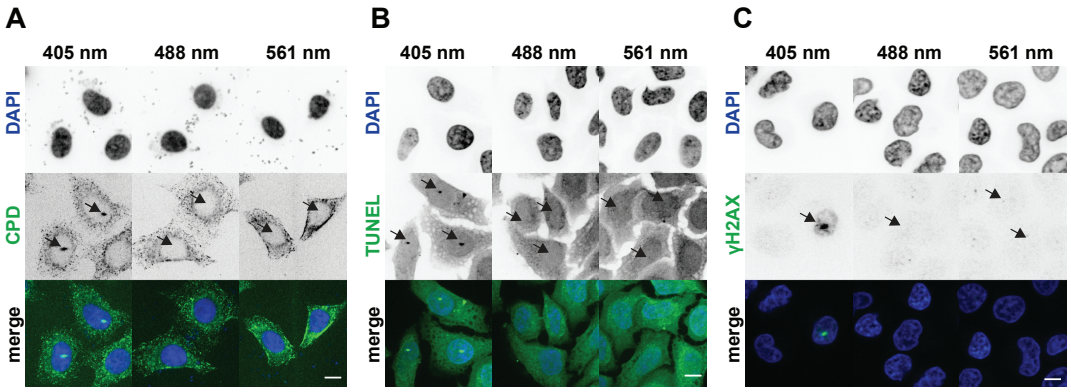

Figure 3.1: Microirradiation with a 405 but not with a 488 or 561 nm laser induces DNA photo damage and strand breaks. HeLa Kyoto cells were microirradiated with 405, 488 or 561 nm laser lines, fixed and subsequently stained for the different DNA damage markers: **(A)** Immunofluorescent detection of cyclobutane dimers; **(B)** terminal deoxynucleotidyl transferase dUTP nick end labeling (TUNEL) and **(C)** immonofluorescence staining against the double strand break marker γH2AX **(C)**. DNA counterstained with DAPI. Arrows indicate the sites of microirradiation. Scale bar = 10 μm.

Taken together we were able to show that using our energy settings CPDs and double strand breaks are only induced after microirradiation with a 405 nm laser but not after microirradiation with a 488 or 561 nm

laser. Only the application of very high energies can lead to induction of this damage when a 488 or 561 nm laser is used. Since we could not find reliable markers for base damage or abasic sites, we can not rule out the possibility for induction of these damage after microirradiation with 488 and 561 nm in our setting. These types of damage result in activation of base excision repair (BER).

The formation of CPDs and DSB after microirradiation with visible light clearly shows that DNA can be damaged by these wavelengths. The mechanisms on how this damage is formed are still unclear. In principle DNA damage by irradiation either with UV or visible light can be accomplished by two different mechanisms. The first one is via direct absorption of a photon by the DNA. Since direct absorption of wavelengths over 300 nm by DNA is very low (Sutherland and Griffin, 1981), these mechanisms seem unlikely to account for all our observed DNA damage. Also two-photon effects, where photons with double the wavelength are simultaneously absorbed, are very unlikely considering the energy density used in these experimental conditions. The second mechanisms is via absorption by endogenous, so far unknown, cellular photo-sensitizers The so formed photoexcited sensitizers can damage DNA either by a direct reaction with a DNA base (type I reaction) or via reaction with molecular oxygen (type II reaction). The latter leads to the formation of reactive oxygen species (ROS), which in turn reacts with DNA and forms oxidative damage like 8-Oxoguanine or single strand breaks (SSB) (Greinert et al., 2012, Kielbassa et al., 1997, Pflaum et al., 1994). When two SSB on opposing DNA strands are induced within a distance of less than 15 base pairs, these SSBs can convert into a DSBs (Povirk et al., 1977). The observed DSBs are therefor likely to be produced by multiple SSBs in close proximity. Formation of CPDs on the other hand could occur via the formation of an excited triplet state of the sensitizer. If the energy of the triplet manifolds is larger than that of thymidine in DNA, a transfer may take place and lead to the formation of CPDs. An alternative explanation would be a weak direct absorption of the DNA (Cadet et al., 2012).

Activation of double strand break repair pathways NHEJ and HR

Since microirradiation with a 405 nm laser led to the formation of γH2AX foci and a positive TUNEL staining, we tested whether non-homologous end joining (NHEJ) and homologous recombination (HR) repair pathways were activated. Key proteins of each pathway are depicted in Figure 3.2 A left.

Activation of homologous recombination was monitored by GFP-tagged Rad51. Since overexpressed Rad51 protein forms higher-order nuclear structures even in the absence of DNA damage (Raderschall et al., 2002), we only selected very low expressing cells for our analysis. Cherry-PCNA serves as a reference, since PCNA shows a strong recruitment after microirradiation (Mortusewicz et al., 2011). Microirradiation with the 405 nm laser at 1 mJoule resulted in a strong (4 fold) (Figure 3.2 B) recruitment of cherry-PCNA and a significant accumulation of GFP-Rad51 (1.5 fold) to sites of DNA damage (Figure 3.2 B). Microirradiation with the longer wavelengths on the other hand did not lead to a detectable accumulation of Rad51 at damage sites (Figure 3.2 B and E).

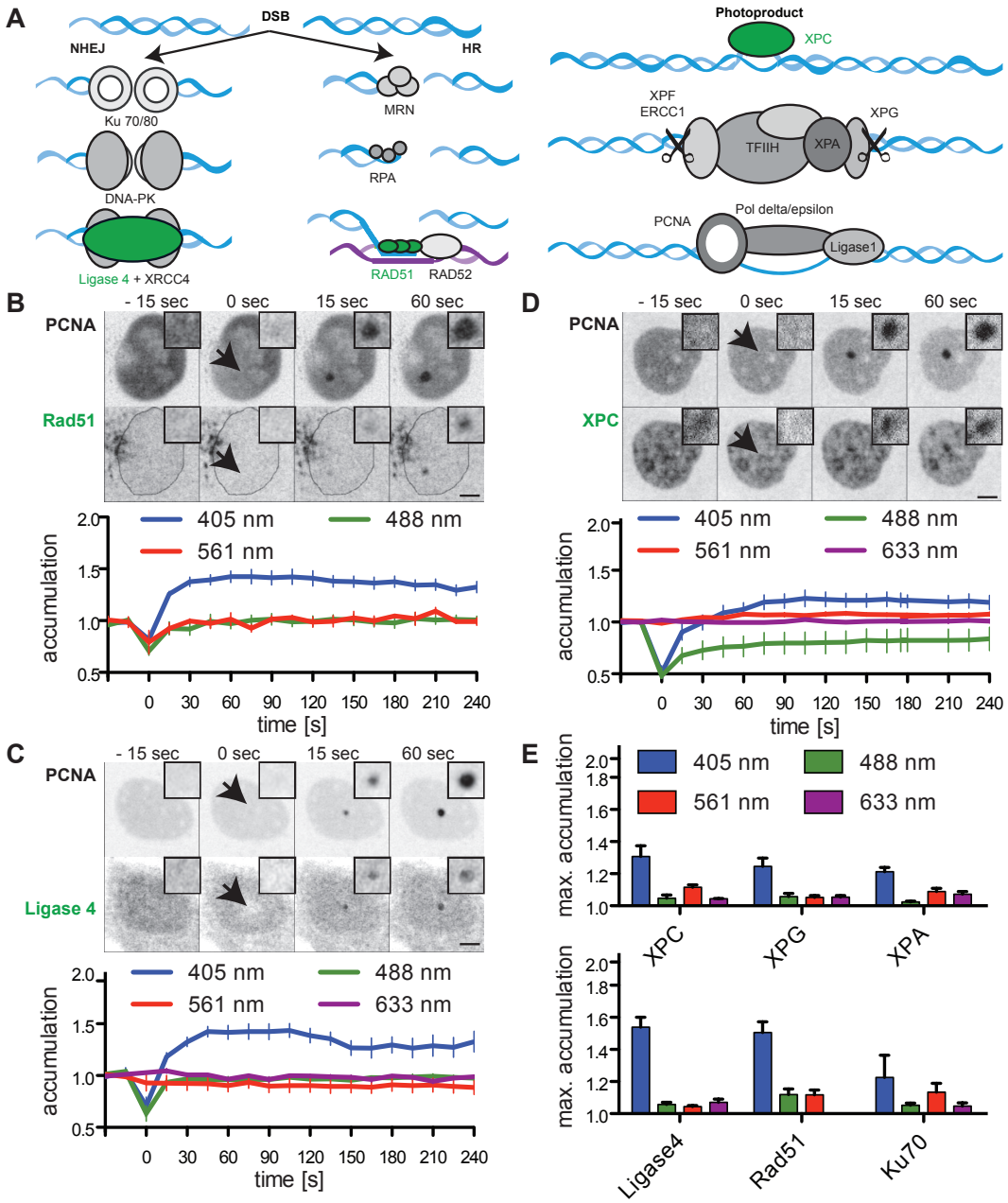

Figure 3.2: 405 nm microirradiation activates HR, NEHJ and NER. Simplified schematic representation of NHEJ and HR (left) and NER (right) **(A)**. HeLa cells, expressing cherry-PCNA and GFP-Rad51 **(B)** or GFP-Ligase 4 **(C)** or XPC-GFP **(D)** were irradiated with different laser lines as indicated. Representative confocal microscopy images are shown from experiments with a 405 nm laser. Arrowheads point to sites of microirradiation, shown enlarged as insets. Plots show accumulation of repair proteins over time as mean value. **(E)** Bar histograms display calculated mean maximal accumulation for repair factors as indicated. Whisker represents standard deviation. Scale bar = 5 μm.

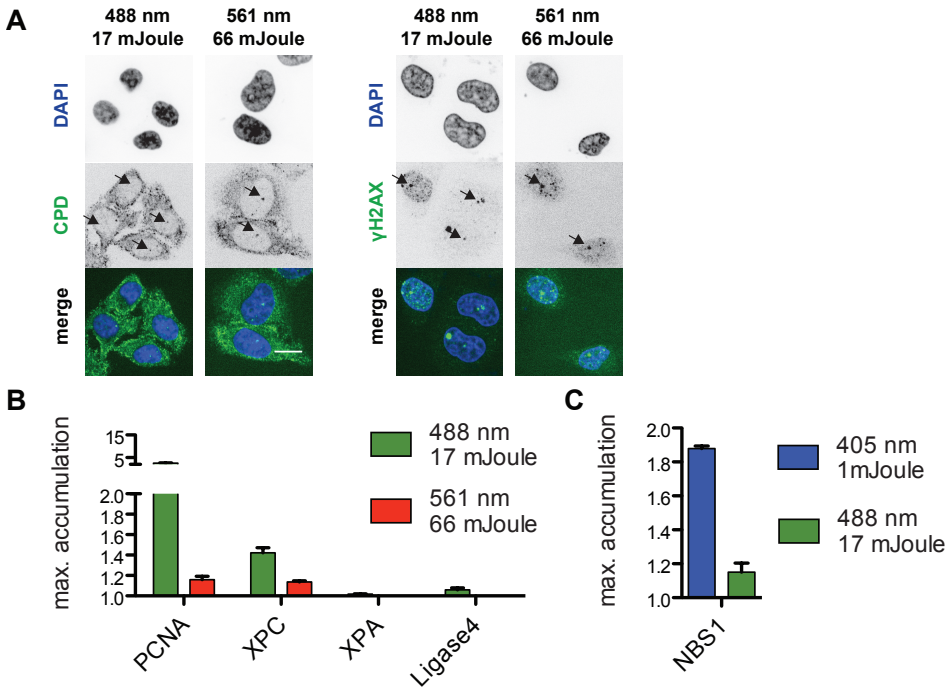

Figure 3.3: Microirradiation with a 488 or 561 nm laser at very high energies. (A) HeLa Kyoto cells were microirradiated with 488 nm at 17 mJoule or 561 nm at 66 mJoule, fixed and subsequently stained with antibodies against γH2AX or against cyclobutane dimers and DNA counterstained with DAPI. Arrows indicate the sites of microirradiation. Scale bar = 10 μm. **(B)** Bar histograms display the mean maximal accumulation for the different repair factors from at least 3 experiments. Whisker represents standard deviation. **(C)** Bar histograms from the mean maximal accumulation of GFP-NBS1 after microirradiation from at least 4 experiments. Whisker represents standard deviation.

As markers for the non-homologous end joining pathway we selected GFP-tagged versions of Ku70 as one of the early acting factors on DSB and Ligase 4, which seals the broken ends at the end of this pathway. Cherry-PCNA was again used as a reference. A representative time-laps series for the recruitment of GFP-Ligase 4 after microirradiation with a 405 nm laser is shown in Figure 3.2 C. Quantitative analysis of the accumulation for GFP-Ligase 4 to sites of microirradiation clearly shows that DNA DSB repair proteins only recruits to sites of 405 nm microirradiation but not after microirradiation with longer wavelengths (Figure 3.2 C). A maximal accumulation of 1.5 fold was found for Ligase 4 (Figure 3.2 E). Similarly, Ku70-GFP accumulates only at sites of 405 nm laser induced damage, but not after microirradiation with longer wavelengths. Here the maximum accumulation reaches levels of approximately 1.3 (Figure 3.2 E). This indicates that both DNA DSB pathways, homologous recombination and non-homologous end joining, get activated after microirradiation with 405 nm even in the absence of exogenous sensitizers, but not after microirradiation with longer wavelengths.

Addition of the sensitizers BrdU or EtBr does not lead to an activation of these pathways using longer wavelengths (shown for Ligase4 and Ku 70 in Table 3.1. Even after microirradiation with the 488 nm laser with 17 mJoule, which resulted in the formation of γH2AX foci (Figure 3.3 A), no accumulation for DSB

repair pathway proteins was detectable (shown for Ligase 4 in Figure 3.3 B). Nevertheless, NBS1, a subunit of the MRN complex, which is involved in foci formation (Figure 3.2 A left) (Trujillo et al., 1998), does accumulate at sites of 488 nm induced DNA DSB (Figure 3.3 C). This indicates that the threshold for measurable accumulation of DNA repair factors is higher than that of factors involved in foci formation. This is due to a cellular amplification of factors involved in foci formation, which result in a multiplication of their accumulation at damaged sites (Fernandez-Capetillo et al., 2003).

Experiments with energy levels equivalent to our initial settings were also performed on a Leica SP5 II for Ligase 4 to show independency of the microscope type. Using this confocal laser scanning microscope we were able to reproduce activation of the DNA DSB repair pathway exclusively after irradiation with a 405 nm laser (Figure 3.4).

Taken together, we could verify that DNA DSB are induced after microirradiation with a 405 nm laser. Former studies routinely used additional sensitizers, mostly BrdU, to enhance the formation of DNA DSB. We demonstrated that 1 mJoule with the 405 nm laser is not only sufficient to induce this type of damage without additional sensitizers, but also that the corresponding DNA repair pathways are activated. This allows the study of these DNA repair pathways in real time with high spatial resolution on conventional confocal microscopes without unwanted side effects from exogenous sensitizers.

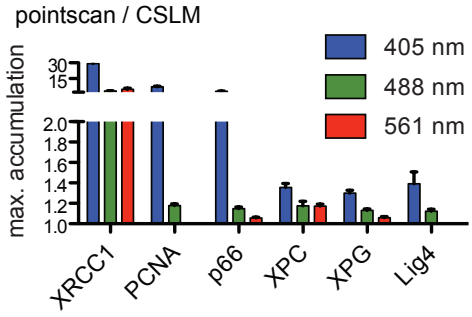

Figure 3.4: Confirmation of pathway activation in another microscope type. Maximal accumulation after microirradiation of HeLa Kyoto cells on a Leica SP5 II confocal laser scan microscope for different fluorescently tagged DNA repair factors. Bars show mean values of at least 6 experiments. Whisker represents standard deviation.

Activation of NER

Micorirradiation with the 405 nm laser does not only lead to formation of γH2AX foci and a positive TUNEL staining, but also to induction of CPDs. Thus, we were interested if nucleotide excision repair (NER), is activated. Therefore we used XPC, one of the first factors in global genomic NER (Figure 3.2 A, right) to study recruitment to the damage site. XPC can bind nonspecific to DNA without damage, but binding is strongly enhanced at DNA with helix distortions where it initiates the NER reaction (Sugasawa et al., 2001). XPC-GFP transfected cells therefor already showed florescent signals in the nucleus with a pattern representing endogenous localization of XPC (Figure 3.2 D). After microirradiation with the 405 nm laser, the NER factors get recruited to sites of damage. Microirradation with longer wavelength on the other hand does not

lead to an accumulation. Irradiation with a 488 nm laser even leads to a persistent lower fluorescence at the irradiated spot due to photobleaching of the bound XPC-GFP fraction with the laser (Figure 3.2 D and 3.5).

Maximal accumulation for XPC-GFP after microirradiation with a 405 nm laser reached an average of 1.3. Since it was shown that XPC binds to DNA helix distortions and needs subsequent verification of the damaged base before proceeding with NER (Dinant et al., 2007, Sugasawa et al., 2001), we validated progression of NER. Thus, microirradiation experiments with fluorescently tagged XPG and XPA, which both act downstream of XPC (Figure 3.2 A, right) were performed. These NER factors also showed a specific recruitment to sites of 405 nm induced damage with a maximum accumulation of approximately 1.3 fold (Figure 3.2 E). Recruitment after microirradiation with a 405 nm laser of XPC and XPG were additionally validated in the confocal Leica SP5 II microscope (Figure 3.4). Addition of sensitizers (BrdU or EtBr) also led to an accumulation of XPC when cells were irradiated with a 488 or 561 nm laser although not as strong. Nevertheless, the accumulation of the downstream NER factor XPG was exclusively detected after microirradiation with the 405 nm laser (Table 3.1). Alternatively XPC accumulation can also be found after 488 and 564 nm irradiation when the higher energy levels were applied (17 and 66 mJoule respectively). But again the accumulation of downstream NER factors can not be detected (Figure 3.3 B). This shows that activation of the whole NER pathways is only achieved after microirradiation with the 405 nm laser. An accumulation of XPC without the recruitment of downstream NER factors was also seen by Menoni *et al*. in 2012. They suggested an additional role for XPC and CSB in the repair of oxidative DNA lesions (Menoni et al., 2012). So far studies on NER with microirradiation were mostly done with the help of UVC laser, which requires special lenses and coupling the UVC laser into the microscope. We show here that it is also possible to induce NER using the 405 nm laser for microirradiation, proving that it is possible to study NER with conventional microscopes. However, the activation is very low.

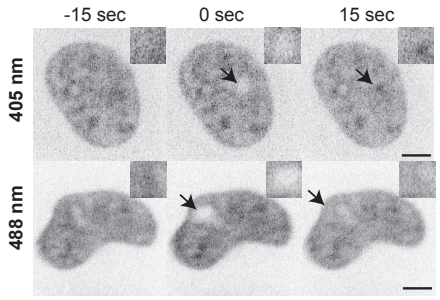

Figure 3.5: Bleaching effect in XPC-GFP expressing cells after microirradiation with a 488 nm laser. Representative confocal mid nuclear sections from XPC-GFP transfected HeLa Kyoto cells microirradiated either with a 405 nm or a 488 nm laser. Arrowheads point to sites of microirradiation, shown enlarged as insets. Scale bar = 5 μm

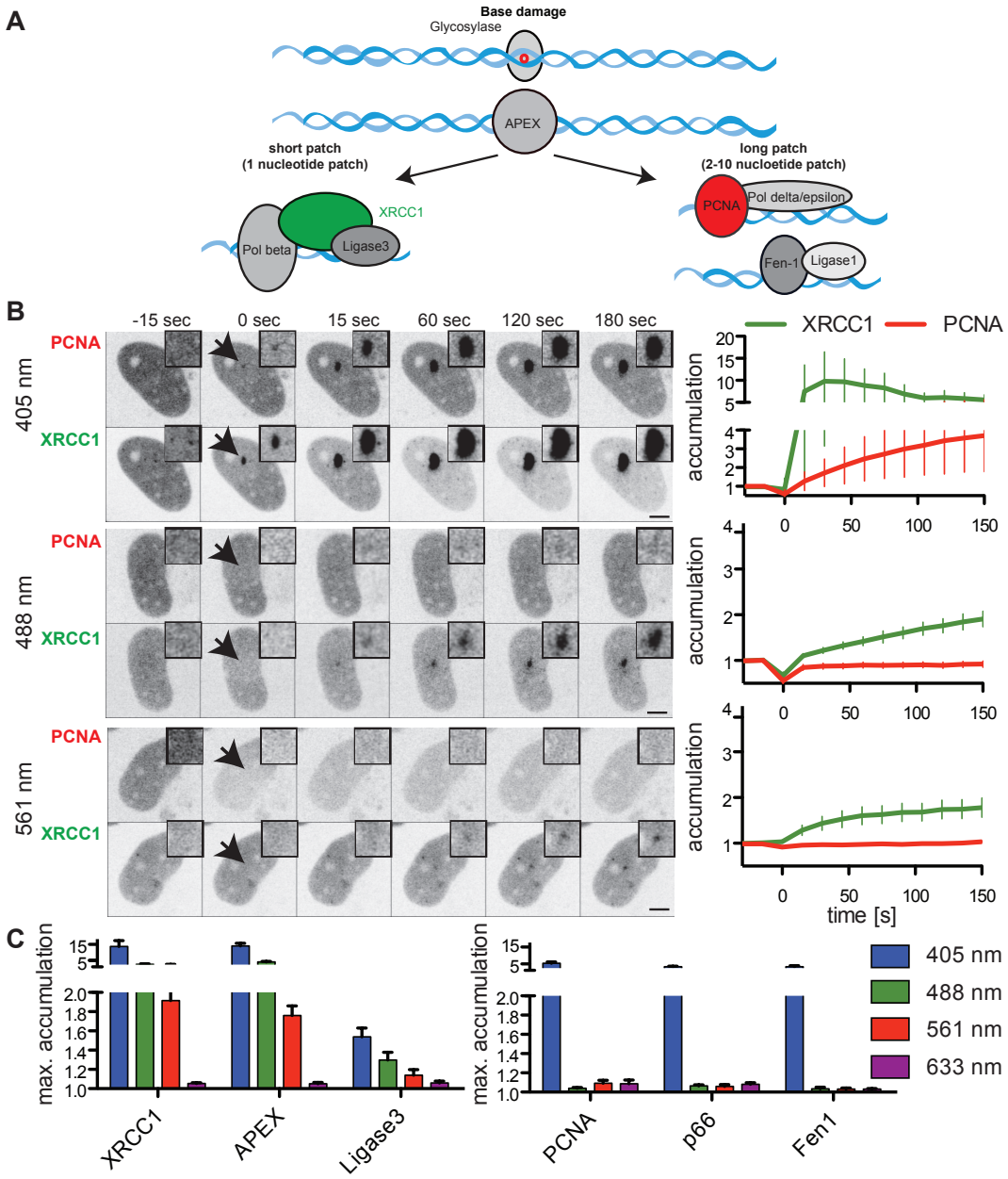

Figure 3.6: Discrimination for short-patch BER. (A) Schematic representation of short- and long-patch BER. **(B)** HeLa cells expressing cherry-PCNA and GFP-XRCC1 were irradiated with the 405, 488 and 561 nm laser. Arrowheads point to the sites of microirradiation, shown enlarged as insets. Plots represent accumulation of repair proteins over time as mean value. **(C)** Bar histograms display calculated mean maximal accumulation for different repair factors as indicated. Whisker represents standard deviation. Scale bar = 5 μm. Only short-patch, but not long-patch, BER proteins accumulate at all three wavelengths (405, 488 and 561 nm)

Discrimination between short-patch and long-patch BER

Since there are no methods available that are sensitive enough to detect small amounts of damaged bases or abasic sites *in situ* and *in vivo*, we could not rule out the possibility that this kinds of damage gets formed after microirradiation. This damage is repaired by base excision repair (BER). BER can be divided into short- and long-patch BER (Figure 3.6 A). During short-patch BER only one nucleotide gets replaced. For this non-processive DNA synthesis reaction XRCC1 serves as a loading platform. Alternatively, in long-patch BER, up to 10 nucleotides are synthesized. In this processive DNA synthesis PCNA is required as a loading platform, as it is in other processive DNA repair pathways e.g. NER.

To distinguish between the different types of BER, we used GFP tagged XRCC1 as a marker for short-patch BER and cherry tagged PCNA as an indicator for long-patch BER. Time laps microscopy revealed a recruitment of both factors after microirradiation with a 405 nm laser, with XRCC1 exhibiting a very strong accumulation (>10 fold). Irradiation with 488 or 561 nm leads to a significant accumulation of XRCC1 and almost no accumulation of PCNA (Figure 3.6 B). Notably, accumulation of XRCC1 is slower after microirradiation with the longer wavelength compared to accumulation after 405 nm laser irradiation. Calculation of the accumulation half-time after microirradiation revealed a prolonged time from approximately 10 seconds for microirradiation with the 405 nm laser and up to 100 seconds for 488 and 561 nm irradiation (Figure 3.7). This might arise from the activation of multiple DNA repair pathways with the 405 nm laser compared to activation of only short-patch BER after microirradiation with longer wavelengths.

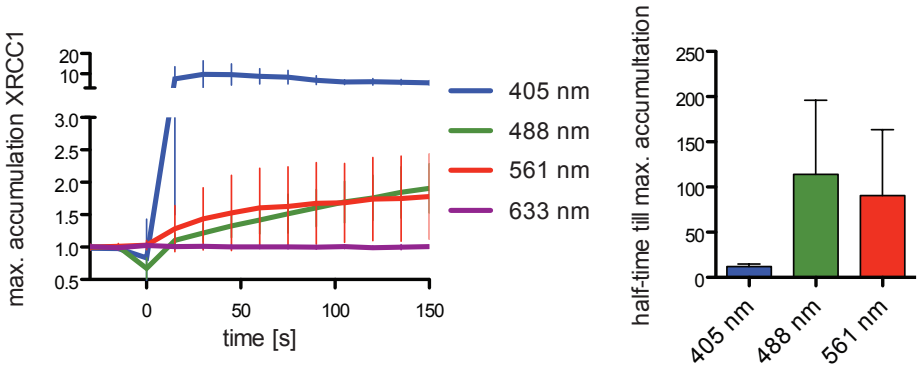

Figure 3.7: Distinct recruitment kinetics of XRCC1 after microirradiation under different conditions. HeLa Kyoto cells expressing GFP-XRCC1 were microirradiated with the 405, 488 or 561 nm laser and accumulation is blotted over time as mean from at least 5 experiments. Half-time was calculated from these curves from time of bleach till maximal accumulation assuming a single exponential accumulation function and mean values are displayed in a bar histogram. Whisker represents standard deviation.

To further validate the selective activation of non-processive short-patch BER without activation of processive long-patch BER after microirradiation with 488 and 561 nm, we also tested other short- and long patch specific BER factors. In line with the observation for XRCC1, fluorescently tagged short-patch BER factors APEX and Ligase 3 get recruited under all three conditions tested. Proteins involved in long-patch BER such as Fen1 and p66 (a subunit of polymerase delta) on the other hand, only get recruited after microirradiation

with a 405 nm laser (Figure 3.6 C). Notably, maximal accumulation of short- and long-patch BER factors after microirradiation with 405 nm lasers is higher than that for DSB repair or NER specific factors. This strengthens the model that the predominant DNA damage produced by low power visible cw lasers arises from absorption by endogenous cellular photosensizers leading mainly to oxidative damage, which are in turn processed by BER.

Irradiation with the 633 nm laser line never led to the recruitment of any tested DNA repair factor, not even in the presence of exogenous sensitizers BrdU or EtBr (Figure 3.6 C, Table 3.1). Sensitization with EtBr, but not BrdU, led to accumulation of PCNA even to sites of 488 or 561 nm laser microirradiation. Nevertheless, this effect cannot be seen for p66, which is another factor in processive DNA synthesis pathways (Table 3.1). Accumulation of PCNA is also detected when microirradiation with 488 or 561 nm was performed using high energies (17 mJoule and 66 mJoule respectively) (Figure 3.3 B).
To confirm these data in another microscope, we microirradiated fluorescently tagged XRCC1, PCNA or p66 expressing cells with the 405, 488 and 561 nm laser at equal energy levels comparable to our initial settings in a confocal laser scanning microscope LeicaSP5 II (point scanner). For XRCC1 we could validate accumulation not only for 405 nm laser induced damage, but also recruitment after 488 and 561 nm laser microirradiation. The processive DNA synthesis related factors PCNA and p66 on the other hand, only accumulate at sites of 405 nm laser induced DNA damage. Also in this system the BER related factors get accumulated at higher levels than factors specific for NER or DSB repair (Figure 3.4).

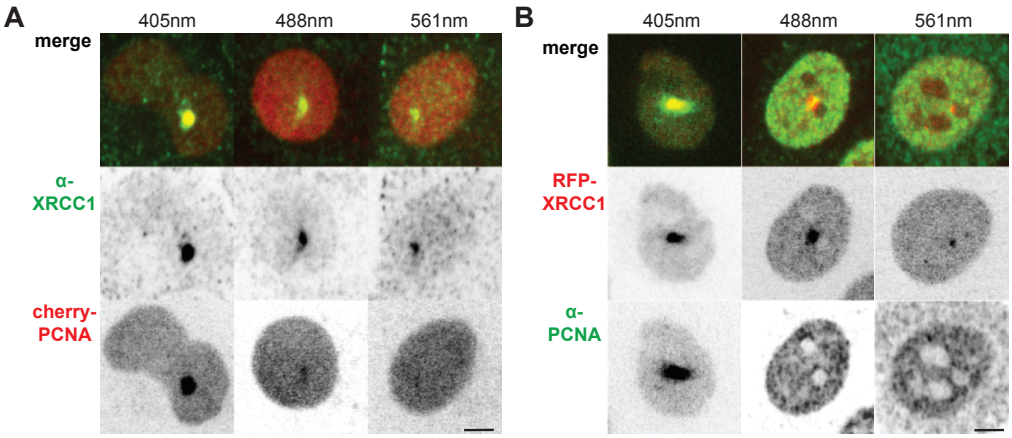

Figure 3.8: Discrimination for short-patch BER with endogenous proteins. HeLa Kyoto cells expressing either cherry-PCNA or RFP-XRCC1 were fixed directly after irradiation and subsequently stained with anti-XRCC1 **(A)** or anti-PCNA **(B)** antibodies as indicated. Scale bar = 5 μm.

To rule out that accumulation only occurs when protein is overexpressed, we tested the accumulation of endogenous XRCC1 and PCNA. After microirradiation cells were directly fixed and stained for the repair factors by indirect immunofluorescence. For direct comparison, antibody staining against XRCC1 was performed in cherry-PCNA transfected cells and PCNA antibody staining in RFP-XRCC1 transfected ones. Microirradiation with a 405 nm laser again showed a strong recruitment of cherry-PCNA to the irradiated site,

whereas irradiation with the two longer wavelengths led to no or not significant accumulation. Immunofluorescence staining for endogenous XRCC1 verified accumulation of this short-patch BER factor to sites of 405, 488 and 561 nm induced damage. Accordingly, in RFP-XRCC1 transfected cells the fusion protein gets recruited after microirradiation with 405, 488 and 561 nm laser, while accumulation of endogenous PCNA is only seen after microirradiation with the 405 nm laser (Figure 3.8).

Taken together we could show that it is possible to induce various types of DNA damage (e.g. DSB and CPDs) with visible light microirradiation. The activation of the corresponding DNA repair pathways NHEJ, HR and NER can be monitored when the 405 nm laser is applied at 1 mJoule. This allows studying these pathways on standard confocal microscopes in the absence of exogenous sensitzers that could potentially result in unwanted side effects. Additionally we could demonstrate that it is possible to discriminate for non-possessive short patch BER over possessive DNA repair pathways with longer wavelength lasers (488 and 564nm) when the energy level is controlled. Moreover, our studies show how important applied energy and wavelength are in a microirradiation setup for induction of DNA damage and repair if quantitative conclusions are drawn.

max. accumulation	without sensitizer			BrdU			EthBr		
Ku70 (DSB repair)	200 ms	800 ms	1200 ms	200 ms	800 ms	1200 ms	200 ms	800 ms	1200 ms
405	1.1	1.1	1.2		1.2	1.3			1.1
488			1.0			1.0			1.1
561			1.1			1.1			1.1
633			1.0			1.1			
Ligase 4 (DSB repair)									
405	1.2	1.3	1.5			1.5	1.1	1.3	1.4
488			1.0			1.1			1.1
561			1.0			1.1			1.2
633			1.0			1.1			1.1
XPC (NER)									
405	1.2	1.4	1.3	3.5		3.0		1.3	2.0
488			1.0			1.2	1.2	1.1	1.3
561		1.1	1.1			1.2			1.7
633	1.0		1.0			1.1			1.1
XPG (NER)									
405			1.2			1.4			1.1
488			1.0			1.0			1.0
561			1.0			1.0			1.1
633			1.0			1.0			1.0
p66 (BER+NER)									
405	1.6	1.5	3.0	1.9	2.3	2.3	1.6	2.1	2.1
488			1.1			1.0			1.1
561			1.1			1.1			1.1
633			1.1			1.0			1.1
PCNA (BER+NER)									
405	2.1	4.2	5.4	5.4	8.1	9.2	2.9	5.2	6.2
488	1.1	1.2	1.1	1.2		1.1	1.1		1.7
561	1.0	1.1	1.1	1.1	1.3	1.1	1.3		2.3
633			1.1			1.0			1.1
XRCC1 (BER)									
405	7.3	12.1	10.6	15.7	7.3	12.8	16.3		10.1
488	1.3	3.3	2.2	3.5	5.9	8.5	2.2		6.1
561	1.2	1.9	1.9	2.6	4.6	3.6	3.8		9.9
633			1.0			1.1			1.1
	< 1	≥ 1.2	> 2						

Table 3.1: Summary of repair factor accumulation at microirradiation sites. Mean maximal accumulation after microirradiation from different fluorescently tagged DNA repair factors from at least 3 experiments. Experiments were performed either with BrdU, EtBr or without any sensitizers. Indicated lasers were used at specified bleaching times. Color-coding illustrates the level of accumulation ranging from red representing no accumulation, over yellow for a mild accumulation of $\geq$ 1.2 and green for a strong accumulation greater or equal $\geq$ 2.

3.2 Processive DNA repair synthesis inside heterochromatin is accompanied by local chromatin decondensation

Britta Muster[1], **Alexander Rapp**[1], **M. Cristina Cardoso**[1]

[1] Cell Biology and Epigenetics, TU Darmstadt, Darmstadt, Germany

Genomic DNA inside eukaryotic cells together with several proteins forms distinct chromatin structures, which lead to an organization and compaction of DNA. The two fundamental chromatin structures are euchromatin and heterochromatin. Euchromatin is considered as more 'open', decondensed, gene rich and transcriptionally active. Heterochromatin on the other hand has the opposite features. It is highly compacted, contains only a few genes and is mostly transcriptionally silent (Tamaru, 2010). Regions that remain condensed throughout the life span of the cell are named constitutive heterochromatin whereas regions that get condensed when genes need to be silenced during development are named facultative heterochromatin. These chromatin types can be distinguished by characteristic histone modifications and variants as well as DNA modifications. Examples for this are methylations of cytosine at CpG sites, which are mostly found in heterochromatic regions (Razin and Cedar, 1977) and the histone variant macroH2A1.2, which is preferentially located at the inactive X chromosome (Costanzi and Pehrson, 1998), the most prominent facultative heterochromatic structure in mammalian females.

It has been shown that induction and repair of DNA damage is affected by the chromatin structure in, which they occur (Goodarzi et al., 2010, Surralles et al., 1998). For instance, ionizing radiation induced double strand breaks (DSBs) occur in lower frequency inside heterochromatic regions (Falk et al., 2008, Obe et al., 2002). It was suggested that radicals induced by radiation react more frequently with the tighter bound chromatin proteins in heterochromatin than in euchromatin and thus prevent the radicals to react with DNA (Davidkova et al., 2006). This would lead to a better protection of DNA in heterochromatin. Highly transcribed euchromatic regions are known to be more fragile due to the DNA being partially single stranded during transcription. Heterochromatin therefore seems to be better protected agains DNA damage induction than euchromatin.

To balance the higher fragility euchromatin on the other hand is preferentially repaired. A transcription coupled repair mechanism (transcription coupled nucleotide excision repair) for UV-induced damage is already known for a long time (Friedberg, 1996, Mullenders et al., 1991) and also DNA DSBs are repaired with faster kinetics in euchromatin, compared to heterochromatin (Falk et al., 2008, Goodarzi et al., 2008). It was hypothesized that heterochromatin may even pose a barrier to DNA repair (Goodarzi et al., 2009) and only after remodeling of the chromatin structure efficient repair is possible. In line with these hypotheses, a local decondensation of heterochromatin following different mechanism of DNA DSB induction was observed (Falk et al., 2007, Jakob et al., 2011, Kruhlak et al., 2006) and a relocation out of heterochromatin was reported for DSBs induced directly inside heterochromatin (Chiolo et al., 2011, Jakob et al., 2011).

So far, all studies on DNA damage induction or repair related to the chromatin structure focused on UV-induced damage or DSBs. This types of damage are repaired either via nucleotide excision repair or the DSB repair pathways non-homologous end joining or homologous recombination. All of them imply processive DNA synthesis.

With the help of our previously established laser microirradiation conditions it is not only possible to in-

flict DNA damage inside specific chromatin regions, but also to discriminate non-processive short-patch base excision repair against processive DNA repair synthesis pathways (see chapter 3.1, Muster et al. in preparation). We used this system to study recruitment of repair factors under both conditions in and outside of euchromatic and heterochromatic structures to answer several questions. First we wanted to know if recruitment kinetics of DNA repair proteins are altered due to different chromatin structures. Second, if heterochromatic decondensation is induced by the damage itself or is mediated by the repair process and third, if DNA repair synthesis is excluded form the inside of heterochromatic regions. Since heterochromatin can be divided further into constitutive and facultative heterochromatin we investigated the dynamics in those chromatin types separately. To distinguish between these two types of heterochromatin in living cells we used fluorescently tagged methyl-CpG binding domain (MBD) proteins to label constitutive heterochromatin in mouse and human cells and fluorescently tagged histone mH2A1.2 in *Microtus cabrera* cells to label the facultative heterochromatic inactive X-Chromosome.

We were the first to show that the local decondensation of heterochromatin only takes place when processive DNA synthesis is induced and that this deconendsation is sufficient to allow processive DNA synthesis repair well within heterochromatic regions.

Materials and Methods

Cell culture and transfection

Human HeLa Kyoto cells (Landry et al., 2013), C2C12 mouse myoblasts (Yaffe and Saxel, 1977) and a permanent fibroblast cell line from *Microtus cabrera* (female) (gift from A. Sanchez group, Universidad de Jaén, Jaén, Spain) were grown at 37 °C 5% CO_2 in DMEM supplemented with either 10% (HeLa and *M. cabrera* fibroblasts) or 20% (C2C12) FCS and 1 μM/ml gentamycin. Stable transfected cherry-PCNA HeLa Kyoto cells were cultivated in the presence of blasticidin (2.5 μg/ml). Cells grown on cover slide dishes or in 8-well chambered coverslip (Sarstedt) were transfected with constructs encoding fluorescence-tagged proteins using polyethylenimin as described elsewhere (Casas-Delucchi et al., 2012). Following constructs were used: cherry-PCNA (Mortusewicz et al., 2011, Sporbert et al., 2005), mRFP-APEX (see chapter 3.1), GFP-MeCP2 (Agarwal et al., 2007, Brero et al., 2005), GFP-MBD1 (Hendrich and Bird, 1998) and GFP-mH2A1.2.

The construct GFP-mH2A1.2 was generated by cloning the corresponding human cDNA into TA cloning vector pCR2.1 (Invitrogen) and subsequently into pEGFP-C1 backbone (Clontech) vector by BglII and XhoI restriction sites. For PCR amplification following primers were used:

mH2A1.2 forward: 5' AAAGATCTACCGCCATGTCGAGCCGC 3'

mH2A1.2 revers: 5' AA AGCGCTGGTTGGCGTCCAGCTTGGC 3'

The construct was verified by sequencing.

Microscopy and microirradiation

Imaging and laser microirradiation experiments were performed using a Leica SP5 II confocal laser-scanning

microscope in a closed live cell microscopy chamber (ACU, Perkin Elmer) at 37 °C with 5% CO_2 and 60% humidity. Images were taken with a HCX PL APO 63x/1.49 NA oil objective. DAPI, GFP, cherry/mRFP and Cy5 were imaged with 405, 488, 561 or 633 nm laser excitation respectively. Live cell two color images were taken simultaneously whereas fixed four colored images were taken in sequential mode to exclude crosstalk. For Laser microirradiation a preselected spot (around 1 μm in diameter) within the nucleus was microirradiated either with a 405 nm or a 488 nm laser resulting in a total energy of 1 or 3 mJoule respectively. Energy output of the lasers was measured with a laser power meter (OPHIR) directly after the objective. Confocal image series of one mid nucleus z section were recorded either at maximal speed for 3 images before and after microirradiation and then in 15 seconds intervals or for the full recovery in 15 seconds intervals. For evaluation of accumulation kinetics images were first corrected for cell movement and mean intensity of the irradiated region was divided by mean intensity of the whole nucleus (both corrected for background) using ImageJ. Maximal accumulation represents the highest ratio from each experiment.

***In situ* heterochromatin decondensation analysis**

Constitutive heterochromatin was visualized by transfecting cells with constructs encoding for GFP-tagged MBD proteins. In mouse C2C12 cells chromocenters were identified as MeCP2 enriched regions and in human HeLa cells constitutive heterochromatin of chromosome 1 was identified as MBD1 enriched regions. The heterochromatic regions were microirradiated with either 1 mJoule of a 405 nm laser or 3 mJoule of a 488 nm laser. For measuring the area of the MBD marked region, images were first cropped to the region of interest, filtered with a Gaussian blur (blur radius 1), thresholded and subsequently the corresponding area was calculated (ImageJ). The area after irradiation was normalized to the area before irradiation and the relative increase in size was measured.

Detection of processive DNA synthesis

Incorporation of BrdU or EdU was taken as a proxy for processive DNA synthesis. To visualize BrdU or EdU incorporation after DNA repair, medium containing 100 μM BrdU or EdU was added to the cells directly before microirradiation. After 1 hour post irradiation incubation time, cells were fixed for 10 minutes with 3.7% formaldehyde and stained for either BrdU or EdU.

For BrdU staining, cells were permeabilized in 0.5% TritonX-100 for 30 minutes and subsequently treated with DNaseI 0.25 μl / 20 μl 1x DNaseI buffer (Sigma Aldrich) for 30 minutes at 37 °C. After blocking for 30 minutes with 2% BSA/PBS at room temperature, the first antibody (rat anti-BrdU clone BU1/75, Gentaur) was diluted 1:100 in 1% BSA/PBS and incubated for 1 hour at room temperature. The secondary antibody (Cy5 coupled anti-rat antibody, Jackson Immuno Research) was diluted 1:200 in 1% BSA/PBS and also incubated for 1 hour at room temperature.

For EdU staining cells were permeabilized in 0.5% TritonX-100 for 20 minutes and ClickIT EDU (Life technologies) solution was added(for 50 μl: 44 μl ClickIT EdU reaction buffer, 2 μl $CuSO_4$, 0.2 μl Alexa Fluor 647, 5 μl ClickITEdU reaction buffer additive). Incubation was done for 45 minutes at room temperature.

DAPI (1 μg/ml, Sigma-Aldrich, Germany) was always used as DNA counterstaining.
Confocal image stacks were taken at a Leica SP5 II confocal laser-scanning microscope as described above. For 3D reconstruction pictures were taken with a voxel size of 56·56·335,7 nm or 40,4·40,4·125,9 nm in C2C12 and HeLa cells respectively. 3D visualization was performed with the UCSF Chimera package. Chimera is developed by the Resource for Biocomputing, Visualization, and Informatics at the University of California, San Francisco (supported by NIGMS P41-GM103311). Intensity analysis over one line (line plot) directly through the heterochromatic region was done on one confocal section after filtering with Gaussian blur (radius 1) using ImageJ.

Results

Recruitment of DNA repair factors after laser microirradiation takes place inside heterochromatic regions

Heterochromatin was suggested to be a barrier for efficient DNA repair (Goodarzi et al., 2009). Nonetheless, Jakob *et al.* could show recruitment of XRCC1 directly inside heterochromatin using ion microbeam irradiation (Jakob et al., 2011). XRCC1 is one of the key proteins from the short-patch base excision repair pathway (BER), which repairs DNA lesions such as base damage by replacing a single nucleotide in a non-processive DNA synthesis manner.
Ion microbeam irradiation produces not only lesions repaired by short-patch BER but also other lesions, for example DSBs (Jakob et al., 2009), resulting in activation of multiple DNA repair pathways. Our previously established laser microirradiation conditions allow not only to target specific regions inside the nucleus but also selective activation of short-patch BER (chapter 3.1, Muster et al. in preparation). We employed this system to investigate recruitment of XRCC1 in and outside of heterochromatic regions related to the induction of specific DNA repair pathways.

Mouse cells harbor large constitutive heterochromatic structures known as chromocenters where pericentric heterochromatin is clustered. Brero *et al.* showed that the fluorescently-tagged MBD family member MeCP2 is located at these structures (Brero et al., 2005) and therefor suitable as a live cell marker for chromocenters. Expression of GFP-tagged MeCP2 in C2C12 mouse myoblasts led to clear visualization of chromocenters (Figure 3.9 A) and enabled direct targeting with the laser beam inside of this constitutive heterochromatic structures. Microirradiation was simultaneously also performed outside of chromocenters to investigate possible differences of XRCC1 recruitment due to chromatin state. We have previously shown that 3 mJoule of 488 nm laser microirradiation results in selective activation of short-patch BER whereas 1 mJoule of 405 nm laser microirradiation of leads to activation of multiple DNA repair pathways (see chapter 3.1, Muster et al. in preparation). Microirradiation with both lasers resulted in accumulation of XRCC1 at irradiated sites with 405 nm laser microirradiation leading to a higher accumulation (Figure 3.9 A). Under both conditions recruitment of XRCC1 could be observed within chromocenters (Figure 3.9 A). Quantification of XRCC1 accumulation revealed an increase in accumulation up to 8 fold after microirradiation with

a 405 nm laser and up to 3.5 fold after microirradiation with 488 nm(Figure 3.9 B + C). Astonishingly, accumulation after the 488 nm laser microirradiation was significantly stronger inside chromocenters than outside (3.5 versus 1.8 fold) (Figure 3.9 B + C).

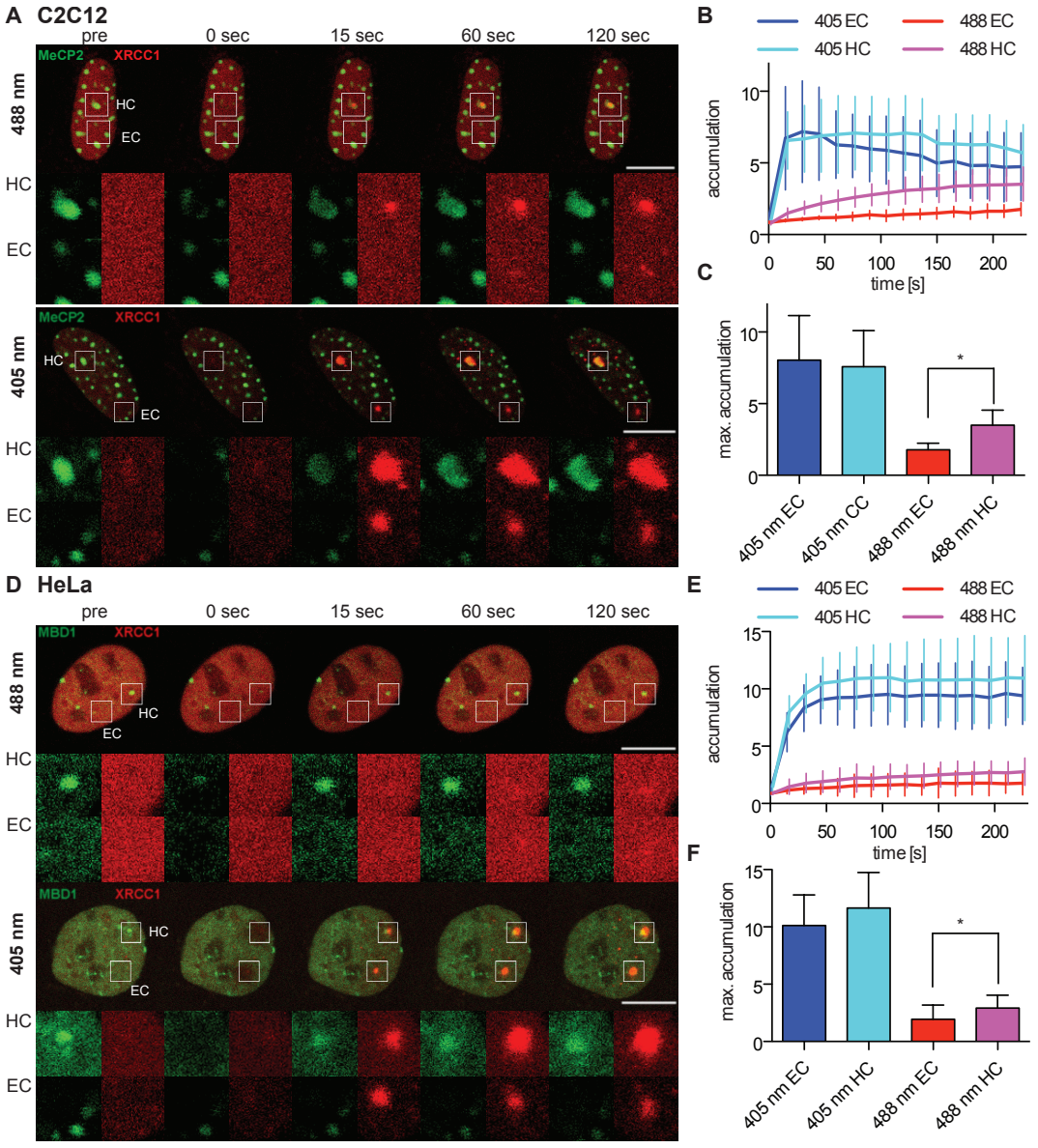

Figure 3.9: XRCC1 gets recruited inside dense constitutive heterochromatic regions in the nuclei of mouse and human cells. Live cell imaging plus 488 or 405 nm laser microirradiation of XRCC1 expressing **(A)** C2C12 or **(C)** HeLa cells. Heterochromatin (HC) was visualized by transfection with GFP-tagged MBD proteins (MeCP2 for chromocenters in C2C12 and MBD1 for pericentric heterochromatin of chromosome 1 in HeLa). Enlarged regions represent sites of irradiation either in heterochromatin (HC) or euchromatin (EC). XRCC1 accumulation in **(B)** C2C12 and **(D)** HeLa over time as mean value and calculation of mean maximal accumulation form these curves. Whisker represents standard deviation. Statistical test was the Mann Whitney test $p < 0.05$ * $n \geq 4$. Scale bar = 10 μm.

To extend our findings to other species, we tested recruitment of XRCC1 in the human cell line HeLa. For visualization of constitutive heterochromatin we used fluorescently-tagged MBD1, another member of the MBD family. MBD1 was shown to be located at constitutive heterochromatin in human cells (Ng et al., 2000) and expression of fluorescently-tagged MBD1 in HeLa cells resulted in an enrichment at pericentric heterochromatin of chromosome 1 (unpublished results by Dr. K. L. Jost), making it a live cell marker for constitutive heterochromatin in HeLa cells. Microirradiation with a 405 or 488 nm laser in- and outside of these heterochromatic regions resulted in accumulation of XRCC1 (Figure 3.9 D) and recruitment directly inside heterochromatin. Quantification showed accumulation up to 11.7 and up to 2.9 fold for 405 and 488 nm microirradiation respectively Figure 3.9 E + F). Similar to C2C12 cells, microirradiation with a 488 nm laser inside heterochromatic regions in Hela cells led to significant stronger accumulation of XRCC1 compared to euchromatic regions (2.9 versus 1.9 fold) (Figure 3.9 E + F).

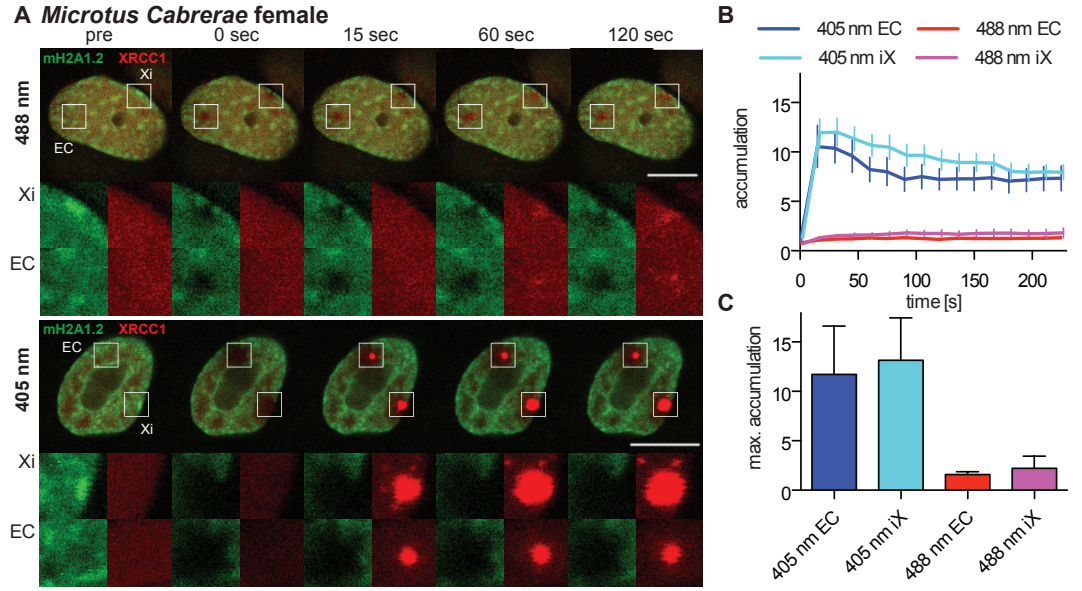

Figure 3.10: Recruitment of XRCC1 inside facultative heterochromatin of inactive X chromosome. (A) Live cell imaging of XRCC1 expressing *Microtus Cabrerae* cells transfected with mH2A1.2 to visualize inactive X. Enlarged regions represent sites of 405 or 488 nm laser microirradiation either in inactive X (Xi) or outside (EC) regions. **(B)** Accumulation of XRCC1 over time as mean value and calculated of mean maximal accumulation from these curves. Whisker represents standard deviation n $\geq$ 8. Scale bar = 10 μm.

To expand our knowledge to other types of heterochromatin, we performed the same kind of experiments in facultative heterochromatic regions. The most prominent facultative heterochromatic structure in mammals is the inactive X (Xi), which is the randomly inactivated X chromosome of female cells. To visualize Xi we made use of a construct coding for a GFP-tagged version of the histone variant macroH2A1.2, which was shown to be expressed in somatic cells and is preferentially concentrate at Xi in female cells (Costanzi and Pehrson, 1998). As a model system we used a *Microtus Cabrerea* fibroblasts cell line, which have enlarged sex chromosomes (known as 'giant sex chromosomes') (Marchal et al., 2003, 2004) and are therefor a very

interesting model system to study the Xi.

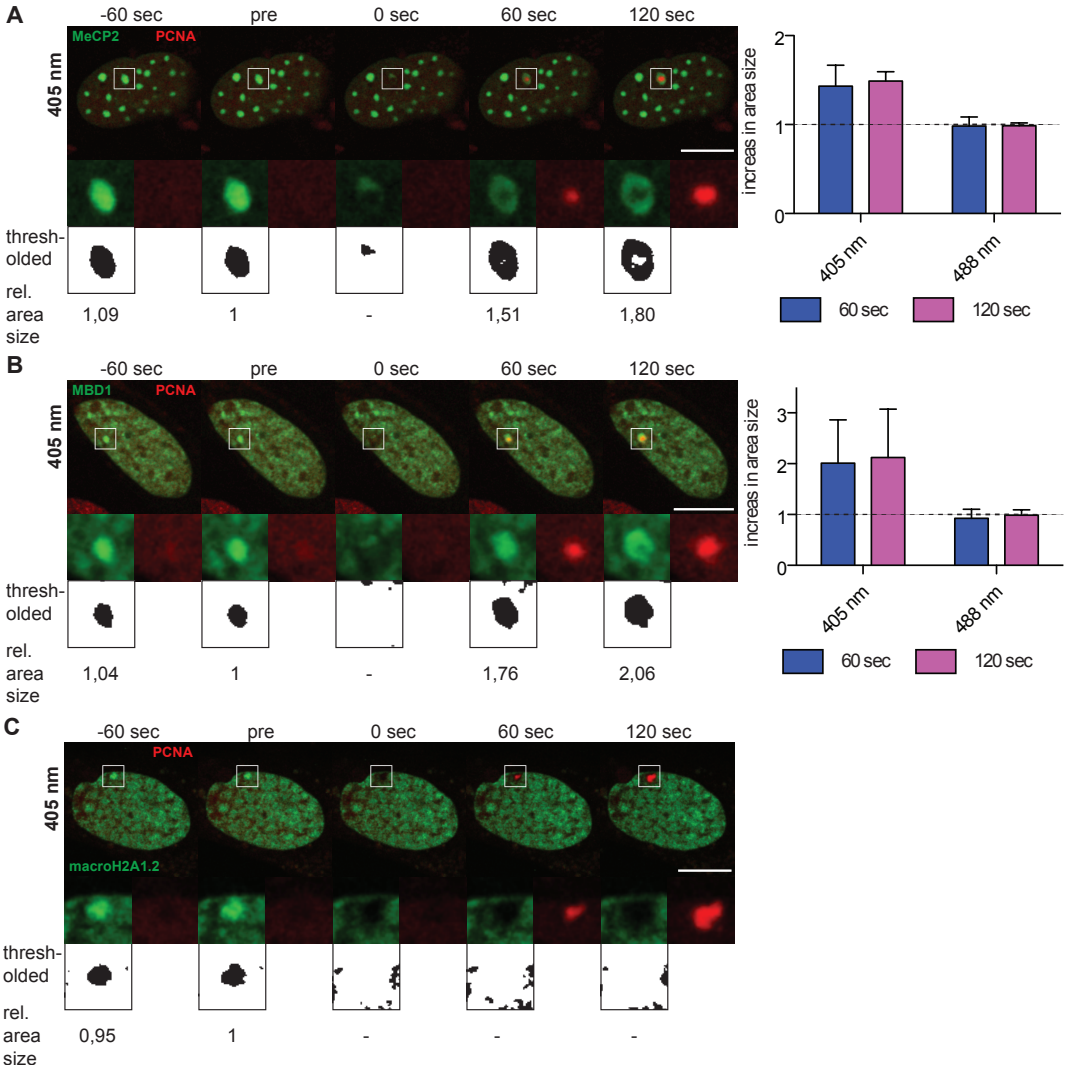

Figure 3.11: Induction of processive DNA synthesis repair leads to decondensation of heterochromatin. Live cell imaging of PCNA expressing **(A)** C2C12, **(B)** HeLa or **(C)** *Microtus Cabrerae* cells. Constitutive heterochromatin was visualized by expressing GFP-tagged MeCP2 and MBD1 in C2C12 and HeLa cells respectively and facultative heterochromatin by GFP-macroH2A1.2 expression in *Microtus Cabrerae* cells. Microirradiation with a 405 nm laser leads to an accumulation of PCNA inside heterochromatin. Enlarged regions represent sites of irradiation. Underneath: thresholded pictures of heterochromatic GFP-tagged markers and area size relative to pre-irradiation image. Evaluation of MeCP2 and MBD1 marked area size 60 seconds and 120 seconds after irradiation normalized to initial size are shown at the right. Whisker represents standard deviation. n $\geq$ 3. Scale bar = 10 μm

GFP-macroH2A1.2 expressing *Microtus Cabrerea* fibroblasts demonstrated a homogenous histone staining with an additional bright stained region located at the nuclear periphery, representing Xi (Figure 3.10 A). Irradiation with either a 405 nm or a 488 nm laser led to persistent bleaching of the histone and accumulation of XRCC1. Maximal accumulation after damage induction with a 405 nm laser reached up to a 13 fold and

with 488 nm up to 2.2 fold increase (Figure 3.10 B + C). Slightly higher accumulation levels were observed after irradiation with 488 inside Xi (1.6 versus 2.2 fold), however these effects are not significant in contrast to those in constitutive heterochromatin.

Local heterochromatin decondensation after induction of processive DNA synthesis repair

Recruitment of XRCC1 directly inside heterochromatic regions shows activation of short-patch BER, which repairs DNA via a non-processive DNA synthesis. To verify activation of processive DNA repair synthesis inside heterochromatin we investigated recruitment of proliferating cell nuclear antigen (PCNA) to sites of laser microirradiation. PCNA is the processivity factor during DNA synthesis. Activation of several DNA repair pathways, including nucleotide excision repair and DSB repair, which imply processive DNA synthesis, were previously shown after 405 nm laser microirradiation (chapter 3.1, Muster et al. in preparation).

We found PCNA recruitment after 405 nm laser microirradiation directly inside constitutive and facultative heterochromatic regions (Figure 3.11). This accumulation was accompanied by a local decondensation of constitutive heterochromatin in C2C12 and HeLa cells (Figure 3.11 A+B) after induction of DSB repair as previously shown by others (Jakob et al., 2011, Kruhlak et al., 2006). A decondensation effect of facultative heterochromatin in *Microtus Cabrerae* cells was not detectable due to a persistent photobleaching effect of the GFP-tagged histone macroH2A1.2 (Figure 3.11 C).

Falk *et al.* proposed that the local decondensation effect is necessary to complete repair by enabling larger repair proteins to access the damaged DNA (Falk et al., 2014). However, we observed no such obvious decondensation effect after irradiation with a 488 nm laser but induction of non-processive short-patch BER. To evaluate whether only processive DNA synthesis repair requires local decondensation or if decondensation can also be measured after induction of exclusive non-processive DNA repair synthesis, we quantified the area of heterochromatin before and after 405 nm and 488 nm laser microirradiation. 405 nm laser microirradiation led to 1.5 and 2 fold area size increase already 60 seconds after damage induction in C2C12 and HeLa cells respectively and we observed no further decondensation effect after 120 seconds post irradiation. On the other hand, 488 nm laser microirradiation did not lead to an increase in area size, neither at 60 seconds nor 120 seconds post irradiation (Figure 3.11 A+B right).

DNA synthesis takes place inside heterochromatic regions

The accumulation of PCNA led to the question whether processive DNA synthesis might take place directly inside heterochromatin. We detected DNA synthesis by incorporation of modified thymidine analogs (BrdU or EdU) as shown in a schematic overview in Figure 3.12 A. Thymidine analogs were added directly to the cells before 405 nm laser microirradiation to detect repair related DNA synthesis after damage induction in non S-Phase cells. To allow synthesis to occur, we incubated the cells for one hour before fixation and subsequently stained against BrdU or EdU. 3D reconstruction of the cells and line plots through one confocal plane revealed PCNA and BrdU positive signals well within heterochromatin (Figure 3.12 C+D). As a

secondary control EdU incorporation was measured (Figure 3.12 E).

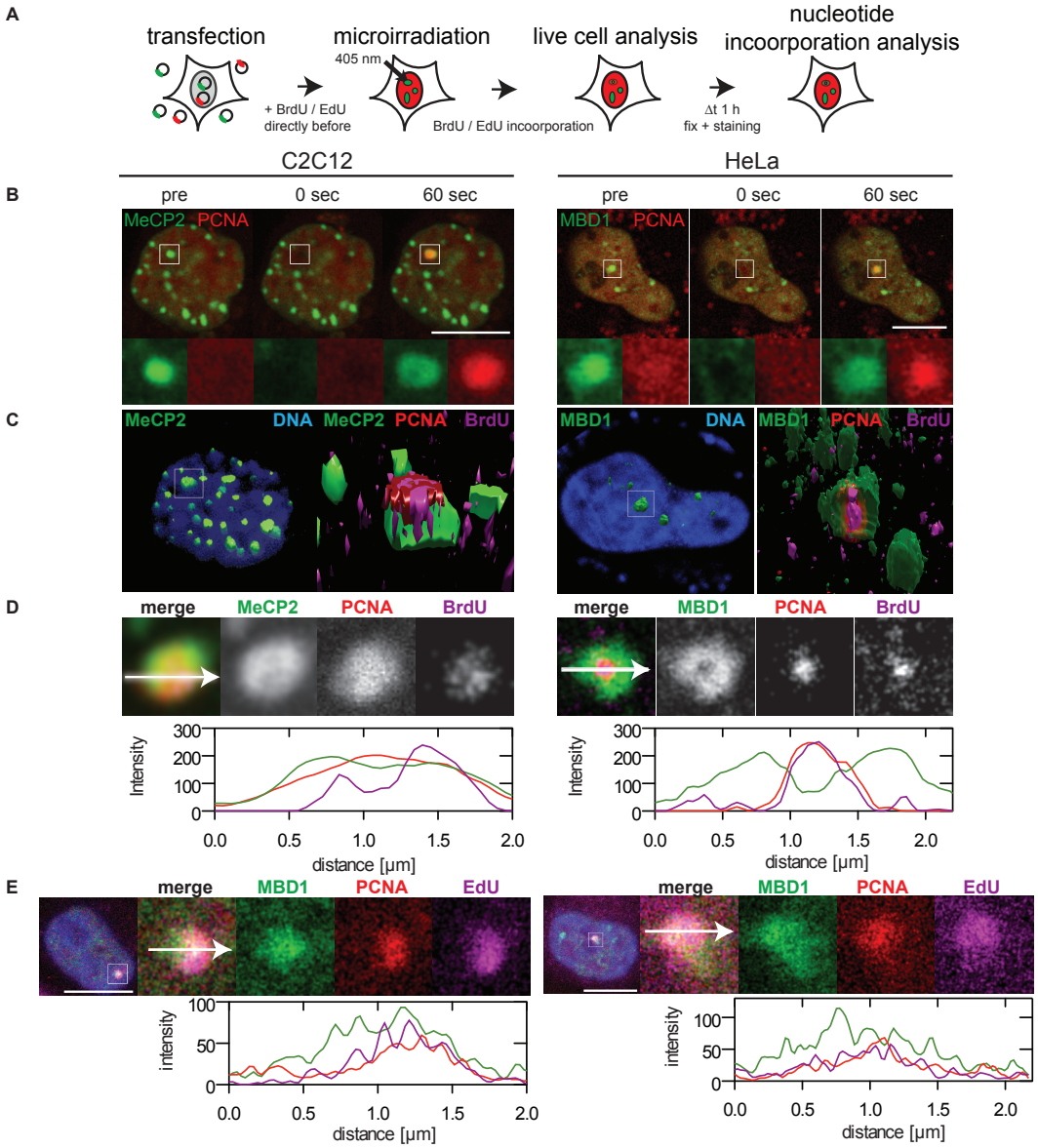

Figure 3.12: Processive DNA synthesis repair takes place inside dense heterochromatic regions. (A) Schematic overview of experimental design. **(B)** – **(D)** Experimental data of C2C12 (left side) and HeLa (right side) cells incubated with BrdU. **(B)** Live cell imaging and 405 nm laser microirradiation of PCNA and GFP-tagged MBD proteins (MeCP2 for C2C12 and MBD1 for HeLa) expressing cells. Enlarged regions represent sites of irradiation. **(C)** 3D reconstruction of irradiated cells. Left: heterochromatic regions and DNA counterstain with DAPI; box represents site of irradiation. Right: enlarged region of irradiated site; heterochromatic regions display PCNA and BrdU signals inside. **(D)** Image of one confocal plane from irradiated heterochromatic region and line plot directly through the center and **(E)** same experiment in HeLa cells incubated with EdU. Scale bar = 10 μm

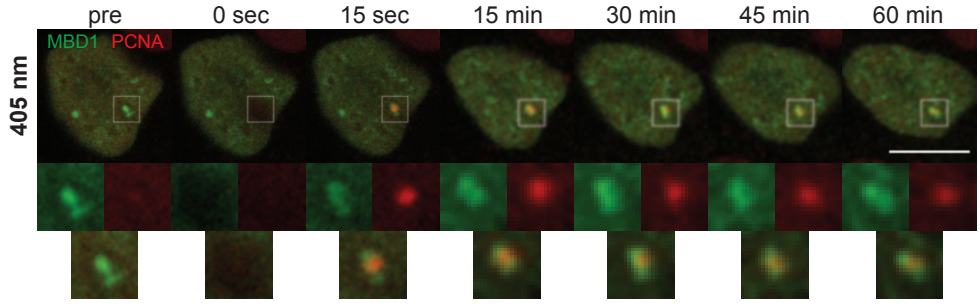

Figure 3.13: Persistent PCNA signal inside heterochromatin. 405 nm microirradiation inside heterochromatin of cherry-PCNA and GFP-MBD1 expressing HeLa cells. Images were taken for over 1 hour. Enlarged regions represent sites of irradiation. Scale bar = 10 μm

Heterochromatic DSBs were reported to relocate to the periphery of the heterochromatic domain for repair (Chiolo et al., 2011, Jakob et al., 2011), but we could measure DNA synthesis at DSBs directly inside heterochromatic regions after microirradiation with a 405 nm laser. To rule out the possibility that we missed the relocation step during the one hour incubation time, we followed PCNA accumulation inside heterochromatin over a longer time-period. Live cell observations after 405 nm laser microirradiation showed a persistent accumulation of PCNA inside heterochromatin up to 60 minutes without a relocation to the periphery (Figure 3.13). This suggests that processive DNA synthesis takes place inside heterochromatic regions.

Discussion

DNA damage induction was suggested to be dependent on the chromatin type in, which it occurs (Falk et al., 2008, Obe et al., 2002). So far most studies focused on DNA doubles strand breaks (DSBs) but with the differential laser microirradiation setup established in chapter 3.1 we can not only study repair of DSBs but also exclusive repair of lesions that activate the non-processive DNA repair pathway short-patch BER.
We found fast recruitment of DNA repair factors in- and outside of heterochromatin independently of the induced damage. Accumulation of the short-patch repair protein XRCC1 after selective activation of this pathway was significantly higher in constitutive heterochromatin than in euchromatin. The reason for elevated XRCC1 accumulation in heterochromatin might simply be due to denser compaction of DNA and therefore more potential targets for the laser beam. This proves for the first time, that not only DSBs, but also lesions, which activate short-patch BER, such as base damage and single strand breaks, are induced directly inside dense heterochromatic regions.

Heterochromatin was proposed to be a barrier to DNA repair (Goodarzi et al., 2009) and it was suggested that a local decondensation is necessary for an efficient repair process (Ziv et al., 2006). We found local decondensation of heterochromatin after 405 nm laser microirradiation, which induced, among other damage, DSBs. This is in line with several other studies, which showed a local decondensation effect after induction

of DSBs inside heterochromatin (Jakob et al., 2011, Kruhlak et al., 2006). Local decondensation could be a passive process by the breaks themselves relieving some torsional energy of the DNA packing (Kruhlak et al., 2006). However, Kruhlak *et al.* already dismissed this hypothesis by showing that the DSB-induced decondensation is ATP dependent (Kruhlak et al., 2006) and Ziv *et al.* could further show the ATM-dependency of this process (Ziv et al., 2006). ATM is a protein kinase and the primary transducer in DSB signaling (Shiloh, 2006), suggesting that the decondensation is dependent on DSB repair. Supporting this theory, exclusive induction of short-patch BER with a 488 nm laser did not lead to a decondensation effect of heterochromatin, demonstrating not only that BER repaired lesions have no effect on large scale chromatin organization, but also accessibility of DNA repair factors is not blocked by heterochromatin. The decondensation effect after induction of DSBs is therefore not necessary to allow DNA repair factors to access the break, but to facilitate later, chromatin confirmation dependent steps. This could enable homology search during homologous recombination or help to prevent miss-rejoining or false recombination in non-homologous end joining and homologous recombination. BER is less related to chromatin confirmation and thus available inside dense heterochromatic structures.

A relocation of DSBs out of heterochromatic regions to complete repair was just recently reported (Chiolo et al., 2011, Jakob et al., 2011). Chiolo *et al.* could show that after ionizing radiation *Drosophila* cells repair heterochromatic DSBs by homologous recombination (HR). While early HR proteins get recruited inside heterochromatic structures, proteins that mediate strand invasion only accumulate at DSBs after relocation out of heterochromatin (Chiolo et al., 2011). Jakob *et al.* could show similar kinetics in mammalian cells using ion microbeam irradiation. Although DNA repair proteins get recruited inside heterochromatin, in 30% of the irradiated cells the DSB gets relocated to the periphery of heterochromatic regions within 20 minutes (Jakob et al., 2011).

We did not observed this relocation step, on the contrary, under our conditions DNA synthesis took place within the volume of heterochromatin. The reason for this might be differences in induced DNA damage quality, which have been proposed to influence DNA repair (Asaithamby et al., 2008, Goodarzi et al., 2010, 2008, Goodhead, 1994, Psonka-Antonczyk et al., 2009, Shibata et al., 2011).

One of the most important endogenous DNA damaging sources are reactive oxygen species (ROS) generated during cell metabolism. ROS evoke oxidative base or sugar damage and single-strand breaks (Lindahl, 1993) that can lead to the formation of DSBs (Greinert et al., 2012, Povirk et al., 1977). These DSBs often feature non-ligatable ends due to association of base or sugar damage but rarely arise in close vicinity to each other. Ionizing radiation or ion microbeam on the other hand results in formation of multiple DSBs in close vicinity, thus representing another quality of DNA damage (Asaithamby et al., 2008, Nikjoo et al., 2001, Psonka-Antonczyk et al., 2009). The DSBs evoked by 405 nm laser microirradiation are more similar to endogenous DSBs since they also resemble oxidative induced DSBs as discussed in chapter 3.1 and arise rarer in close vicinity to each other than ionizing radiation or ion microbeam induced ones. The relocation step seen for ionizing radiation or ion microbeam induced DSBs could therefore be only necessary when

multiple DSBs arise in close vicinity. This could help to avoid illegitimate joining of free ends from different DNA DSBs (Sachs et al., 1997) and, in case of homologous recombination, avoid incorrect recombination of repetitive sequences as proposed by Chiolo *et al.* (Chiolo et al., 2011). Whether relocation plays a role for physiological arising DNA damage has yet to be determined.

In conclusion, our studies showed that damage induction and repair takes place inside heterochromatin not only in the case of DSBs but also for other DNA lesions. Non-processive DNA synthesis repair does not induce visible chromatin changes whereas processive DNA synthesis is accompanied by a decondensation of the surrounding heterochromatin, as we proved by damage induction using our differentiated laser microirradiation setup. Furthermore, we could show that this processive DNA synthesis takes place well within heterochromatin without relocation to the periphery of the heterochromatic domain.

3.3 Altered dynamics of RNase H2 at replication and repair sites in Aicardi-Goutières syndrome

Britta Muster[1], **Henry Herce**[2], **Barbara Kind**[3], **Min Ae Lee-Kirsch**[2], **Alexander Rapp**[1], **M. Cristina Cardoso**[1]

[1] Cell Biology and Epigenetics, TU Darmstadt, Darmstadt, Germany

[2] Department of Physics, Applied Physics and Astronomy, Rensselaer Polytechnic Institute; New York 12180-3590, USA

[3] Department of Pediatrics, Technische Universität Dresden, 01307 Dresden, Germany

Ribonucleases H (RNase H) was first isolated from calf thymus and described in Peter Hausen's laboratory (Hausen and Stein, 1970). It has the ability to degrade RNA in RNA/DNA hybrids. Such hybrids can be formed during a variety of different cellular processes, including DNA replication (Machida et al., 1977) and transcription (Huertas and Aguilera, 2003, Li and Manley, 2006).

There are two main types of RNase H, and at least one of them is present in most organisms. In eukaryotes they are named RNase H1 and RNase H2.

RNase H1 is a monomeric protein. Its mRNA bears two in-frame methionines at the 5' end that give rise to either an isoform with or without a mitochondrial targeting sequence. It was shown that the mitochondrial RNase H1 population is essential for mitochondrial DNA replication (Cerritelli et al., 2003). Nevertheless, the role of the nuclear RNase H1 population is unknown so far (Cerritelli and Crouch, 2009). RNase H2 exhibits the major RNase H activity in eukaryotes. Unlike RNase H1, which requires a substrate with at least four successive ribonucleotides (Cerritelli and Crouch, 2009), RNase H2 can recognize and release single ribonucleotides embedded in a DNA duplex (Eder et al., 1993).

RNase H2 is a heterotrimeric complex consisting of the catalytic RNase H2A subunit with a metal binding DEDD motif (D24, E35, D141, D169) and two auxiliary subunits RNase H2B and RNase H2C (Crow et al., 2006, Figiel et al., 2011, Rychlik et al., 2010, Shaban et al., 2010). The three subunits of the complex are arranged in a line, with the C subunit located in the middle and the B and A subunits on its sides (Figure 3.15 A) (Figiel et al., 2011). All three subunits are required for enzymatic activity (Figiel et al., 2011, Jeong et al., 2004). Although the exact functions of the B and C subunits are not fully understood, they may be involved in interactions with other proteins (Chon et al., 2009). In line with this theory, the RNase H2B subunit harbors a PIP-Box motif at its C-terminus, which mediates its interaction with proliferating cell nuclear antigen (PCNA) (Chon et al., 2009). Bubeck *et al.* showed that RNase H2 binds via this PIP-box domain to replication sites during S-Phase (Bubeck et al., 2011).

Several functions were proposed for RNase H2, including a role in Okazaki fragment maturation and the removal of misincorporated ribonucleotides during replication. Recent models suggest fragment maturation as an unlikely primary function of RNase H2 since those models show Fen1 and/or Dna2 are responsible for RNA primer removal from Okazaki fragments and do not require any participation of RNase H (Burgers, 2009, Rossi et al., 2006). The removal of misincorporated ribonucleotieds was already postulated by Eder *et al.* in 1993. They described a role for RNase H2 in an excision-repair pathway for the removal of ribose residues misincorporated into DNA and pointed out that the vast excess of ribotriphosphates compared to deoxyribotriphosphates (100- to 1000-fold) present within cells enhances the probability that such errors occur (Eder et al., 1993). Recently it was shown that replicative DNA-polymerases indeed incorporate RNA into genomic DNA in a relatively high frequency (every few thousand base pairs) (McElhinny et al., 2010) and that ribonucleotides are the most frequent alteration in genomic DNA (one in approximately 7000 base pairs) of replicating cells (Reijns et al., 2012).

The DNA repair pathway handling these misincorporated ribonucleotides was named ribonucleotide excision repair (RER). The first complete reconstitution *in vitro* from this excision repair pathway suggests that after a first cleavage by RNase H2, strand displacement synthesis takes place via Pol δ/ϵ followed by flap cutting via FEN/Exo1, both in a PCNA-dependent manner (Sparks et al., 2012). This repair pathway is absolutely dependent on RNase H2, since RNase H1 can not compensate for RNase H2 deficiency (Sparks et al., 2012). The consequence of unrepaired ribonucleotides inside genomic DNA are a DNA backbone more susceptible to strand cleavage and hence it was shown that RNase H2 plays a crucial role in the maintenance of genomic stability (Hiller et al., 2012, McElhinny et al., 2010, Reijns et al., 2012). The importance of RNase H2 is further underlined by the fact that RNase H2 knock-out mice die during early development. They show reduced cellular proliferation during gastrulation, elevated DNA damage and a p53-dependent DNA-damage response and, implicating RNase H2 having a role in processing misincoporated ribonculeotides, they accumulate large numbers of single (or di-) ribonucleotides embedded in their genomic DNA (Reijns et al., 2012).

In humans, mutations in any of the three subunits cause the disorder Aicardi-Goutières syndrome (AGS) (Crow et al., 2006). AGS is a rare autosomal recessive disorder first described and subsequently named after Aicardi and Goutière in 1984 (Lee-Kirsch et al., 2013). It is characterized as an inflammatory encephalopathy that clinically mimics *in utero* acquired viral infection, including elevated interferon-α levels in the cerebrospinal fluid, despite the absence of any detectable viral infection. Affected infants exhibit a progressive disorder of the central nervous system with bilateral spasticity and dystonia, acquired microcephaly, and a rapid course toward profound deterioration and death (Aicardi and Goutieres, 1984). It has been proposed that AGS is an autoimmune-like disorder that results from problems with nucleic acids metabolism (Crow et al., 2006). Mutations in at least three other genes encoding for enzymes involved in the metabolism of nucleic acids can as well cause AGS, supporting this theory (Lee-Kirsch et al., 2013). However, the majority of all known AGS cases are attributed to mutations in one of the three RNase H2 subunits (Rice et al., 2007).

To reveal the impact of AGS related mutations on enzyme activity, extensive *in vitro* studies were performed (Chon et al., 2009, Coffin et al., 2011, Crow et al., 2006, Figiel et al., 2011, Perrino et al., 2009, Reijns et al., 2011, Shaban et al., 2010). The G37S substitution in the RNase H2A subunit, which is in close proximity to the catalytic domain (Coffin et al., 2011), showed a 30-fold lower catalytic activity using single ribonucleotide substrate relative to the wild type RNase H2 (Shaban et al., 2010). Nevertheless the reduction of enzymatic activity is apparently not the only determinant of RNase H2 function. Most mutations showed no effect on enzyme activity, including the A177T substitution in the RNase H2B subunit, which is the most common amino acid substitution in AGS patients (Chon et al., 2009, Coffin et al., 2011, Crow et al., 2006, Figiel et al., 2011, Perrino et al., 2009, Reijns et al., 2011, Shaban et al., 2010). Reijns *et al.* could show *in vitro* that some of the mutations lead to a significant destabilization of the RNase H2 complex as measured by a reduction in thermal stability of recombinant RNase H2 (Reijns et al., 2011). Therefor it is likely that not only substrate binding/hydrolysis, but also complex formation/stability and interactions with other pro-

teins could play a role in total RNase H2 activity (Perrino et al., 2009, Shaban et al., 2010). However, these effects do not necessarily have a direct *in vivo* correlation.

Our aim was therefor to examine the effects of AGS related mutations *in vivo* on newly synthesized DNA. Using living human cells, we investigate the binding and mobility of the different RNase H2 subunits during DNA replication and repair and furthermore elucidate the effects of AGS related mutations on these features to gain more insight in the pathogenic processes underlying AGS.

Materials and Methods

Cell culture and transfection

HeLa cells stably expressing cherry-PCNA (Rottach et al., 2008) or wild type HeLa cells were grown at 37 °C 5% CO_2 in DMEM supplemented with 10% FCS, 1 μM/ml gentamycin and, in case of stable transfection, blasticidin (2.5 μg/1ml). Cells grown on cover slides were transfected as described elsewhere (Casas-Delucchi et al., 2012). Constructs coding for following RNaseH2 subunits were used: N-terminally fluroesecently-tagged (eGFP or mCherry or CFP) and untagged either wild type subunits of RNaseH2 (A_wt, B_wt, C_wt), or with mutations identified in AGS patients (A_G37S, B_A177T, C_D39Y, C_R69W, C_D115fs) and one artificial PIP-box mutation in subunit B (Bubeck et al., 2011) (B_ΔPIP). All plasmids coding for RNase H2 subunits are a kindly gift from Prof. Dr. med. Min Ae Lee-Kirsch (Department of Pediatrics, Technische Universität Dresden, Germany). For experiments all three subunits were always cotransfected (one fluorescently-tagged together with its corresponding untagged RNase H2 subunits). RFP-XRCC1 (see chapter 3.1), cherry-PCNA (Rottach et al., 2008) and CFP-PCNA were used as positive control for DNA damage induction after microirradiation and/or, in case of PCNA, to visualize DNA replication forks.

Live cell microscopy, microirradiation and photobleaching experiments

Live cell imaging, microirradiation and photobleaching experiments were performed using an UltraVIEW VoX spinning disc confocal system (PerkinElmer) in a closed live cell microscopy chamber (ACU, Perkin Elmer) at 37 °C with 5% CO_2 and 60% humidity, mounted on a Nikon TI microscope (Nikon). Images were taken with CFI Apochromat 60x/1.49 NA oil immersion objective. CFP, GFP and cherry were imaged with 405 nm, 488 nm and 561 nm laser excitation and 445 $\pm$ 60 nm, 527 $\pm$ 55 nm and 612 $\pm$ 70 nm (full width at half Maximum) emission filters, respectively.

For microirradiation, a preselected spot within the nucleus was microirradiated for 1.2 seconds either with a 405 nm, 488 nm or 561 nm laser set to 100% corresponding to 1, 3 or 8 mJoule respectively. Before and after microirradiation, confocal image series of a mid nuclear section were recorded. For evaluation of the accumulation kinetics, the mean intensity of the irradiated region was divided by the mean intensity of the whole nucleus (both corrected for background) using ImageJ software. One phase association equation (single exponential function: $Y = Y_0 + (Plateau - Y_0) \cdot (1 - e^{(-K \cdot x)})$ was used to calculate the plateau level

of the accumulation curves using Prism 5 (GraphPad Software, Inc.).

For FRAP analysis spots of previously microirradiated sites were bleached using a circular ROI (approximatly 1.5 μm diameter) at 600 ms with a 488 nm or 561 nm laser set to 100% resulting in 1.5 and 4 mJoule respectively. Identical bleach regions were selected at sites of DNA replication or repair and in the nucleoplasm (control). Before and after photobleaching, confocal image series of mid nuclear sections were recorded at 200 mseconds time intervals (5 seconds pre- and 30 seconds postbleach). Double normalization (normalized to value of bleach point at time of bleach and to bleaching of the sample) was done in ImageJ as previously described (Phair et al., 2004, Sprague and McNally, 2005) and half-times were calculated from these curves with one phase association equation (single exponential function: $Y = Y_0 + (Plateau - Y_0) \cdot (1 - e^{(-K \cdot x)})$ using Prism 5 (GraphPad Software, Inc.).

For colocalisation analysis one confocal plane of living cells was imaged using constant settings (488 nm: 30% laser power, 500 ms exposure; 561nm: 30% laser power, 400 ms exposure time). Spatially resolved colocalisation was calculated using the Hcoeff as previously described (Herce et al., 2013).

Alkaline Comet-assay

Alkaline Comet-assay was performed according to Singh and Tice (Singh et al., 1988, Tice et al., 2000) and is described in detail elsewhere (Rapp et al., 2000).

HeLa cells were transfected either with wild type or PIP-box mutated RNase H2B and harvested 48 hours later. Rough microcope-slides (Dakin Slide, Electron Microscopy Sciences) were coated with a first thin layer of 0.5 % Agarose Type 2 (Sigma) in PBS (around 50 μl per slide) and dried. The middle layer of 1 % Agarose Type 2 (Sigma) in PBS (400 μl per slide) was flattened with a coverslip until the agarose turned solid. $5 \cdot 10^5$ cells in 150 μl PBS were mixed with 600 μl 1 % Agarose Type VII (Simga). 100 μl of this suspension was put as final layer on the coverslide, flattened with a coverslip and transferred immediately to a cold plate for gelling. After the agarose was cooled down, the coverslips were removed and slides were immersed in lysis buffer containing 2.5 M NaCl, 0.1 M EDTA, 10 mM Tris and 1 % Triton X-100, pH 10 over night at 4 °C. Following a 20 min washing step with alkaline buffer (0.3 M NaOH, 1mM Na_2EDTA, pH 13), electrophoresis was performed in fresh alkaline buffer for 35 min and 1 V/cm. After neutralization in 0.5 M Tris pH 7.5, DNA was stained with propidiumiodid (500 nM) and images were taken using a fluorescence microscope (Axiovert 200, Zeiss, Germany) with a 20x Plan-Neofluar 0.5 NA air objective and a AxioCam mRM camera. Quantitative comet analysis of at least 100 images was performed using Komet 4.0 (Kinetic Imaging).

Statistical analysis

Data where analyzed with Mann-Whitney U-test using GraphPad Prism. P-values of $P < 0.05$ were considered significant.

RNase H2 binds exclusively to sites of processive DNA synthesis

RNase H2 facilitates the removal of ribonucleotides misincorporated during DNA replication by a ribonucleotide excision repair mechanism (Clausen et al., 2013, Sparks et al., 2012). This misincorporation of ribonucleotides could in principle occur during any kind of DNA synthesis. Thus one would expect RNase H2 dependent nucleotide repair not only after DNA replication, but also after processive, PCNA-dependent DNA repair.

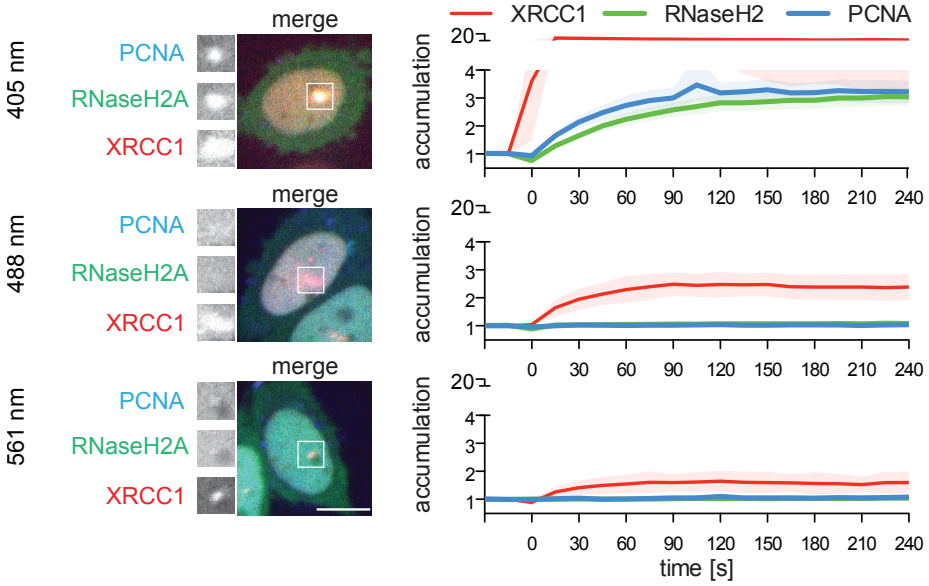

Figure 3.14: Recruitment of RNase H2 to sites of DNA damage. Live cell imaging of HeLa Kyoto cells overexpressing all three RNase H2 subunits with the indicated one GFP-tagged, PCNA CFP-tagged and XRCC1 RFP-tagged. Microirradiation was done with 405, 488 or 561 nm laser as indicated. Pictures were taken every 15 seconds for 240 seconds after microirradiation. Representative images show cells 240 seconds after microirradiation. Boxes show magnification of the microirradiation sites. Quantitative evaluation of the accumulation is shown at the right. Scale bar = 10 μm. n $\geq$ 14, color shaded areas represent SD.

To test this hypothesis we made use of the laser micorirradiation conditions established in chapter 3.1. Under these settings, microirradiation with a 405 nm laser inflicts DNA damage that leads to processive DNA repair whereas microirradiation with 488 or 561 nm only led to the activation of non-processive short-patch base excision repair. To analyze under, which conditions RNase H2 gets recruited, we cotransfected HeLa Kyoto cells with all three RNaseH2 subunits, PCNA and the base excision repair protein XRCC1. To follow recruitment after microirradiation of all three proteins simultaneously, subunit A of RNase H2 was GFP labeled, PCNA with CFP and XRCC1 with mRFP. All three tagged proteins accumulated at the irradiated spot after microirradiation with 405 nm. XRCC1 reached an increase in mean intensity at the irradiated spot compared to the whole nucleus of 20 fold. RNase H2A and PCNA both reached accumulation levels of approximately 3. Microirradiation with a 488 and 561 nm laser only led to a recruitment of XRCC1 without

an accumulation of either PCNA nor RNase H2A (Figure 3.14).

Altered binding of AGS mutants to sites of DNA repair

Since microirradiation with the 405 nm laser led to an accumulation of wild type RNase H2A, we aimed to study the kinetics of the other wild type subunits under these conditions. Furthermore, we wanted to investigate the influences of AGS related mutations on accumulation at sites of processive DNA repair. For this we made use of GFP-tagged constructs of wild type and mutated subunits.

We choose 5 mutations in the different subunits, which were already reported to be present in AGS patients (Ramantani et al., 2010, Rice et al., 2007). Four of them lead to an amino acid alteration (A_G37S, B_A177T, C_D39Y, C_R69W) and one leads to a truncated form of subunit C (C_D155fs). Additonally, we tested one artificial PIP-box mutation in subunit B (_ΔPIP) (Figure 3.15).

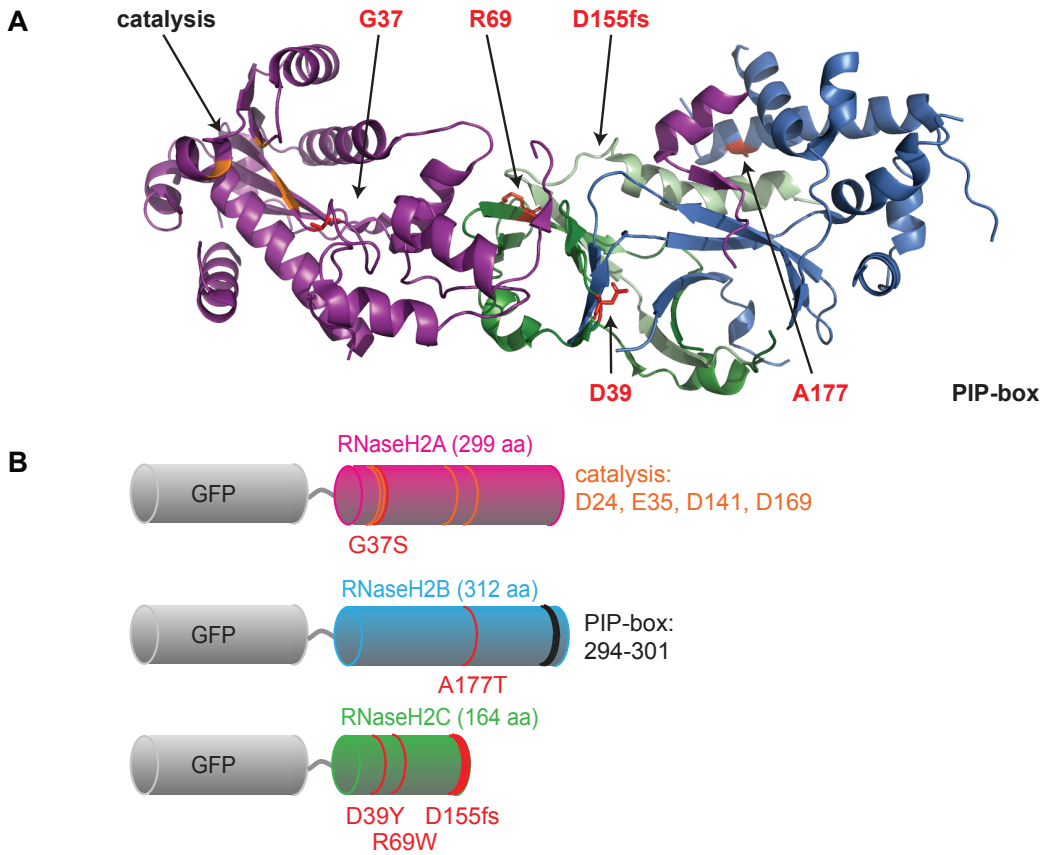

Figure 3.15: Structure of RNase H2. AGS mutations analyzed in this study on **(A)** the 3D-structure of the human RNase H2 complex (PBD 3P56) and **(B)** cartoon of the used constructs. The human RNase H2 is a heterotrimeric complex consisting of a catalytic subunit RNase H2A (magenta) containing the active center (orange) closely connected to the two subunits RNase H2B (cyan) and RNase H2C (green), with the C subunit located in the middle and the B and the A subunits on its sides. In the present study analyzed AGS amino acid alterations are indicated in red.

To confirm activation of processive PCNA dependent DNA repair, we used HeLa Kyoto cells stably expressing cherry-PCNA. All three subunits of RNase H2 were transiently transfected. Each time one subunit was GFP-tagged and analyzed. PCNA and RNase H2A get accumulated at sites of 405 nm laser microirradiation already 4 seconds after irradiation (Figure 3.16 A). Quantification of accumulation revealed similar plateau and recruitment kinetics for all three wild type subunits (Figure 3.16 B + C). The G37S substitution in subunit A showed a significant decreased plateau compared to wild type subunit A. The B_ΔPIP and C_D115fs mutations showed nearly no accumulation after damage induction. Mutation A177T in the B subunit exhibits no changes in accumulation compared to wild type subunit B. The two other studied mutations in subunit C, C_D39Y and C_R69W also showed no significant changes (Figure 3.16 B + C).

To investigate kinetics of the different subunits, we performed FRAP experiments at sites of processive DNA repair. For this, we allowed the proteins to accumulate for 200 seconds after 405 nm laser microirradiation before photobleaching. Fluorescence recovery was monitored every 200 milliseconds (Figure 3.17 A top). PCNA revealed slow recovery, whereas RNase H2A showed full recovery already 3 seconds after bleaching (Figure 3.17 A) indicating a high protein turnover for RNase H2 and slow exchange of PCNA at sites of DNA repair. Control experiments were performed in non-irradiated cells, thus representing corresponding diffusion dynamics of non accumulated protein. To quantify protein turnover, halt-times of full recovery were calculated. No significant decrease in protein turnover was measured for any subunits (Figure 3.17 B).

Altered binding and mobility of AGS mutants at sites of replication

Since it was already shown that RNase H2B binds via PCNA to replication sites (Bubeck et al., 2011), we wanted to validate the binding in S-Phase for the other subunits. Images of HeLa Kyoto cells expressing cherry-PCNA and the different GFP-tagged RNaseH2 subunits were recorded in living cells to avoid fixation artifacts.

All but one subunit showed an exclusive nuclear localization. The frame shift mutation in subunit C (C_D115fs) was evenly distributed in the nucleus as well as in the cytoplasm (Fig. 3.18 B). All wild type subunits colocalized with PCNA in S-Phase (Fig. 3.18 A). Mutant subunits B_ΔPIP and C_D115fs showed no clear colocalization with PCNA in S-Phase. All other mutants also colocalized to PCNA (Fig. 3.18 B). The catalytic impaired mutant A_G37S exhibited a weaker binding compared to wild type as seen by a reduced colocalization (Fig. 3.18 B).

For quantitative colocalization analysis between the subunits and PCNA we used the Hcoeff. The Hcoeff tests the colocalization of two fluorescence signals depending on the pixel distance. If the proteins do not interact, or are randomly distributed, the Hcoeff is 1. A Hcoeff above 1 therefor reflects interaction (Herce et al., 2013). The Hcoeff confirmed the visual observation by showing significant lower values for A_G37S, B_ΔPIP and C_D115fs compared to corresponding wt subunits (Fig. 3.18 C). Remarkably, the B_ΔPIP showed a

significant higher Hcoeff than C_D115fs indicating a weak binding at replication sites for this mutant.

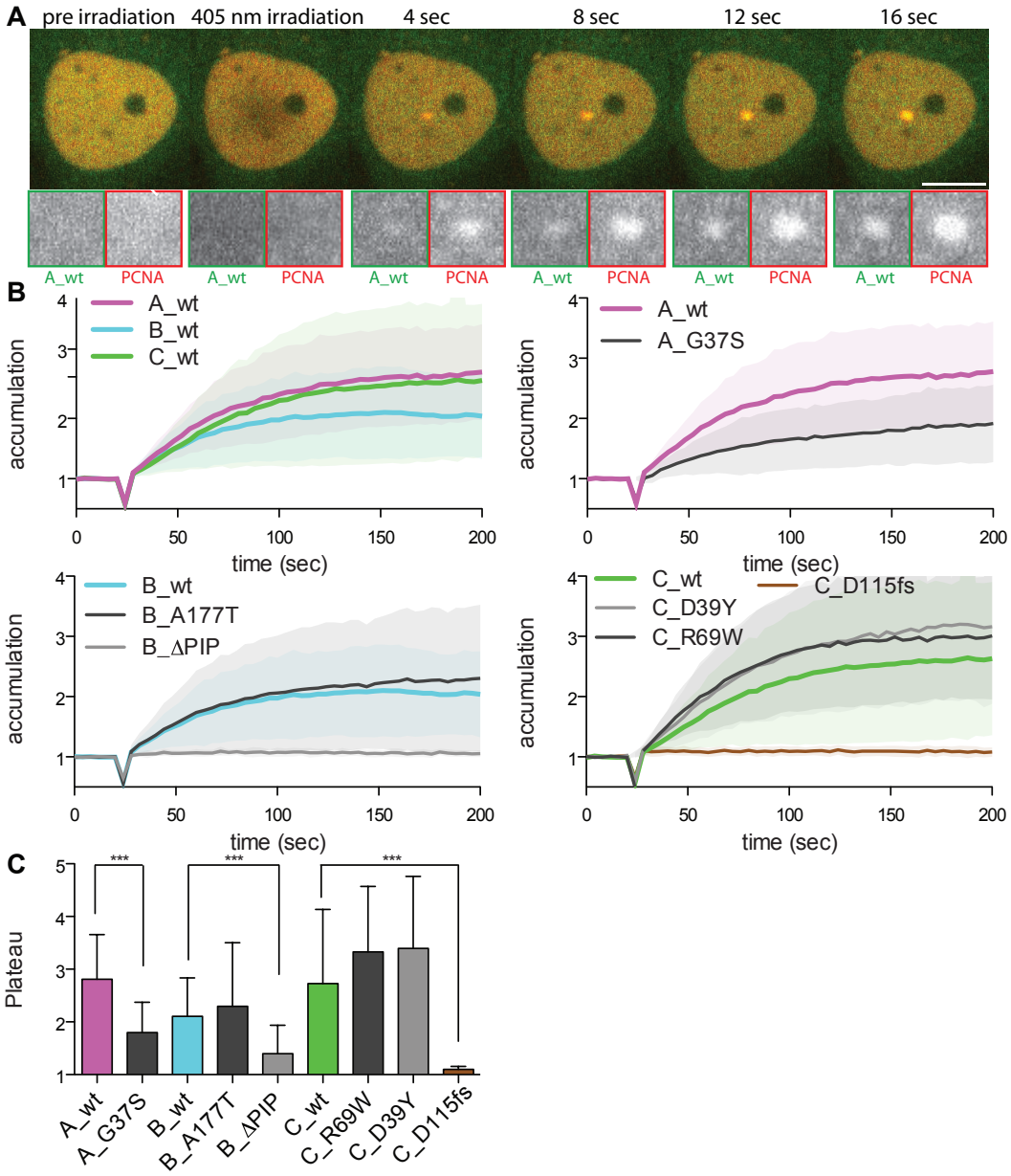

Figure 3.16: Recruitment of RNase H2 subunits to sites of PCNA dependent DNA repair. (A) Live cell imaging of microirradiated cherry-PCNA and RNase H2 expressing cells (RNase H2A GFP tagged). Pictures were taken every 4 seconds. Boxes show magnification of the microirradiation sites. **(B)** Quantitative evaluation of accumulation kinetics from RNase H2 subunits to sites of DNA damage and calculation of Plateau levels from these curves. Scale bar = 10 μm. Statistical test was the Mann Whitney test p< 0.001 ***; n $\geq$ 5, color shaded areas and error bars represent SD.

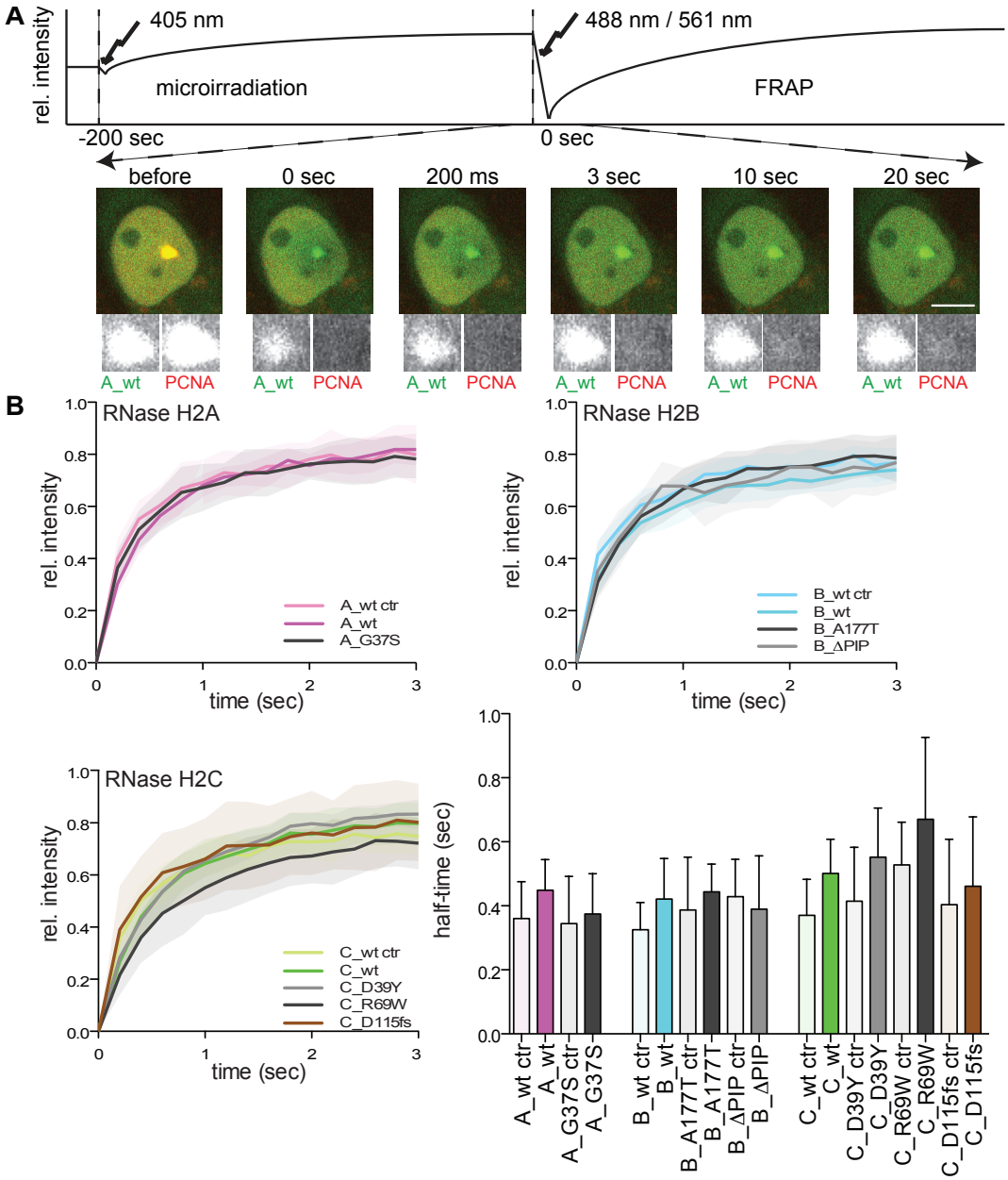

Figure 3.17: Kinetics of wild type and mutant RNase H2 at repair sites. (A) Schematic overview of experimental setup and live cell imaging of cherry-PCNA and RNase H2 expressing cells (RNase H2A GFP tagged). 200 seconds after microirradiation accumulated proteins are bleached and recovery is recorded. Boxes show magnification of the microirradiation and photobleached sites. **(B)** Quantitative evaluation of the FRAP recovery. Controls represent nucleoplasm at not irradiated sites. Scale bar = 10 μm. Statistical test was the Mann Whitney test; n $\geq$ 5, color shaded areas and error bars represent SD

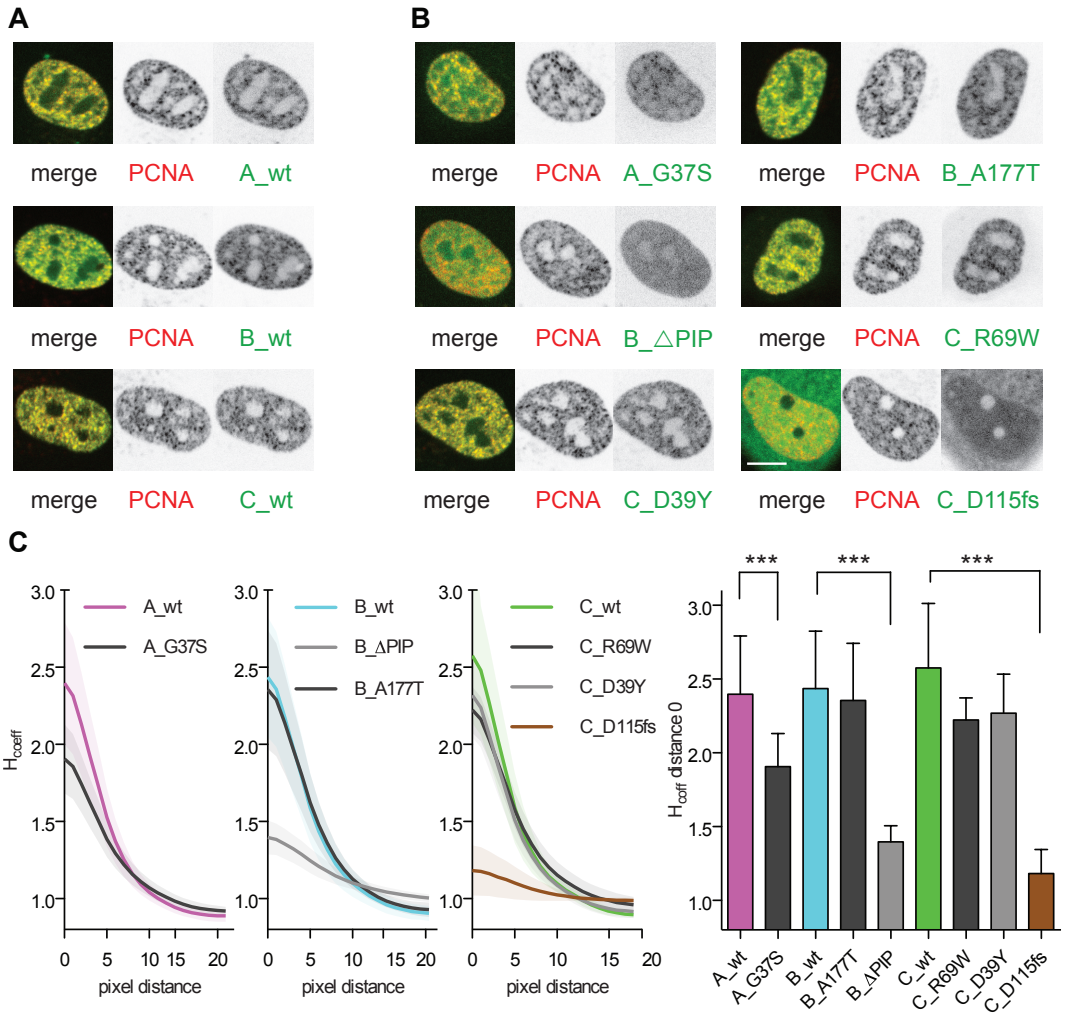

Figure 3.18: Recruitment of RNase H2 subunits to sites of DNA replication. Confocal images of living cells in S-Phase expressing cherry-PCNA and RNase H2 with **(A)** wild type tagged and **(B)** mutant tagged subunits. **(C)** Hcoeff colocalization quantification of RNase H2 subunits and PCNA. Scale bar = 10 μm. Statistical test was the Mann Whitney test p< 0.05 *, p< 0.01 **, p< 0.001 ***; n $\geq$ 5, color shaded areas and error bars represent SD

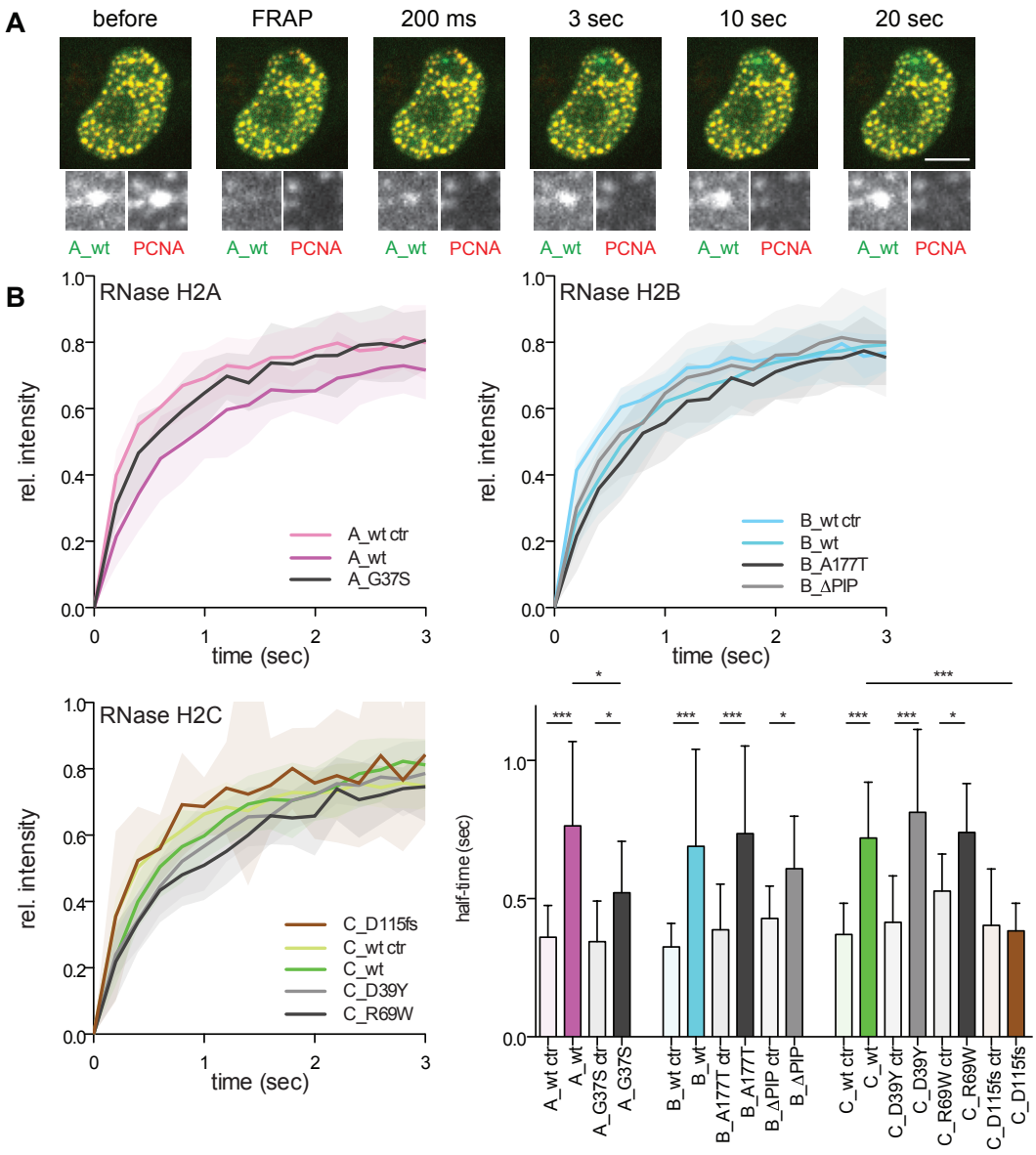

Figure 3.19: Kinetics of RNase H2 subunits to sites of DNA replication. (A) Live cell images of bleached S-Phase cells expressing cherry-PCNA and RNase H2 (RNase H2A GFP tagged). Boxes show magnification of the microirradiation and photobleached sites. **(B)** Quantitative evaluation of recovery and calculated half-times. Controls represent nucleoplasm in non S-Phase cells. Scale bar = 10 μm. Statistical test was the Mann Whitney test p< 0.05 *, p< 0.01 **, p< 0.001 ***; n $\geq$ 5. color shaded areas and error bars represent SD

The majority of DNA synthesis occurs during DNA replication in S-Phase and McElhinny *et al.* calculated that during this process several million ribonuclotides get incorporated into DNA (McElhinny et al., 2010). Therefor, we expected longer retention at sites of DNA replication than for repair sites. To study the dynamics of RNase H2 at sites of DNA replication we performed FRAP at replication foci in S phase cells. As expected, PCNA shows a very slow turnover at sites of DNA replication. RNase H2A in contrast recovers very fast and is fully recovered after 3 seconds (Figure 3.19 A) as it is on sites of DNA repair. Control experiments

were performed in non-S-Phase cells, thus representing corresponding non-accumulated protein diffusion. All three wild type subunits show a slowdown in recovery compared to corresponding controls, resulting in a twice as long half-time (0.35 seconds for controls compared to 0.72 seconds for sites of DNA replication) (Fig. 3.19 B). Except from C_D115fs, which is as fast as the control, all other mutant subunits show a significant delay in turnover compared to their controls (Figure 3.19 B). Comparison between wild type and mutant subunits revealed a significant faster turnover at sites of DNA replication for the A_G37S and for the C_D115fs mutant (Figure 3.19 B).

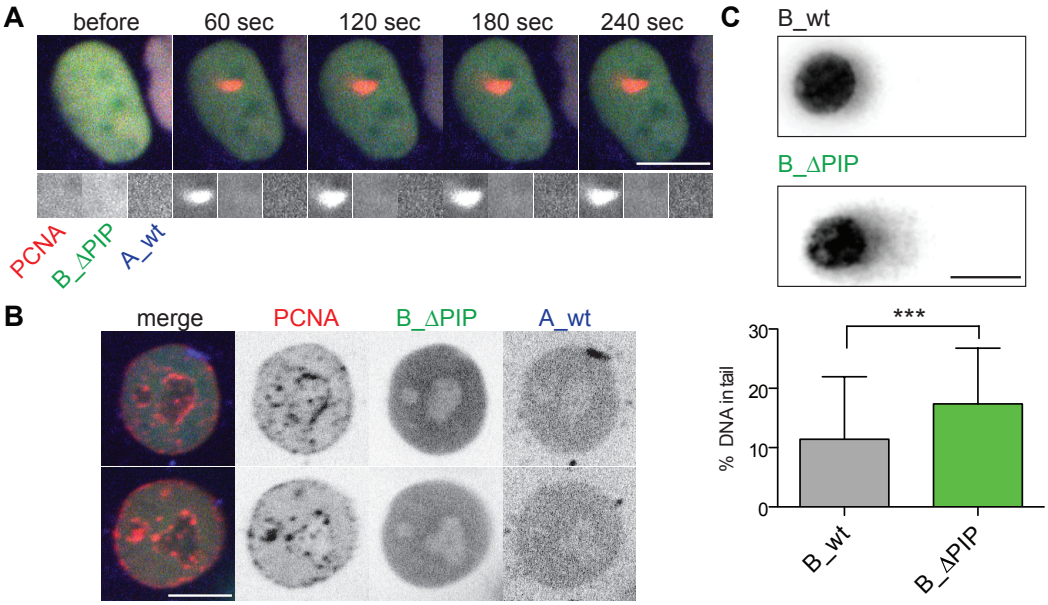

Figure 3.20: Dominat negative effect of over expressed B_ΔPIP mutant. Confocal images of cherry-PCNA, CFP-RNase H2A_and GFP-B_Δ-PIP mutant expressing cells **(A)** after 405 nm laser microirradiation or **(B)** in S-Phase. Boxes show magnification of the microirradiation sites. **(C)** Representative images of alkaline comets from B_wt and B_ΔPIP expressing cells and quantification of the percentage tail DNA of at least 100 cells. Statistical test was the Mann Whitney test, p< 0.001 *** n = 1. Error bars represent SD. Scale bar = 10 μm.

PCNA binding is important for accumulation and activity of RNase H2

Overexpression of the PIP-box mutated B_ΔPIP revealed a hindrance in accumulation for wt A and C subunits to sites of DNA replication and repair (shown for subunit A in Figure 3.20 A+B). This points to a dominant negative effect of this mutation. To unravel if activity is hindered in addition to accumulation, we performed an alkaline Comet assay. The Comet assays enable detection of DNA damage on the level of the whole genome on single cells using the detection of fragmented DNA that migrates in an electrical field. Undamaged DNA is to large to move whereas damaged DNA migrates in the electric field and generates the so called comet tail (Ostling and Johanson, 1984). With an alkaline Comet assay DNA double- and single-strand breaks as well as alkali-labile sites, such as ribonucleotides, can be quantified (Singh et al., 1988, Tice et al., 2000). Preliminary results showed an increased level of fragmented DNA after overexpression of

B_ΔPIP compared to B_wt seen as an increased percentage of DNA in the comet tail (Figure 3.20 C).

Discussion

The key function of RNase H2 is to mediate the removal of ribonucleotides misincorporated by DNA polymerases during DNA synthesis (Bubeck et al., 2011, Chon et al., 2009, Hiller et al., 2012, McElhinny et al., 2010, Reijns et al., 2012) via a new DNA repair pathway known as ribonucleotide excision repair (RER) (Sparks et al., 2012). The RER pathway was only proposed for the removal of misincorporated ribonucleotides after DNA replication. DNA damage can also lead to processive, PCNA dependent DNA synthesis and therefor could also lead to the misincorporation of ribonucleotides into genomic DNA.
Taking advantage of the differential laser microirradiation setup established in chapter 3.1, we tested whether RNase H2 gets recruited to sites of non-processive and processive DNA repair. In line with the proposed function for RNase H2 during RER, RNase H2 only accumulated at sites of 405 nm induced damage. Under these conditions processive DNA synthesis is induced, which involves PCNA recruitment. PCNA is necessary for progression of RER, since it was shown that the following strand displacement synthesis and the flap removal are PCNA dependent (Sparks et al., 2012).
We could proof that RNase H2 plays not only a role at sites of DNA replication but also at sites of processive DNA repair. To further study the dynamics of RNase H2 we investigated the accumulation at sites of DNA repair and replication for the different wild type subunits. All three wild type subunits of RNase H2 get recruited to sites of 405 nm laser microirradiation induced DNA damage with similar kinetics. Binding at sites of DNA replication was confirmed by strong colocalization with PCNA in S-Phase. This proofs the accumulation of trimeric RNase H2 complexes at sites of replication and repair.

This accumulation could in principle be dependent on two parameters: the association and the dissociation rate. To examine the dissociation part, we looked for retention at replication and repair sites using Fluorescence Recovery after Photobleaching (FRAP) measurements.
FRAP measurements revealed slow turnover for PCNA and fast turnover for RNase H2 subunits at sites of DNA repair. This matches observations from Mortusewicz *et al.*. They showed that PCNA remains stably bound over a long time period at DNA damage sites, whereas several PCNA interacting proteins (e.g. DNA Ligase I) show a high turnover (Mortusewicz et al., 2008). Turnover rates for RNase H2 subunits were not decreased significantly compared to unbound protein. The inability to demonstrate differences in retention time could originate from only a miniscule amount of ribonucleotides incorporated during repair and a nearly immediate release of RNase H2.
McElhinny *et al.* calculated that in the yeast genome (1.2×10^7 base pairs) more than 13,000 ribonucleotides could be incorporated during DNA replication by DNA polymerases (McElhinny et al., 2010). Assuming that homologous mammalian polymerases have similar rates, this would mean that several million ribonucleotides would get incorporated into the genome ($\sim 3 \times 10^9$ base pairs) during DNA replication.

One would expect a longer retention of RNase H2 at sites of DNA replication. We measured the retention of RNase H2 at replication sites by FRAP. The RNase H2 subunits showed a fast turnover compared to PCNA similar to DNA repair. Different to repair sites, the turnover of all three RNase H2 wild type subunits was slowed down significantly compared to unbound protein, reflecting the higher catalytic activity of RNase H2 in DNA replication than in DNA repair.

To uncover the effect of AGS causing mutations, we compared the accumulation of wild type and mutated subunits at sites of DNA replication and repair. We found significant differences in accumulation for the PIP-box mutant B_ΔPIP, the catalytic impaired mutant A_G37S and the frameshift mutation C_D115fs (Figure 3.21).

A

RNase H2 subunit	repair binding	repair mobility*	replication binding	replication mobility*
A_wt	↑	high	↑	low
A_G37S	↓	high	↓	middle
B_wt	↑	high	↑	low
B_A177T	↑	high	↑	low
B_ΔPIP	no	high	weak	low
C_wt	↑	high	↑	low
C_R69W	↑	high	↑	low
C_D39Y	↑	high	↑	low
C_D115fs	no	high	no	high

* compared to unirradiated non S-Phase cells

B

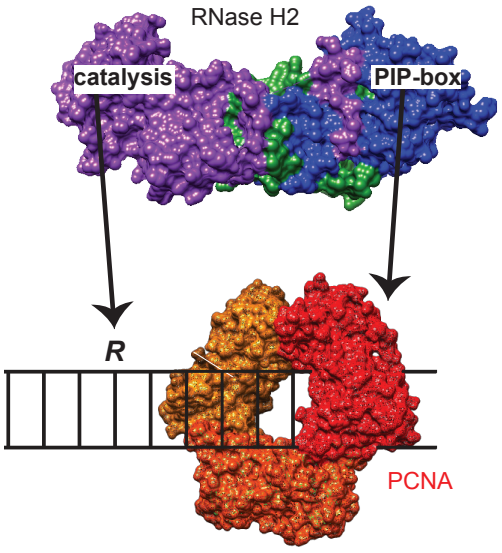

Figure 3.21: Binding and mobility of RNaseH2 to sites of DNA synthesis (A) Schematic overview of binding and mobility characteristic of mutant and wild type RNase H2 subunits during DNA repair and replication. Upward arrows correspond to binding as strong as wild type, arrows facing down indicate weaker binding and 'no' represents non-binding mutant. High mobility denotes kinetics as fast as unbound protein, low mobility stands for delayed turnover and middle an intermediate turnover. Effects on binding and/or mobility can be seen for A_G37S, B_Δ-PIP and C_D115fs. **(B)** Graphical overview of binding sites for RNaseH2. *R* represents a misincorporated ribonucleotide. The catalytic site is important for direct substrate binding, whereas the PIP-box domain mediates binding to DNA over PCNA. The frame shift mutation D115fs in the C subunit leads to a disruption of the complex and to a loss of function. RNase H2: PBD 3P56 and PCNA: PBD 1vym

The PIP-box mutant B_ΔPIP was not recruited to sites of PCNA dependent DNA repair, indicating that PCNA binding is essential for accumulation comparable to other proteins, e.g. Ligase1 or Dnmt1 during DNA repair (Mortusewicz et al., 2006, Schermelleh et al., 2007) via the conserved PIP-box domain. Bubeck *et al.* showed in COS7 cells an unaltered nuclear localization for the articifal B_ΔPIP mutant, but it no longer colocalized with PCNA in S-Phase. Thus, RNase H2 interacts with PCNA in COS7 cells in a PIP-box

dependent manner (Bubeck et al., 2011). We also observed an unaltered nuclear localization for B_ΔPIP but no clear colocalization with PCNA during S-Phase in human cells. However, a slight binding to sites of replication is measurable using sophisticated colocalization algorithms. FRAP at sites of replication revealed a slower recovery compared to unbound protein. We hypothesize that this retention and the slight binding at replication sites is due to complex formation. The wild type subunit A binds via its catalytic activity and slows down dissociation of B_ΔPIP. Catalysis would therefor be more important for retention at replication sites than PCNA binding. Schneider *et al.* observed a similar effect investigating FRAP kinetics of Dnmt1 in S-Phase. They found a slowed down turnover compared to freely diffusing protein even when they mutated the PIP-box and assumed an additional interaction through the targeting sequence (TS) domain of Dnmt1 (Schneider et al., 2013).
However, the slight binding and retention at sites of DNA synthesis are not sufficient to complete RER. We showed that overexpression of B_ΔPIP increases the amount of DNA damage measured by an alkaline comet assay. This matches with data from Sparks *et al*. who could show that PCNA is necessary for progression of RER (Sparks et al., 2012).

Catalytic impaired mutant A_G37S also showed an unaltered nuclear localization. Its defect is apparent at sites of DNA replication and repair. In both cases it shows a weaker accumulation. At repair foci it reaches a lower plateau level and during S-Phase the binding to PCNA was less pronounced compared to the wild type subunit. This supports *in vitro* data from *Shaban et al.*, which show that the G37S mutation distorts binding to the active site. It only allows binding of the wider minor groove present in a RNA-DNA hybrid with a longer stretch of ribonucleotides and not the smaller minor groove expected in a DNA-DNA duplex with only a single ribonucleotide (Shaban et al., 2010). In conclusion, this shows that direct interaction with DNA via the catalytic domain is important for binding at sites of DNA repair and replication. Highlighting the importance of catalysis for association, the A_G37S mutant shows a significant faster turnover measured by FRAP compared to A_wt.
RNase H2C frameshift mutation D115fs was not exclusively located in the nucleus and showed no specific binding to sites of DNA repair or replication. FRAP measurements demonstrate unbound protein like behavior as well and the only possible conclusion is lack of binding and retention to sites of DNA synthesis. The C_D115fs mutant was shown to disrupt the formation of the complex (Kind *et al*., in preparation). Therefor, complex formation is important for binding to sites of DNA synthesis and for retention/import of the complex in the nucleus.
In the present study, the other AGS-causing mutations (B_A177T, C_D39Y, C_R69W) showed no significant differences to RNase H2 wild type subunits in dynamics at repair and replication sites.

Taken together, this demonstrates an impairment of RNase H2 mutations on several levels.
First, complex formation is essential for RNase H2 function. The complex disrupting C_D115fs mutation is not located exclusively in the nucleus and can not bind or be retained at sites of DNA synthesis and therefor

can not fulfill its enzymatic activity. Matching with this, there are only heterozygous patients with this mutation, indicating that a homozygous state might be incompatible with life. Second, RNase H2 mutations have an influence on substrate binding. We show here that direct DNA binding via the catalytic domain (effects of A_G37S mutant) and binding to DNA via PCNA (effects of BΔPIP mutant) are important for accumulation at sites of DNA synthesis and progression of RER.

The other AGS related mutations showed no altered localization or significant changes in binding or retention at sites of DNA synthesis. One explanation could be that the effect of these mutations is so low on complex formation or localization that we can not detect the differences between them and wild type subunits.

Furthermore, there are other possible functions for RNase H2 which could be impaired by these mutations. RNase H2 was shown to be essential for resolving R-loops (Chon et al., 2013, Lazzaro et al., 2012). R-loops are three-strand nucleic acid structures formed by an RNA:DNA hybrid plus a displaced DNA strand (ssDNA), which can be generated during DNA transcription (Aguilera and Garcia-Muse, 2012) In addition, RNase H2 may deliver PCNA in an orientation-dependent manner to the nascent leading strand after replication in order to participate in signaling for MMR (Clausen et al., 2013, Ghodgaonkar et al., 2013, Yao et al., 2013). These multiple activities of RNase H2 can provide different functions *in vivo*. Therefore it will be necessary to modify the experimental setup in a way that will make it possible to distinguish between the various RNase H2 functions to get a deeper insight in the impacts of AGS-causing mutations on specific RNase H2 functions.

4 Conclusion and outlook

The aim of this thesis was to shed more light into the complex processes of DNA repair inside living mammalian cells.

Even though the DNA repair pathways have been reconstructed *in vitro* (Aboussekhra et al., 1995, Bowen et al., 2013, Dianov and Lindahl, 1994, Sebesta et al., 2011, Sharma and Raghavan, 2010, Sparks et al., 2012) there are still many open questions concerning the *in vivo* situation. To address specific questions about kinetics and influence of chromatin states on DNA damage induction and repair, we chose laser microirradiation to induce damage. This technique allows not only to inflict DNA damage at a pre-selected spot with high spatial resolution at specific time points but also to study kinetics of fluorescently tagged DNA repair factors with high temporal resolution.

Establishment of laser microirradiation conditions selective for specific DNA repair pathways

405 nm laser microirradiation was shown to induce a mixture of DNA damage, which results in activation of multiple DNA repair pathways when the cells were pre-sensitized with e.g. BrdU or Hoechst (Dinant et al., 2007, Mortusewicz and Leonhardt, 2007, Mortusewicz et al., 2006, 2005). Therefor it was not possible to study DNA repair pathways separately.

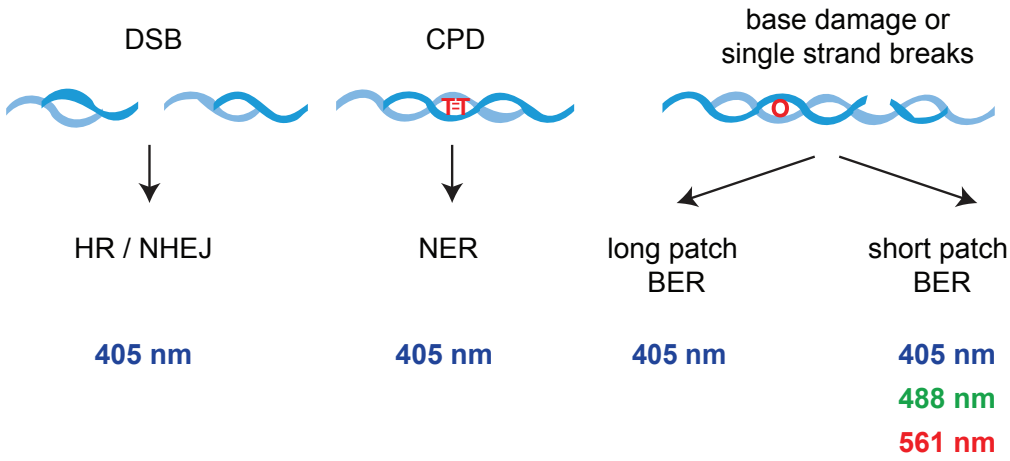

Figure 4.1: Discrimination for short-patch base excision repair with 488 or 561 nm laser microirradiation. Induced damage and resulting DNA repair pathway after laser microirradiation with indicated wavelengths. DSB = double strand break, CPD = cyclobutane pyrimidine dimer, HR = homologous recombination, NHEJ = non homologous end joining, NER = nucleotide excision repair, BER = base excision repair.

To overcome this problem, we studied the relationship between laser wavelength and power and the DNA repair pathways that gets activated. We established the selective induction of short-patch BER by using 488 or 561 laser microirradiation while irradiation with a 405 laser led to activation of DNA double strand break (DSB) repair, nucleotide excision repair (NER) and base excision repair (BER) (Figure 4.1). We further validated the induction of thymidine dimers (cylobutane pyrimidine dimer) and DSBs with specific markers after 405 nm laser microirradiation. In conclusion, we were the first to show that it is possible to discriminate between non-processive DNA repair (short-patch BER) and processive DNA repair pathways using lasers installed on most confocal systems.

Activation of short-patch BER could be due to formation of damaged bases or single strand breaks (Figure 4.1). Campalans *et al.* demonstrated a predominant induction of single strand breaks for their 405 nm laser microirradiation setup (Campalans et al., 2013). The recruitment of BER factor XRCC1 to sites of single strand breaks but not to sites of base damage is dependent on poly (ADP-ribose) polymerase (PARP) activity (Campalans et al., 2013). Exploring recruitment of XRCC1 to sites of laser microirradiation induced damage in PARP knock out cells or after treatment with PARP inhibitors could therefor be one possible way to verify induction of single strand breaks after 488 or 561 nm laser microirradiation. One possibility to prove base damage would be to monitor accumulation of DNA glycosylases at sites of microirradiation, which recognize and process damaged bases.

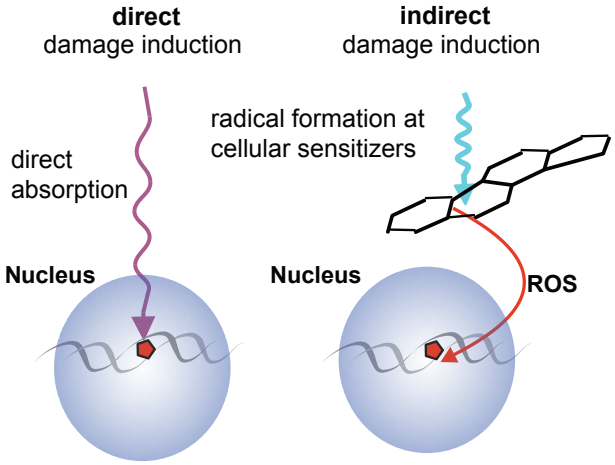

Figure 4.2: DNA damage induction with light. Direct and indirect mechanisms for the induction of DNA damage (Graphic by Dr. Alexander Rapp).

The underlying mechanism of damage induction by laser microirradiation in the visible range is still under discussion. Direct absorption of photons at these wavelengths by DNA is unlikely to be the main trigger for damage induction, since absorption at these wavelengths is very low (Sutherland and Griffin, 1981). A more likely explanation is absorption by endogenous, so far unknown, cellular photosensitizes and formation of radicals, mostly reactive oxygen species (ROS), that subsequently damage DNA (Kielbassa et al., 1997, Pflaum et al., 1994) (Figure 4.2). It would be intriguing to investigate the formation of ROS after laser microirradiation since those wavelengths are not only common in confocal microscopes but also in the

spectra of our sun.

The influence of chromatin state on DNA repair

The level of DNA compaction was shown to have an influence on DNA damage repair (Goodarzi et al., 2010, Surralles et al., 1998). For DNA DSB repair it was suggested that highly condensed heterochromatic regions pose a barrier (David, 2013, Goodarzi et al., 2010) and that a local decondensation or a relocation out of compacted chromatin is necessary to complete repair (Falk et al., 2007, 2008).

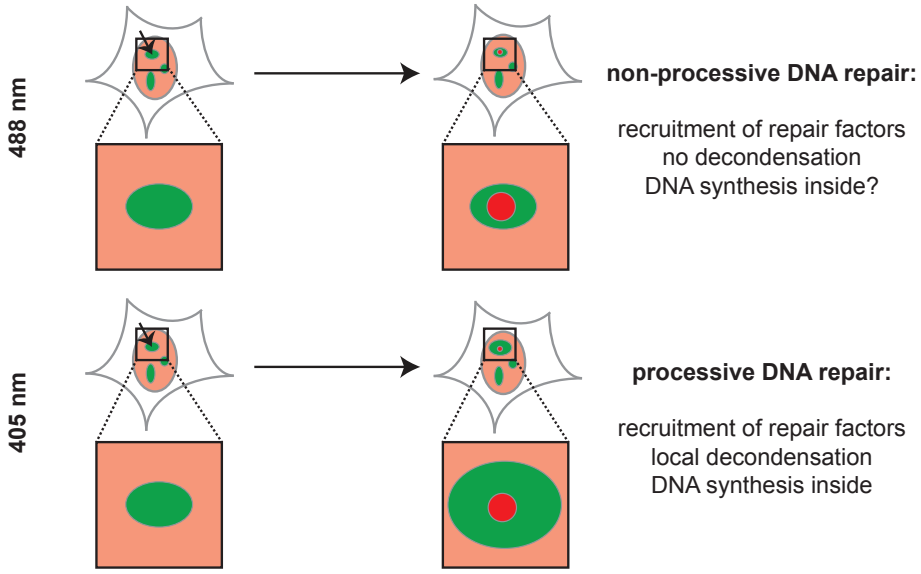

Figure 4.3: DNA repair in heterochromatin dependent on induced damage. DNA repair proteins are indicated in red and heterochromatin in green. 488 nm laser microirradiation induced non-processive DNA repair leads to recruitment of DNA repair factors without a local decondensation. DNA synthesis is not measurable due to low levels of newly incorporated DNA. Induction of processive DNA repair with 405 nm laser microirradiation results in a local decondensation additionally to repair factor recruitment. Newly synthesized DNA can be detected inside heterochromatin.

We could prove the accessibility of dense heterochromatic structures to DNA repair factors for non-processive and processive DNA repair (Figure 4.3). XRCC1 has a role in single strand break rejoining and is associated with ligase 3 (Caldecott et al., 1994, 1995). Therefor the recruitment of XRCC1 suggests that at least short-patch BER is completed inside heterochromatin since the last step of this repair pathway can be detected. Further experiments might prove that not only short-patch BER but also other DNA repair pathways can get completed inside heterochromatin. To investigate this one could monitor recruitment of Ligase 1 or 4, which carry out the ligation step after processive DNA synthesis.

Direct detection of DNA synthesis during non-processive DNA repair is difficult due to the low levels of newly incorporated DNA. Induction of processive DNA synthesis on the other hand enabled us to measure DNA synthesis inside heterochromatin (Figure 4.3), strengthening our hypothesis that DNA repair can get completed inside heterochromatin.

We demonstrated that the recruitment of DNA repair proteins was only accompanied by a local deconden-

sation in case of processive DNA repair (Figure 4.3). This local decondensation of heterochromatin was also seen at sites of DNA replication (unpublished results by Dr. V. O. Chagin). Unlike others (Chiolo et al., 2011, Jakob et al., 2011), we did not observed a relocation out of heterochromatin for the damaged DNA (or the replicating DNA), but the decondensation was sufficient to allow DNA synthesis. This discrepancy is most likely due to differences in induced damage. Jakob *et al.* used ion microbeam irradiation while Chiolo *et al.* applied ionizing radiation, both resulting in the generation of multiple DSBs in close proximity, which represent highly complex lesions (Asaithamby et al., 2008, Nikjoo et al., 2001, Psonka-Antonczyk et al., 2009). It could be that for this type of damage a relocation out of heterochromatin is necessary to avoid misrejoining or false recombination in non-homologous end joining and homologous recombination.

Chiolo *et al.* used *Drosophila* cells as a model system and showed that DSBs occurring in heterochromatic regions are repaired by homologous recombination in this cell line. Early homologous recombination proteins were recruited inside heterochromatin while proteins, which mediate strand invasion only accumulate at DSB after relocation out of heterochromatin (Chiolo et al., 2011). They proposed increased genome stability by preventing incorrect homologous recombination of repetitive sequences (Chiolo et al., 2011). However, *Drosophila* cells differ from mammalian systems. It would be intriguing to investigate if strand invasion during homologous recombination only takes place outside heterochromatin in mammalian cells as well. To gain further insights into strand invasion in and outside of heterochromatic regions laser induced Rad51 recruitment could be achieved with 405 nm laser microirradiation. Accumulation inside heterochromatin would suggest a strand invasion event inside densely packed heterochromatin.

Binding and kinetics of the newly discovered repair protein RNase H2

RNase H2 is a trimeric protein that has been implicated in the newly found DNA repair pathways ribonucleotide excision repair (RER) and mediates recognition and excision of ribonucleotides misincorporated during DNA replication. The pathway was just recently reconstructed *in vitro* (Sparks et al., 2012), but nothing is known so far about the *in vivo* kinetics in mammalian cells.

We used our established laser microirradiation conditions and showed that RNase H2 subunits not only accumulate at sites of DNA replication but also at sites of DNA repair. FRAP analysis revealed fast turnover rates at both accumulation sites. We would expect more misincorporation events during replication due to the increased amount of DNA that is synthesized. The slightly slower turnover rates measured at sites of replication compared to repair sites, matched this hypothesis and resemble the proposed higher enzymatic activity at sites of replication.

Mutations in any of the three RNase H2 subunits have been shown to cause the genetic disorder Aicardi-Goutières syndrome (AGS) (Crow et al., 2006). To elucidate the molecular consequences of mutations in RNase H2 we investigated several mutations found in AGS patients plus an artificial mutant in the PCNA interacting peptide (PIP) box (B _ΔPIP).

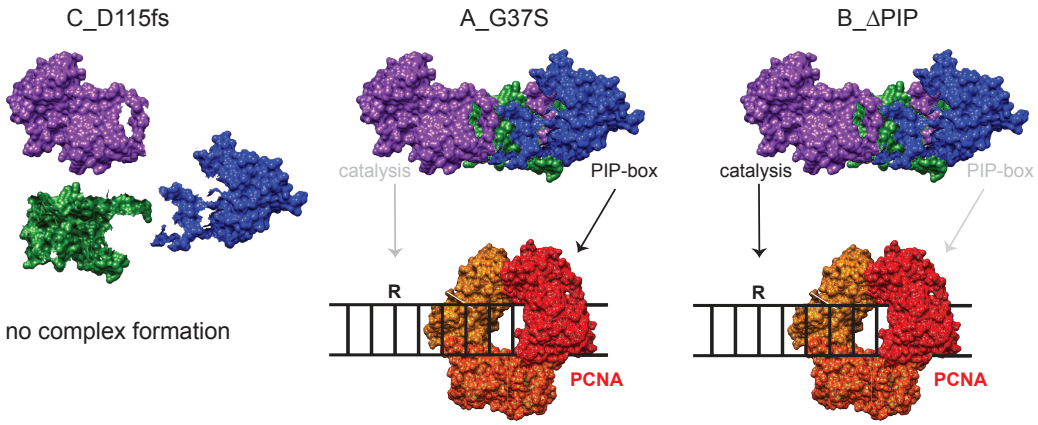

Figure 4.4: Effect of mutants on RNase H2. Assembly of trimeric RNAse H2 complex is hindered by C_D155fs mutation. Mutant A_G37S inhibits binding to single ribonucleotides and PIP box mutant B _ΔPIP can not mediate binding to PCNA. Structures of RNase H2: PBD 3P56 and PCNA: PBD 1vym

We have shown a connection between AGS related mutations and RNase H2 localization and kinetics *in vivo*. Complex formation is not only essential for correct localization and nuclear import but also for retention at DNA replication and repair sites (effect of complex disrupting mutant C_D155fs, Kind *et al.* in preparation), PCNA binding (effect of PIP-box mutant B _ΔPIP) and direct substrate binding (effect of catalytic impaired A_G37S) are crucial for accumulation at sites of DNA synthesis. Impaired catalysis furthermore leads to a defect in retention at these sites (Figure 4.4). We propose that RNase H2 function is dependent on complex formation and binding to sites of misincorporated ribonucleotides.

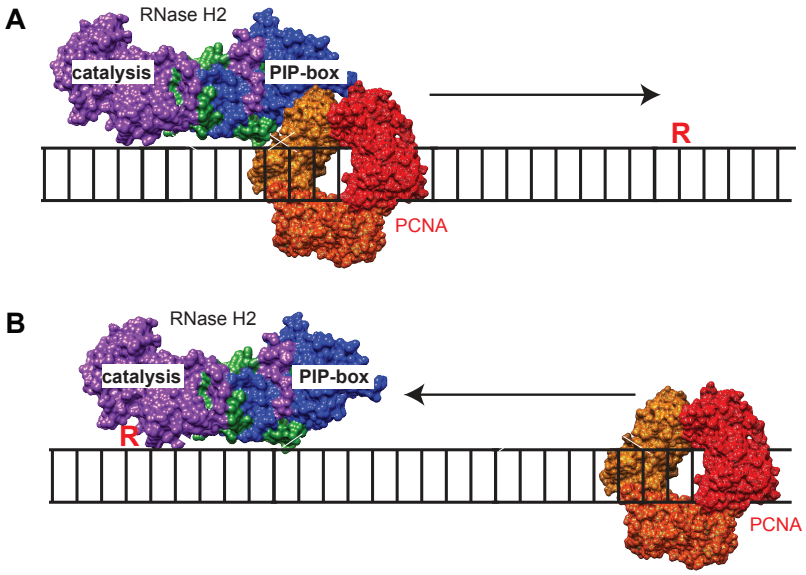

Figure 4.5: RNase H2 binding models. (A) PCNA:RNase H2 complex scans for misincorporated ribonucleotides **(B)** RNase H2 recognizes and binds ribonucleotide inside DNA and PCNA stabilizes binding. Red R indicates a misincorporated ribonucleotide.

PCNA was reported to stimulate ribonucleotide excision (Bubeck et al., 2011), suggesting that binding of RNase H2 to PCNA is not only important for accumulation but also for its catalytic function. The best way to prove this assumption would be to quantify the increase in numbers of ribonucleotides after expression of the PIP-box mutant. One possibility would be to measure incorporation of modified nucleoside analogs, such as uridine analog 5-ethynyl uridine detectable by click chemistry. Another approach would be a single cell gel electrophoresis (Comet) assay. Neutral Comet assays enables detection of DNA DSBs whereas alkaline Comet assays (pH $\geq$ 13) facilitate detection of DNA single-strand breaks and alkali-labile sites (Singh et al., 1988, Tice et al., 2000). High pH conditions not only detect single strand breaks but also results in degradation of RNA (Singh 1988), making ribonucleotide incorporation detectable as single strand breaks. Preliminary results from the alkaline Comet assay showed indeed more incorporated ribonucleotides after overexpression of B.

Binding of RNase H2 to DNA replication and repair sites could be facilitated either via a first loose interaction over the PIP-box with PCNA stabilized by catalytic activity or via a binding to ribonucleotides through the catalytic domain and subsequently stabilization by PCNA binding (Figure 4.5). The first possibility was proposed by Bubeck *et al.* who predicted a complex of PCNA:RNase H2 would scan for misincorporated ribonucleotides (Bubeck et al., 2011). The second was shown in a reconstituted, purified yeast system were RNase H2 processed first cleavage of ribonucleotides in a PCNA independent manner (Sparks et al., 2012). However, there is very little conservation between human and yeast RNase H2B and C subunits (Cerritelli and Crouch, 2009).
Our experiments favor the latter model since protein turnover measured by FRAP is not affected by the PIP-box mutant, which would be unlikely if a complex of PCNA:RNase H2 would be necessary in the first place. Binding via the catalytic domain seems to be more important since the catalytic impaired mutant A_G37S exhibit accelerated turnover at sites of DNA replication.

RNase H2 in Aicardi-Goutières syndrome pathology

Mutations in RNase H2 cause Aicardi-Goutières syndrome (AGS), which is a neuroinflammatory disorder that mimics congenital viral infection (Crow et al., 2006). As previously described, the majority of ribonucleotides are misincorporated during S-Phase. This explains why proliferating cells, which misincorporate ribonucleotides during DNA replication, suffer from RNase H2 failure. This can be clearly seen in RNase H2 knock out mice, which exhibit reduced cellular proliferation and elevated DNA damage during gastrulation (Reijns et al., 2012). Why post-mitotic neurons in AGS patients are affected is less clear.
Neurons are exposed to high levels of oxidative stress (the brain consumes 20% of inhaled oxygen), which result in DNA damage that needs to be repaired (Caldecott, 2014). The amount of ribonucleotides relative to deoxyribonucletotides is particularly high in post-mitotic cells increasing the likelihood for ribonucleotide misincorporation during the synthesis step in DNA repair (Caldecott, 2014, Gosavi et al., 2012). Research of DNA repair and misincorporation of ribonucleoides in postmitotic cells could therefor lead to relevant

insights in AGS.

While yeast cells can tolerate RNase H2 knock out by cleaving ribonucleotides inside genomic DNA with Topoisomerase (Top1), this pathway seems to be avoided when RER is functional because of its mutagenic potential by promoting deletions (Kim et al., 2011, Williams et al., 2013). In addition, yeast DNA polymerases have been shown to tolerate ribonucleotide containing templates with the risk of higher mutation rates (Clausen et al., 2013, Lazzaro et al., 2012). RNase H2 knock out mice die during gastrulation but their early embryogenesis proceeds normally (Reijns et al., 2012) suggesting that this potentially mutagenic mechanisms could also be relevant in mammals.

Alternative functions of RNase H2

Apart from its role in processing misincorporated ribonucleotides, RNase H2 has been suggested to have additional functions, which could be relevant in AGS.

After DNA replication mismatch repair (MMR) factors must be directed to the nascent DNA strand to correct false base pairing. It has been suggested that strand discrimination by MMR may be due to strand discontinuities such as gaps between Okazaki fragments on the lagging strand (Holmes et al., 1990, Thomas et al., 1991). Recently it was shown that single ribonucleotides in close proximity of a mismatch can act as an initiation site for MMR in a RNase H2 dependent manner (Ghodgaonkar et al., 2013, Yao et al., 2013), giving an explanation on how strand discrimination is achieved on the leading strand. Additionally RNase H2 was shown to be essential for resolving R-loops (Chon et al., 2013, Lazzaro et al., 2012). R-loops are three-strand nucleic acid structures formed by an RNA:DNA hybrid plus a displaced DNA strand, which can be generated during DNA transcription (Aguilera and Garcia-Muse, 2012).

Mutations in RNase H2 could therefor lead to increased mismatch mutations or problems in resolving R-loops.

5 References

Aboussekhra, A., Biggerstaff, M., Shivji, M. K., Vilpo, J. A., Moncollin, V., Podust, V. N., Protic, M., Hübscher, U., Egly, J. M., and Wood, R. D. (**1995**). "Mammalian DNA nucleotide excision repair reconstituted with purified protein components." *Cell*, 80(6): 859–868.

Agarwal, N., Hardt, T., Brero, A., Nowak, D., Rothbauer, U., Becker, A., Leonhardt, H., and Cardoso, M. C. (**2007**). "MeCP2 interacts with HP1 and modulates its heterochromatin association during myogenic differentiation." *Nucleic Acids Research*, 35(16): 5402–5408.

Aguilera, A. and Garcia-Muse, T. (**2012**). "R Loops: From Transcription Byproducts to Threats to Genome Stability." *Mol Cell*, 46(2): 115–124.

Aicardi, J. and Goutieres, F. (**1984**). "A Progressive Familial Encephalopathy in Infancy with Calcifications of the Basal Ganglia and Chronic Cerebrospinal-Fluid Lymphocytosis." *Annals of Neurology*, 15(1): 49–54.

Araki, M., Masutani, C., Takemura, M., Uchida, A., Sugasawa, K., Kondoh, J., Ohkuma, Y., and Hanaoka, F. (**2001**). "Centrosome protein centrin 2/caltractin 1 is part of the xeroderma pigmentosum group C complex that initiates global genome nucleotide excision repair." *The Journal of biological chemistry*, 276(22): 18 665–18 672.

Asaithamby, A., Uematsu, N., Chatterjee, A., Story, M. D., Burma, S., and Chen, D. J. (**2008**). "Repair of HZE-particle-induced DNA double-strand breaks in normal human fibroblasts." *Radiat Res*, 169(4): 437–446.

Bae, S. H., Bae, K. H., Kim, J. A., and Seo, Y. S. (**2001**). "RPA governs endonuclease switching during processing of Okazaki fragments in eukaryotes." *Nature*, 412(6845): 456–461.

Bannister, A. J., Zegerman, P., Partridge, J. F., Miska, E. A., Thomas, J. O., Allshire, R. C., and Kouzarides, T. (**2001**). "Selective recognition of methylated lysine 9 on histone H3 by the HP1 chromo domain." *Nature*, 410(6824): 120–124.

Berkovich, E., Monnat, R. J. J., and Kastan, M. B. (**2007**). "Roles of ATM and NBS1 in chromatin structure modulation and DNA double-strand break repair." *Nat Cell Biol*, 9(6): 683–690.

Bird, A. P. and Wolffe, A. P. (**1999**). "Methylation-induced repression - Belts, braces, and chromatin." *Cell*, 99(5): 451–454.

Bonisch, C. and Hake, S. B. (**2012**). "Histone H2A variants in nucleosomes and chromatin: more or less stable?" *Nucleic Acids Research*, 40(21): 10 719–10 741.

Bowen, N., Smith, C. E., Srivatsan, A., Willcox, S., Griffith, J. D., and Kolodner, R. D. (**2013**). "Reconstitution of long and short patch mismatch repair reactions using Saccharomyces cerevisiae proteins." *Proc Natl Acad Sci U S A*, 110(46): 18 472–18 477.

Bradsher, J., Coin, F., and Egly, J. M. (**2000**). "Distinct roles for the helicases of TFIIH in transcript initiation and promoter escape." *The Journal of biological chemistry*, 275(4): 2532–2538.

Brero, A., Easwaran, H. P., Nowak, D., Grunewald, I., Cremer, T., Leonhardt, H., and Cardoso, M. C. (**2005**). "Methyl CpG-binding proteins induce large-scale chromatin reorganization during terminal differentiation." *Journal of Cell Biology*, 169(5): 733–743.

Bubeck, D., Reijns, M. A., Graham, S. C., Astell, K. R., Jones, E. Y., and Jackson, A. P. (**2011**). "PCNA directs type 2 RNase H activity on DNA replication and repair substrates." *Nucleic Acids Research*, 39(9): 3652–3666.

Burgers, P. M. (**2009**). "Polymerase dynamics at the eukaryotic DNA replication fork." *The Journal of biological chemistry*, 284(7): 4041–4045.

Cadet, J., Mouret, S., Ravanat, J. L., and Douki, T. (**2012**). "Photoinduced damage to cellular DNA: direct and photosensitized reactions." *Photochem Photobiol*, 88(5): 1048–1065.

Caldecott, K. W. (**2014**). "Molecular biology. Ribose–an internal threat to DNA." *Science*, 343(6168): 260–261.

Caldecott, K. W., Mckeown, C. K., Tucker, J. D., Ljungquist, S., and Thompson, L. H. (**1994**). "An Interaction between the Mammalian DNA-Repair Protein Xrcc1 and DNA Ligase-Iii." *Mol Cell Biol*, 14(1): 68–76.

Caldecott, K. W., Tucker, J. D., Stanker, L. H., and Thompson, L. H. (**1995**). "Characterization of the XRCC1-DNA ligase III complex in vitro and its absence from mutant hamster cells." *Nucleic Acids Research*, 23(23): 4836–4843.

Campalans, A., Kortulewski, T., Amouroux, R., Menoni, H., Vermeulen, W., and Radicella, J. P. (**2013**). "Distinct spatiotemporal patterns and PARP dependence of XRCC1 recruitment to single-strand break and base excision repair." *Nucleic Acids Research*, 41(5): 3115–3129.

Casas-Delucchi, C. S., Becker, A., Bolius, J. J., and Cardoso, M. C. (**2012**). "Targeted manipulation of heterochromatin rescues MeCP2 Rett mutants and re-establishes higher order chromatin organization." *Nucleic Acids Research*, 40(22): e176.

Cerritelli, S. M. and Crouch, R. J. (**2009**). "Ribonuclease H: the enzymes in eukaryotes." *FEBS J*, 276(6): 1494–1505.

Cerritelli, S. M., Frolova, E. G., Feng, C., Grinberg, A., Love, P. E., and Crouch, R. J. (**2003**). "Failure to produce mitochondrial DNA results in embryonic lethality in Rnaseh1 null mice." *Mol Cell*, 11(3): 807–815.

Chagin, V. O., Stear, J. H., and Cardoso, M. C. (**2010**). "Organization of DNA Replication." *Cold Spring Harb Perspect Biol*, 2(4).

Chiolo, I., Minoda, A., Colmenares, S. U., Polyzos, A., Costes, S. V., and Karpen, G. H. (**2011**). "Double-Strand Breaks in Heterochromatin Move Outside of a Dynamic HP1a Domain to Complete Recombinational Repair." *Cell*, 144(5): 732–744.

Chon, H., Sparks, J. L., Rychlik, M., Nowotny, M., Burgers, P. M., Crouch, R. J., and Cerritelli, S. M. (**2013**). "RNase H2 roles in genome integrity revealed by unlinking its activities." *Nucleic Acids Research*, 41(5): 3130–3143.

Chon, H., Vassilev, A., DePamphilis, M. L., Zhao, Y., Zhang, J., Burgers, P. M., Crouch, R. J., and Cerritelli, S. M. (**2009**). "Contributions of the two accessory subunits, RNASEH2B and RNASEH2C, to the activity and properties of the human RNase H2 complex." *Nucleic Acids Research*, 37(1): 96–110.

Clausen, A. R., Murray, M. S., Passer, A. R., Pedersen, L. C., and Kunkel, T. A. (**2013**). "Structure-function analysis of ribonucleotide bypass by B family DNA replicases." *Proc Natl Acad Sci U S A*, 110(42): 16 802–16 807.

Coffin, S. R., Hollis, T., and Perrino, F. W. (**2011**). "Functional Consequences of the RNase H2A Subunit Mutations That Cause Aicardi-Goutieres Syndrome." *The Journal of biological chemistry*, 286(19): 16 984–16 991.

Costanzi, C. and Pehrson, J. R. (**1998**). "Histone macroH2A1 is concentrated in the inactive X chromosome of female mammals." *Nature*, 393(6685): 599–601.

Craig, J. M. (**2005**). "Heterochromatin–many flavours, common themes." *BioEssays*, 27(1): 17–28.

Cremer, C., Cremer, T., Fukuda, M., and Nakanishi, K. (**1980**). "Detection of laser–UV microirradiation-induced DNA photolesions by immunofluorescent staining." *Human Genetics*, 54(1): 107–110.

Crow, Y. J., Leitch, A., Hayward, B. E., Garner, A., Parmar, R., Griffith, E., Ali, M., Semple, C., Aicardi, J., Babul-Hirji, R., Baumann, C., Baxter, P., Bertini, E., Chandler, K. E., Chitayat, D., Cau, D., Dery, C., Fazzi, E., Goizet, C., King, M. D., Klepper, J., Lacombe, D., Lanzi, G., Lyall, H., Martinez-Frias, M. L., Mathieu, M., McKeown, C., Monier, A., Oade, Y., Quarrell, O. W., Rittey, C. D., Rogers, R. C., Sanchis, A., Stephenson, J. B., Tacke, U., Till, M., Tolmie, J. L., Tomlin, P., Voit, T., Weschke, B., Woods, C. G., Lebon, P., Bonthron, D. T., Ponting, C. P., and Jackson, A. P. (**2006**). "Mutations in genes encoding ribonuclease H2 subunits cause Aicardi-Goutieres syndrome and mimic congenital viral brain infection." *Nature genetics*, 38(8): 910–916.

David, R. (**2013**). "DNA repair: A sensor for chromatin damage." *Nature Reviews Molecular Cell Biology*, 14(7): 400–401.

Davidkova, M., Stisova, V., Goffinont, S., Gillard, N., Castaing, B., and Spotheim-Maurizot, M. (**2006**). "Modification of DNA radiolysis by DNA-binding proteins: structural aspects." *Radiat Prot Dosimetry*, 122(1-4): 100–105.

Dianov, G. and Lindahl, T. (**1994**). "Reconstitution of the DNA base excision-repair pathway." *Current biology : CB*, 4(12): 1069–1076.

Dinant, C., de Jager, M., Essers, J., van Cappellen, W. A., Kanaar, R., Houtsmuller, A. B., and Vermeulen, W. (**2007**). "Activation of multiple DNA repair pathways by sub-nuclear damage induction methods." *Journal of Cell Science*, 120(Pt 15): 2731–2740.

Eder, P. S., Walder, R. Y., and Walder, J. A. (**1993**). "Substrate specificity of human RNase H1 and its role in excision repair of ribose residues misincorporated in DNA." *Biochimie*, 75(1-2): 123–126.

Eissenberg, J. C. and Elgin, S. C. R. (**2000**). "The HP1 protein family: getting a grip on chromatin." *Current Opinion in Genetics & Development*, 10(2): 204–210.

Falk, M., Lukasova, E., Gabrielova, B., Ondrej, V., and Kozubek, S. (**2007**). "Chromatin dynamics during DSB repair." *Biochimica Et Biophysica Acta-Molecular Cell Research*, 1773(10): 1534–1545.

Falk, M., Lukasova, E., and Kozubek, S. (**2008**). "Chromatin structure influences the sensitivity of DNA to gamma-radiation." *Biochimica et biophysica acta*, 1783(12): 2398–2414.

Falk, M., Lukasova, E., Stefancikova, L., Baranova, E., Falkova, I., Jezkova, L., Davidkova, M., Bacikova, A., Vachelova, J., Michaelidesova, A., and Kozubek, S. (**2014**). "Heterochromatinization associated with cell differentiation as a model to study DNA double strand break induction and repair in the context of higher-order chromatin structure." *Appl Radiat Isot*, 83 Pt B: 177–185.

Fernandez-Capetillo, O., Celeste, A., and Nussenzweig, A. (**2003**). "Focusing on foci: H2AX and the recruitment of DNA-damage response factors." *Cell Cycle*, 2(5): 426–427.

Ferrando-May, E., Tomas, M., Blumhardt, P., Stockl, M., Fuchs, M., and Leitenstorfer, A. (**2013**). "Highlighting the DNA damage response with ultrashort laser pulses in the near infrared and kinetic modeling." *Front Genet*, 4: 135.

Figiel, M., Chon, H., Cerritelli, S. M., Cybulska, M., Crouch, R. J., and Nowotny, M. (**2011**). "The structural and biochemical characterization of human RNase H2 complex reveals the molecular basis for substrate recognition and Aicardi-Goutieres syndrome defects." *The Journal of biological chemistry*, 286(12): 10 540–10 550.

Fortini, P. and Dogliotti, E. (**2007**). "Base damage and single-strand break repair: Mechanisms and functional significance of short- and long-patch repair subpathways." *DNA Repair*, 6(4): 398–409.

Friedberg, E. C. (**1996**). "Relationships between DNA repair and transcription." *Annual Review of Biochemistry*, 65: 15–42.

Fujita, N., Watanabe, S., Ichimura, T., Tsuruzoe, S., Shinkai, Y., Tachibana, M., Chiba, T., and Nakao, M. (**2003**). "Methyl-CpG binding domain 1 (MBD1) interacts with the Suv39h1-HP1 heterochromatic complex for DNA methylation-based transcriptional repression." *The Journal of biological chemistry*, 278(26): 24 132–24 138.

Ghodgaonkar, M. M., Lazzaro, F., Olivera-Pimentel, M., Artola-Boran, M., Cejka, P., Reijns, M. A., Jackson, A. P., Plevani, P., Muzi-Falconi, M., and Jiricny, J. (**2013**). "Ribonucleotides Misincorporated into DNA Act as Strand-Discrimination Signals in Eukaryotic Mismatch Repair." *Mol Cell*, 50(3): 323–332.

Goodarzi, A. A., Jeggo, P., and Lobrich, M. (**2010**). "The influence of heterochromatin on DNA double strand break repair: Getting the strong, silent type to relax." *DNA Repair*, 9(12): 1273–1282.

Goodarzi, A. A. and Jeggo, P. A. (**2013**). "The repair and signaling responses to DNA double-strand breaks." *Adv Genet*, 82: 1–45.

Goodarzi, A. A., Noon, A. T., Deckbar, D., Ziv, Y., Shiloh, Y., Lobrich, M., and Jeggo, P. A. (**2008**). "ATM signaling facilitates repair of DNA double-strand breaks associated with heterochromatin." *Mol Cell*, 31(2): 167–177.

Goodarzi, A. A., Noon, A. T., and Jeggo, P. A. (**2009**). "The impact of heterochromatin on DSB repair." *Biochemical Society Transactions*, 37: 569–576.

Goodhead, D. T. (**1994**). "Initial events in the cellular effects of ionizing radiations: clustered damage in DNA." *Int J Radiat Biol*, 65(1): 7–17.

Gosavi, R. A., Moon, A. F., Kunkel, T. A., Pedersen, L. C., and Bebenek, K. (**2012**). "The catalytic cycle for ribonucleotide incorporation by human DNA Pol lambda." *Nucleic Acids Research*, 40(15): 7518–7527.

Greinert, R., Volkmer, B., Henning, S., Breitbart, E. W., Greulich, K. O., Cardoso, M. C., and Rapp, A. (**2012**). "UVA-induced DNA double-strand breaks result from the repair of clustered oxidative DNA damages." *Nucleic Acids Research*, 40(20): 10 263–10 273.

Gunther, K., Rust, M., Leers, J., Boettger, T., Scharfe, M., Jarek, M., Bartkuhn, M., and Renkawitz, R. (**2013**). "Differential roles for MBD2 and MBD3 at methylated CpG islands, active promoters and binding to exon sequences." *Nucleic Acids Research*, 41(5): 3010–3021.

Hausen, P. and Stein, H. (**1970**). "Ribonuclease H. An enzyme degrading the RNA moiety of DNA-RNA hybrids." *Eur J Biochem*, 14(2): 278–283.

Heiss, M., Fischer, B. E., Jakob, B., Fournier, C., Becker, G., and Taucher-Scholz, G. (**2006**). "Targeted irradiation of mammalian cells using a heavy-ion microprobe." *Radiat Res*, 165(2): 231–239.

Hendrich, B. and Bird, A. (**1998**). "Identification and characterization of a family of mammalian methyl-CpG binding proteins." *Mol Cell Biol*, 18(11): 6538–6547.

Herce, H. D., Casas-Delucchi, C. S., and Cardoso, M. C. (**2013**). "New image colocalization coefficient for fluorescence microscopy to quantify (bio-)molecular interactions." *J Microsc*, 249(3): 184–194.

Hiller, B., Achleitner, M., Glage, S., Naumann, R., Behrendt, R., and Roers, A. (**2012**). "Mammalian RNase H2 removes ribonucleotides from DNA to maintain genome integrity." *Journal of Experimental Medicine*, 209(8): 1419–1426.

Hoeijmakers, J. H. (**2001**). "Genome maintenance mechanisms for preventing cancer." *Nature*, 411(6835): 366–374.

Hoeijmakers, J. H. (**2009**). "DNA damage, aging, and cancer." *N Engl J Med*, 361(15): 1475–1485.

Holmes, J., Clark, S., and Modrich, P. (**1990**). "Strand-Specific Mismatch Correction in Nuclear Extracts of Human and Drosophila-Melanogaster Cell-Lines." *Proc Natl Acad Sci U S A*, 87(15): 5837–5841.

Huertas, P. and Aguilera, A. (**2003**). "Cotranscriptionally formed DNA:RNA hybrids mediate transcription elongation impairment and transcription-associated recombination." *Mol Cell*, 12(3): 711–721.

Ichimura, T., Watanabe, S., Sakamoto, Y., Aoto, T., Fujita, N., and Nakao, M. (**2005**). "Transcriptional repression and heterochromatin formation by MBD1 and MCAF/AM family proteins." *The Journal of biological chemistry*, 280(14): 13 928–13 935.

Jackson, S. P. and Bartek, J. (**2009**). "The DNA-damage response in human biology and disease." *Nature*, 461(7267): 1071–1078.

Jakob, B., Rudolph, J. H., Gueven, N., Lavin, M. E., and Taucher-Scholz, G. (**2005**). "Live cell imaging of heavy-ion-induced radiation responses by beamline microscopy." *Radiat Res*, 163(6): 681–690.

Jakob, B., Splinter, J., Conrad, S., Voss, K. O., Zink, D., Durante, M., Lobrich, M., and Taucher-Scholz, G. (**2011**). "DNA double-strand breaks in heterochromatin elicit fast repair protein recruitment, histone H2AX phosphorylation and relocation to euchromatin." *Nucleic Acids Research*, 39(15): 6489–6499.

Jakob, B., Splinter, J., Durante, M., and Taucher-Schoiz, G. (**2009**). "Live cell microscopy analysis of radiation-induced DNA double-strand break motion." *Proc Natl Acad Sci U S A*, 106(9): 3172–3177.

Jasin, M. (**1996**). "Genetic manipulation of genomes with rare-cutting endonucleases." *Trends Genet*, 12(6): 224–228.

Jenuwein, T. (**2001**). "Translating the Histone Code." *Science*, 293(5532): 1074–1080.

Jeong, H. S., Backlund, P. S., Chen, H. C., Karavanov, A. A., and Crouch, R. J. (**2004**). "RNase H2 of Saccharomyces cerevisiae is a complex of three proteins." *Nucleic Acids Research*, 32(2): 407–414.

Johnson, R. D. and Jasin, M. (**2000**). "Sister chromatid gene conversion is a prominent double-strand break repair pathway in mammalian cells." *The EMBO journal*, 19(13): 3398–3407.

Jost, K. L., Bertulat, B., and Cardoso, M. C. (**2012**). "Heterochromatin and gene positioning: inside, outside, any side?" *Chromosoma*, 121(6): 555–563.

Kass, E. M. and Jasin, M. (**2010**). "Collaboration and competition between DNA double-strand break repair pathways." *FEBS letters*, 584(17): 3703–3708.

Kielbassa, C., Roza, L., and Epe, B. (**1997**). "Wavelength dependence of oxidative DNA damage induced by UV and visible light." *Carcinogenesis*, 18(4): 811–816.

Kim, N., Huang, S. Y. N., Williams, J. S., Li, Y. C., Clark, A. B., Cho, J. E., Kunkel, T. A., Pommier, Y., and Jinks-Robertson, S. (**2011**). "Mutagenic Processing of Ribonucleotides in DNA by Yeast Topoisomerase I." *Science*, 332(6037): 1561–1564.

Klungland, A. and Lindahl, T. (**1997**). "Second pathway for completion of human DNA base excision-repair: Reconstitution with purified proteins and requirement for DNase IV (FEN1)." *The EMBO journal*, 16(11): 3341–3348.

Kong, X., Mohanty, S. K., Stephens, J., Heale, J. T., Gomez-Godinez, V., Shi, L. Z., Kim, J. S., Yokomori, K., and Berns, M. W. (**2009**). "Comparative analysis of different laser systems to study cellular responses to DNA damage in mammalian cells." *Nucleic Acids Research*, 37(9): e68.

Kruhlak, M. J., Celeste, A., Dellaire, G., Fernandez-Capetillo, O., Muller, W. G., McNally, J. G., Bazett-Jones, D. P., and Nussenzweig, A. (**2006**). "Changes in chromatin structure and mobility in living cells at sites of DNA double-strand breaks." *Journal of Cell Biology*, 172(6): 823–834.

Kunz, C., Saito, Y., and Schar, P. (**2009**). "DNA Repair in mammalian cells: Mismatched repair: variations on a theme." *Cell Mol Life Sci*, 66(6): 1021–1038.

Lan, L., Nakajima, S., Komatsu, K., Nussenzweig, A., Shimamoto, A., Oshima, J., and Yasui, A. (**2005**). "Accumulation of Werner protein at DNA double-strand breaks in human cells." *Journal of Cell Science*, 118(Pt 18): 4153–4162.

Lan, L., Nakajima, S., Oohata, Y., Takao, M., Okano, S., Masutani, M., Wilson, S. H., and Yasui, A. (**2004**). "In situ analysis of repair processes for oxidative DNA damage in mammalian cells." *Proc Natl Acad Sci U S A*, 101(38): 13 738–13 743.

Landry, J. J. M., Pyl, P. T., Rausch, T., Zichner, T., Tekkedil, M. M., Stütz, A. M., Jauch, A., Aiyar, R. S., Pau, G., Delhomme, N., Gagneur, J., Korbel, J. O., Huber, W., and Steinmetz, L. M. (**2013**). "The Genomic and Transcriptomic Landscape of a HeLa Cell Line." *G3 (Bethesda, Md.)*, pages –.

Law, J. A. and Jacobsen, S. E. (**2010**). "Establishing, maintaining and modifying DNA methylation patterns in plants and animals." *Nat Rev Genet*, 11(3): 204–220.

Lazzaro, F., Novarina, D., Amara, F., Watt, D. L., Stone, J. E., Costanzo, V., Burgers, P. M., Kunkel, T. A., Plevani, P., and Muzi-Falconi, M. (**2012**). "RNase H and postreplication repair protect cells from ribonucleotides incorporated in DNA." *Mol Cell*, 45(1): 99–110.

Lee-Kirsch, M. A., Wolf, C., and Gunther, C. (**2013**). "Aicardi-Goutieres syndrome: a model disease for systemic autoimmunity." *Clin Exp Immunol*.

Leonhardt, H. and Cardoso, M. C. (**2000**). "DNA methylation, nuclear structure, gene expression and cancer." *Journal of Cellular Biochemistry*, pages 78–83.

Li, X. L. and Manley, J. L. (**2006**). "Cotranscriptional processes and their influence on genome stability." *Genes Dev*, 20(14): 1838–1847.

Lindahl, T. (**1993**). "Instability and decay of the primary structure of DNA." *Nature*, 362(6422): 709–715.

Lindahl, T. and Wood, R. D. (**1999**). "Quality control by DNA repair." *Science*, 286(5446): 1897–1905.

Lukas, C., Falck, J., Bartkova, J., Bartek, J., and Lukas, J. (**2003**). "Distinct spatiotemporal dynamics of mammalian checkpoint regulators induced by DNA damage." *Nat Cell Biol*, 5(3): 255–260.

Lukas, C., Melander, F., Stucki, M., Falck, J., Bekker-Jensen, S., Goldberg, M., Lerenthal, Y., Jackson, S. P., Bartek, J., and Lukas, J. (**2004**). "Mdc1 couples DNA double-strand break recognition by Nbs1 with its H2AX-dependent chromatin retention." *The EMBO journal*, 23(13): 2674–2683.

Machida, Y., Okazaki, T., and Okazaki, R. (**1977**). "Discontinuous replication of replicative form DNA from bacteriophage phiX174." *Proc Natl Acad Sci U S A*, 74(7): 2776–2779.

Marchal, J. A., Acosta, M. J., Bullejos, M., de la Guardia, R. D., and Sánchez, A. (**2003**). "Sex chromosomes, sex determination, and sex-linked sequences in Microtidae." *Cytogenetic and genome research*, 101(3-4): 266–273.

Marchal, J. A., Acosta, M. J., Nietzel, H., Sperling, K., Bullejos, M., de la Guardia, R. D., and Sánchez, A. (**2004**). "X chromosome painting in Microtus: Origin and evolution of the giant sex chromosomes." *Chromosome Research*, 12(8): 767–776.

Matsunaga, T., Mu, D., Park, C. H., Reardon, J. T., and Sancar, A. (**1995**). "Human DNA repair excision nuclease. Analysis of the roles of the subunits involved in dual incisions by using anti-XPG and anti-ERCC1 antibodies." *The Journal of biological chemistry*, 270(35): 20 862–20 869.

McElhinny, S. A. N., Watts, B. E., Kumar, D., Watt, D. L., Lundstrom, E. B., Burgers, P. M. J., Johansson, E., Chabes, A., and Kunkel, T. A. (**2010**). "Abundant ribonucleotide incorporation into DNA by yeast replicative polymerases." *Proc Natl Acad Sci U S A*, 107(11): 4949–4954.

Menoni, H., Hoeijmakers, J. H., and Vermeulen, W. (**2012**). "Nucleotide excision repair-initiating proteins bind to oxidative DNA lesions in vivo." *Journal of Cell Biology*, 199(7): 1037–1046.

Mone, M. J., Volker, M., Nikaido, O., Mullenders, L. H., van Zeeland, A. A., Verschure, P. J., Manders, E. M., and Van Driel, R. (**2001**). "Local UV-induced DNA damage in cell nuclei results in local transcription inhibition." *EMBO reports*, 2(11): 1013–1017.

Mortusewicz, O., Fouquerel, E., Ame, J. C., Leonhardt, H., and Schreiber, V. (**2011**). "PARG is recruited to DNA damage sites through poly(ADP-ribose)- and PCNA-dependent mechanisms." *Nucleic Acids Research*, 39(12): 5045–5056.

Mortusewicz, O. and Leonhardt, H. (**2007**). "XRCC1 and PCNA are loading platforms with distinct kinetic properties and different capacities to respond to multiple DNA lesions." *BMC molecular biology*, 8: 81.

Mortusewicz, O., Leonhardt, H., and Cardoso, M. C. (**2008**). "Spatiotemporal dynamics of regulatory protein recruitment at DNA damage sites." *Journal of Cellular Biochemistry*, 104(5): 1562–1569.

Mortusewicz, O., Rothbauer, U., Cardoso, M. C., and Leonhardt, H. (**2006**). "Differential recruitment of DNA Ligase I and III to DNA repair sites." *Nucleic Acids Research*, 34(12): 3523–3532.

Mortusewicz, O., Schermelleh, L., Walter, J., Cardoso, M. C., and Leonhardt, H. (**2005**). "Recruitment of DNA methyltransferase I to DNA repair sites." *Proc Natl Acad Sci U S A*, 102(25): 8905–8909.

Mullenders, L. H. F., Vrieling, H., Venema, J., and Vanzeeland, A. A. (**1991**). "Hierarchies of DNA-Repair in Mammalian-Cells - Biological Consequences." *Mutation Research*, 250(1-2): 223–228.

Nan, X., Tate, P., Li, E., and Bird, A. (**1996**). "DNA methylation specifies chromosomal localization of MeCP2." *Mol Cell Biol*, 16(1): 414–421.

Ng, H. H., Jeppesen, P., and Bird, A. (**2000**). "Active repression of methylated genes by the chromosomal protein MBD1." *Mol Cell Biol*, 20(4): 1394–1406.

Nikjoo, H., O'Neill, P., Wilson, W. E., and Goodhead, D. T. (**2001**). "Computational approach for determining the spectrum of DNA damage induced by ionizing radiation." *Radiat Res*, 156(5): 577–583.

Nouspikel, T. (**2009**). "DNA repair in mammalian cells : Nucleotide excision repair: variations on versatility." *Cell Mol Life Sci*, 66(6): 994–1009.

Obe, G., Pfeiffer, P., Savage, J. R., Johannes, C., Goedecke, W., Jeppesen, P., Natarajan, A. T., Martinez-Lopez, W., Folle, G. A., and Drets, M. E. (**2002**). "Chromosomal aberrations: formation, identification and distribution." *Mutation Research*, 504(1-2): 17–36.

O'Donovan, A., Davies, A. A., Moggs, J. G., West, S. C., and Wood, R. D. (**1994**). "XPG endonuclease makes the 3' incision in human DNA nucleotide excision repair." *Nature*, 371(6496): 432–435.

Okazaki, R., Okazaki, T., Sakabe, K., Sugimoto, K., and Sugino, A. (**1968**). "Mechanism of DNA chain growth. I. Possible discontinuity and unusual secondary structure of newly synthesized chains." *Proc Natl Acad Sci U S A*, 59(2): 598–605.

Ostling, O. and Johanson, K. J. (**1984**). "Microelectrophoretic study of radiation-induced DNA damages in individual mammalian cells." *Biochemical and Biophysical Research Communications*, 123(1): 291–298.

Pardo, B., Gomez-Gonzalez, B., and Aguilera, A. (**2009**). "DNA repair in mammalian cells: DNA double-strand break repair: how to fix a broken relationship." *Cell Mol Life Sci*, 66(6): 1039–1056.

Perrino, F. W., Harvey, S., Shaban, N. M., and Hollis, T. (**2009**). "RNaseH2 mutants that cause Aicardi-Goutieres syndrome are active nucleases." *Journal of Molecular Medicine-Jmm*, 87(1): 25–30.

Perumal, S. K., Yue, H. J., Hu, Z. X., Spiering, M. M., and Benkovic, S. J. (**2010**). "Single-molecule studies of DNA replisome function." *Biochimica Et Biophysica Acta-Proteins and Proteomics*, 1804(5): 1094–1112.

Petermann, E., Ziegler, M., and Oei, S. L. (**2003**). "ATP-dependent selection between single nucleotide and long patch base excision repair." *DNA Repair*, 2(10): 1101–1114.

Pflaum, M., Boiteux, S., and Epe, B. (**1994**). "Visible light generates oxidative DNA base modifications in high excess of strand breaks in mammalian cells." *Carcinogenesis*, 15(2): 297–300.

Phair, R. D., Gorski, S. A., and Misteli, T. (**2004**). "Measurement of dynamic protein binding to chromatin in vivo, using photobleaching microscopy." *Methods Enzymol*, 375: 393–414.

Pierce, A. J., Hu, P., Han, M., Ellis, N., and Jasin, M. (**2001**). "Ku DNA end-binding protein modulates homologous repair of double-strand breaks in mammalian cells." *Genes Dev*, 15(24): 3237–3242.

Pohler, J. R., Otterlei, M., and Warbrick, E. (**2005**). "An in vivo analysis of the localisation and interactions of human p66 DNA polymerase delta subunit." *BMC molecular biology*, 6: 17.

Povirk, L. F., Wubter, W., Kohnlein, W., and Hutchinson, F. (**1977**). "DNA double-strand breaks and alkali-labile bonds produced by bleomycin." *Nucleic Acids Research*, 4(10): 3573–3580.

Psonka-Antonczyk, K., Elsasser, T., Gudowska-Nowak, E., and Taucher-Scholz, G. (**2009**). "Distribution of double-strand breaks induced by ionizing radiation at the level of single DNA molecules examined by atomic force microscopy." *Radiat Res*, 172(3): 288–295.

Raderschall, E., Bazarov, A., Cao, J., Lurz, R., Smith, A., Mann, W., Ropers, H. H., Sedivy, J. M., Golub, E. I., Fritz, E., and Haaf, T. (**2002**). "Formation of higher-order nuclear Rad51 structures is functionally linked to p21 expression and protection from DNA damage-induced apoptosis." *Journal of Cell Science*, 115(Pt 1): 153–164.

Ramantani, G., Kohlhase, J., Hertzberg, C., Innes, A. M., Engel, K., Hunger, S., Borozdin, W., Mah, J. K., Ungerath, K., Walkenhorst, H., Richardt, H. H., Buckard, J., Bevot, A., Siegel, C., von Stulpnagel, C., Ikonomidou, C., Thomas, K., Proud, V., Niemann, F., Wieczorek, D., Hausler, M., Niggemann, P., Baltaci, V., Conrad, K., Lebon, P., and Lee-Kirsch, M. A. (2010). "Expanding the Phenotypic Spectrum of Lupus Erythematosus in Aicardi-Goutieres Syndrome." *Arthritis and Rheumatism*, 62(5): 1469–1477.

Rapp, A., Bock, C., Dittmar, H., and Greulich, K. O. (2000). "UV-A breakage sensitivity of human chromosomes as measured by COMET-FISH depends on gene density and not on the chromosome size." *J Photochem Photobiol B*, 56(2-3): 109–117.

Razin, A. and Cedar, H. (1977). "Distribution of 5-methylcytosine in chromatin." *Proc Natl Acad Sci U S A*, 74(7): 2725–2728.

Reijns, M. A., Bubeck, D., Gibson, L. C., Graham, S. C., Baillie, G. S., Jones, E. Y., and Jackson, A. P. (2011). "The structure of the human RNase H2 complex defines key interaction interfaces relevant to enzyme function and human disease." *The Journal of biological chemistry*, 286(12): 10 530–10 539.

Reijns, M. A. M., Rabe, B., Rigby, R. E., Mill, P., Astell, K. R., Lettice, L. A., Boyle, S., Leitch, A., Keighren, M., Kilanowski, F., Devenney, P. S., Sexton, D., Grimes, G., Holt, I. J., Hill, R. E., Taylor, M. S., Lawson, K. A., Dorin, J. R., and Jackson, A. P. (2012). "Enzymatic Removal of Ribonucleotides from DNA Is Essential for Mammalian Genome Integrity and Development." *Cell*, 149(5).

Rice, G., Patrick, T., Parmar, R., Taylor, C. F., Aeby, A., Aicardi, J., Artuch, R., Montalto, S. A., Bacino, C. A., Barroso, B., Baxter, P., Benko, W. S., Bergmann, C., Bertini, E., Biancheri, R., Blair, E. M., Blau, N., Bonthron, D. T., Briggs, T., Brueton, L. A., Brunner, H. G., Burke, C. J., Carr, I. M., Carvalho, D. R., Chandler, K. E., Christen, H. J., Corry, P. C., Cowan, F. M., Cox, H., D'Arrigo, S., Dean, J., De Laet, C., De Praeter, C., Dery, C., Ferrie, C. D., Flintoff, K., Frints, S. G. M., Garcia-Cazorla, A., Gener, B., Goizet, C., Goutieres, F., Green, A. J., Guet, A., Hamel, B. C. J., Hayward, B. E., Heiberg, A., Hennekam, R. C., Husson, M., Jackson, A. P., Jayatunga, R., Jiang, Y. H., Kant, S. G., Kao, A., King, M. D., Kingston, H. M., Klepper, J., van der Knaap, M. S., Kornberg, A. J., Kotzot, D., Kratzer, W., Lacombe, D., Lagae, L., Landrieu, P. G., Lanzi, G., Leitch, A., Lim, M. J., Livingston, J. H., Lourenco, C. M., Lyall, E. G. H., Lynch, S. A., Lyons, M. J., Marom, D., McClure, J. P., McWilliam, R., Melancon, S. B., Mewasingh, L. D., Moutard, M. L., Nischal, K. K., Ostergaard, J. R., Prendiville, J., Rasmussen, M., Rogers, R. C., Roland, D., Rosser, E. M., Rostasy, K., Roubertie, A., Sanchis, A., Schiffmann, R., Scholl-Burgi, S., Seal, S., Shalev, S. A., Corcoles, C. S., Sinha, G. P., Soler, D., Spiegel, R., Stephenson, J. B. P., Tacke, U., Tan, T. Y., Till, M., Tolmie, J. L., Tomlin, P., Vagnarelli, F., Valente, E. M., Van Coster, R. N. A., Van der Aa, N., Vanderver, A., Vles, J. S. H., Voit, T., Wassmer, E., Weschke, B., Whiteford, M. L., Willemsen, M. A. A., Zankl, A., Zuberi, S. M., Orcesi, S., Fazzi, E., Lebon, P., and Crow, Y. J. (2007). "Clinical and molecular phenotype of Aicardi-Goutieres syndrome." *American journal of human genetics*, 81(4): 713–725.

Robertson, A. B., Klungland, A., Rognes, T., and Leiros, I. (**2009**). "DNA repair in mammalian cells: Base excision repair: the long and short of it." *Cell Mol Life Sci*, 66(6): 981–993.

Rodgers, W., Jordan, S. J., and Capra, J. D. (**2002**). "Transient association of Ku with nuclear substrates characterized using fluorescence photobleaching." *J Immunol*, 168(5): 2348–2355.

Rodrigue, A., Lafrance, M., Gauthier, M. C., McDonald, D., Hendzel, M., West, S. C., Jasin, M., and Masson, J. Y. (**2006**). "Interplay between human DNA repair proteins at a unique double-strand break in vivo." *The EMBO journal*, 25(1): 222–231.

Rogakou, E. P., Boon, C., Redon, C., and Bonner, W. M. (**1999**). "Megabase chromatin domains involved in DNA double-strand breaks in vivo." *Journal of Cell Biology*, 146(5): 905–916.

Rossi, M. L., Purohit, V., Brandt, P. D., and Bambara, R. A. (**2006**). "Lagging strand replication proteins in genome stability and DNA repair." *Chem Rev*, 106(2): 453–473.

Rottach, A., Kremmer, E., Nowak, D., Boisguerin, P., Volkmer, R., Cardoso, M. C., Leonhardt, H., and Rothbauer, U. (**2008**). "Generation and characterization of a rat monoclonal antibody specific for PCNA." *Hybridoma (Larchmt)*, 27(2): 91–98.

Rychlik, M. P., Chon, H., Cerritelli, S. M., Klimek, P., Crouch, R. J., and Nowotny, M. (**2010**). "Crystal structures of RNase H2 in complex with nucleic acid reveal the mechanism of RNA-DNA junction recognition and cleavage." *Mol Cell*, 40(4): 658–670.

Sachs, R. K., Chen, A. M., and Brenner, D. J. (**1997**). "Review: proximity effects in the production of chromosome aberrations by ionizing radiation." *Int J Radiat Biol*, 71(1): 1–19.

Schermelleh, L., Haemmer, A., Spada, F., Rosing, N., Meilinger, D., Rothbauer, U., Cardoso, M. C., and Leonhardt, H. (**2007**). "Dynamics of Dnmt1 interaction with the replication machinery and its role in postreplicative maintenance of DNA methylation." *Nucleic Acids Research*, 35(13): 4301–4312.

Schneider, K., Fuchs, C., Dobay, A., Rottach, A., Qin, W., Wolf, P., Alvarez-Castro, J. M., Nalaskowski, M. M., Kremmer, E., Schmid, V., Leonhardt, H., and Schermelleh, L. (**2013**). "Dissection of cell cycle-dependent dynamics of Dnmt1 by FRAP and diffusion-coupled modeling." *Nucleic Acids Research*, 41(9): 4860–4876.

Sebesta, M., Burkovics, P., Haracska, L., and Krejci, L. (**2011**). "Reconstitution of DNA repair synthesis in vitro and the role of polymerase and helicase activities." *DNA Repair*, 10(6): 567–576.

Shaban, N. M., Harvey, S., Perrino, F. W., and Hollis, T. (**2010**). "The structure of the mammalian RNase H2 complex provides insight into RNA.NA hybrid processing to prevent immune dysfunction." *The Journal of biological chemistry*, 285(6): 3617–3624.

Sharma, S. and Raghavan, S. C. (**2010**). "Nonhomologous DNA end joining in cell-free extracts." *J Nucleic Acids*, 2010.

Shibata, A., Conrad, S., Birraux, J., Geuting, V., Barton, O., Ismail, A., Kakarougkas, A., Meek, K., Taucher-Scholz, G., Lobrich, M., and Jeggo, P. A. (**2011**). "Factors determining DNA double-strand break repair pathway choice in G2 phase." *The EMBO journal*, 30(6): 1079–1092.

Shiloh, Y. (**2006**). "The ATM-mediated DNA-damage response: taking shape." *Trends in biochemical sciences*, 31(7): 402–410.

Singh, N. P., Mccoy, M. T., Tice, R. R., and Schneider, E. L. (**1988**). "A Simple Technique for Quantitation of Low-Levels of DNA Damage in Individual Cells." *Experimental cell research*, 175(1): 184–191.

Sjolund, A. B., Senejani, A. G., and Sweasy, J. B. (**2013**). "MBD4 and TDG: multifaceted DNA glycosylases with ever expanding biological roles." *Mutation Research*, 743-744: 12–25.

Solarczyk, K. J., Zarebski, M., and Dobrucki, J. W. (**2012**). "Inducing local DNA damage by visible light to study chromatin repair." *DNA Repair*, 11(12): 996–1002.

Sparks, J. L., Chon, H., Cerritelli, S. M., Kunkel, T. A., Johansson, E., Crouch, R. J., and Burgers, P. M. (**2012**). "RNase H2-initiated ribonucleotide excision repair." *Mol Cell*, 47(6): 980–986.

Sporbert, A., Domaing, P., Leonhardt, H., and Cardoso, M. C. (**2005**). "PCNA acts as a stationary loading platform for transiently interacting Okazaki fragment maturation proteins." *Nucleic Acids Research*, 33(11): 3521–3528.

Sprague, B. L. and McNally, J. G. (**2005**). "FRAP analysis of binding: proper and fitting." *Trends in Cell Biology*, 15(2): 84–91.

Sugasawa, K., Okamoto, T., Shimizu, Y., Masutani, C., Iwai, S., and Hanaoka, F. (**2001**). "A multistep damage recognition mechanism for global genomic nucleotide excision repair." *Genes Dev*, 15(5): 507–521.

Surralles, J., Puerto, S., Ramirez, M. J., Creus, A., Marcos, R., Mullenders, L. H., and Natarajan, A. T. (**1998**). "Links between chromatin structure, DNA repair and chromosome fragility." *Mutation Research*, 404(1-2): 39–44.

Sutherland, J. C. and Griffin, K. P. (**1981**). "Absorption spectrum of DNA for wavelengths greater than 300 nm." *Radiat Res*, 86(3): 399–409.

Tamaru, H. (**2010**). "Confining euchromatin/heterochromatin territory: jumonji crosses the line." *Genes Dev*, 24(14): 1465–1478.

Tashiro, S., Walter, J., Shinohara, A., Kamada, N., and Cremer, T. (**2000**). "Rad51 accumulation at sites of DNA damage and in postreplicative chromatin." *Journal of Cell Biology*, 150(2): 283–291.

Thomas, D. C., Roberts, J. D., and Kunkel, T. A. (**1991**). "Heteroduplex Repair in Extracts of Human Hela-Cells." *The Journal of biological chemistry*, 266(6): 3744–3751.

Tice, R. R., Agurell, E., Anderson, D., Burlinson, B., Hartmann, A., Kobayashi, H., Miyamae, Y., Rojas, E., Ryu, J. C., and Sasaki, Y. F. (**2000**). "Single cell gel/comet assay: Guidelines for in vitro and in vivo genetic toxicology testing." *Environmental and Molecular Mutagenesis*, 35(3): 206–221.

Tornaletti, S. (**2009**). "DNA repair in mammalian cells: Transcription-coupled DNA repair: directing your effort where it's most needed." *Cell Mol Life Sci*, 66(6): 1010–1020.

Trautlein, D., Deibler, M., Leitenstorfer, A., and Ferrando-May, E. (**2010**). "Specific local induction of DNA strand breaks by infrared multi-photon absorption." *Nucleic Acids Research*, 38(3): e14.

Trujillo, K. M., Yuan, S. S., Lee, E. Y., and Sung, P. (**1998**). "Nuclease activities in a complex of human recombination and DNA repair factors Rad50, Mre11, and p95." *The Journal of biological chemistry*, 273(34): 21 447–21 450.

Turchi, J. J., Huang, L., Murante, R. S., Kim, Y., and Bambara, R. A. (**1994**). "Enzymatic Completion of Mammalian Lagging-Strand DNA-Replication." *Proc Natl Acad Sci U S A*, 91(21): 9803–9807.

Voet, D., Gratzer, W. B., Cox, R. A., and Doty, P. (**1963**). "Absorption Spectra of Nucleotides, Polynucleotides, and Nucleic Acids in the Far Ultraviolet." *Biopolymers*, 1(3): 193–208.

Waga, S., Bauer, G., and Stillman, B. (**1994**). "Reconstitution of Complete Sv40 DNA-Replication with Purified Replication Factors." *The Journal of biological chemistry*, 269(14): 10 923–10 934.

Ward, J. F. (**1995**). "Radiation mutagenesis: the initial DNA lesions responsible." *Radiat Res*, 142(3): 362–368.

Williams, J. S., Smith, D. J., Marjavaara, L., Lujan, S. A., Chabes, A., and Kunkel, T. A. (**2013**). "Topoisomerase 1-mediated removal of ribonucleotides from nascent leading-strand DNA." *Mol Cell*, 49(5): 1010–1015.

Wolffe, A. P. and Pruss, D. (**1996**). "Deviant nucleosomes: the functional specialization of chromatin." *Trends Genet*, 12(2): 58–62.

Woodcock, C. L. and Ghosh, R. P. (**2010**). "Chromatin higher-order structure and dynamics." *Cold Spring Harb Perspect Biol*, 2(5): a000 596.

Yaffe, D. and Saxel, O. (**1977**). "Serial passaging and differentiation of myogenic cells isolated from dystrophic mouse muscle." *Nature*, 270(5639): 725–727.

Yao, N. Y., Schroeder, J. W., Yurieva, O., Simmons, L. A., and O'Donnell, M. E. (**2013**). "Cost of rNTP/dNTP pool imbalance at the replication fork." *Proc Natl Acad Sci U S A*, 110(32): 12 942–12 947.

Yildirim, O., Li, R., Hung, J. H., Chen, P. B., Dong, X., Ee, L. S., Weng, Z., Rando, O. J., and Fazzio, T. G. (**2011**). "Mbd3/NURD complex regulates expression of 5-hydroxymethylcytosine marked genes in embryonic stem cells." *Cell*, 147(7): 1498–1510.

Zheng, L. and Shen, B. H. (**2011**). "Okazaki fragment maturation: nucleases take centre stage." *Journal of Molecular Cell Biology*, 3(1): 23–30.

Ziv, Y., Bielopolski, D., Galanty, Y., Lukas, C., Taya, Y., Schultz, D. C., Lukas, J., Bekker-Jensen, S., Bartek, J., and Shiloh, Y. (**2006**). "Chromatin relaxation in response to DNA double-strand breaks is modulated by a novel ATM and KAP-1 dependent pathway." *Nat Cell Biol*, 8(8): 870–U142.

Zou, X. Q., Ma, W., Solov'yov, I. A., Chipot, C., and Schulten, K. (**2012**). "Recognition of methylated DNA through methyl-CpG binding domain proteins." *Nucleic Acids Research*, 40(6): 2747–2758.

6 Annex

6.1 Abbreviations

(6-4)PP	6,4-photoproduct
5hmC	5-hydroxymethylcytosine
5mC	5-methylcytosine
AGS	Aicardi-Goutières syndrome
AP site	apurinic/apyrimidinic site
AP site	apurinic-apyrimidinic endonuclease
ATM	ataxia telangiectasia mutated
ATP	adenosine triphosphate
BER	base excision repair
BrdU	bromodeoxyuridine
BSA	bovine serum albumin
CFP	cyan fluorescent protein
CPD	cyclobutane pyrimidine dimer
D-loop	displacement loop
DAPI	4',6-diamidino-2-phenylindole
DMEM	Dulbecco's modified Eagle's medium
DNA	deoxyribonucleic acid
DNA-PK	DNA-dependent protein kinase
Dna2	DNA Replication helicase/nuclease 2
DSB	double-strand break
EdU	5-ethynyl-2'-deoxyuridine
ERCC1	excision repair cross-complementing rodent repair deficiency, complementation group 1
EthBr	ethidium bromide
EU	5-ethynyl uridine
FCS	fetal calf serum
Fen1	flap structure-specific endonuclease 1
FRAP	fluorescence recovery after photobleaching
GFP	green fluorescent protein

HCl	hydrogen chloride
HR	homologous recombination
IdU	iododeoxyuridine
IgG	Immunoglobulin G
MBD	methyl-CpG binding domain
MeOH	methanol
MMR	mismatch repair
mRFP	monomeric red fluorescent protein
NA	numerical aperture
NBS1	Nijmegen Breakage Syndrome 1
NER	nucleotide excision repair
NHEJ	non-homologous end joining
p66	DNA polymerase delta subunit p66
PARP	poly (ADP-ribose) polymerase
PBS	phosphate buffered saline
PCNA	proliferating cell nuclear antigen
PIP	PCNA interaction peptide
R-loops	RNA:DNA hybrid structures
RER	ribonucleotide excision repair
RNA	ribonucleic acid
ROS	reactive oxygen species
RPA	replication protein A
RT	room temperature
S phase	synthesis phase
SSB	singel strand break
ssDNA	singel stranded DANN
TC-NER	transcription coupled NER
TUNEL	terminal deoxynucleotidyl transferase dUTP nick end labeling
UV	ultraviolet
Xi	incacitve X chromosome
XPA, B, C or G	xeroderma pigmentosum, complementation group A, B, C or G
XRCC1 or 4	X-ray repair complementing defective repair in Chinese hamster cells 1 or 4

6.2 List of contributions

chapter 3.1.:

Britta Muster	Carried out cloning of Rad51 construct and all experiments, writing of the manuscript and figure preparation
Alexander Rapp	Designed the project, carried out cloning of XRCC1 and APEX1 constructs, writing of ImageJ macro for Data analysis and supervised the manuscript writing
M. Cristina Cardoso	Designed the project

chapter 3.2.:

Britta Muster	Carried out all experiments, writing of the manuscript and figure preparation
Alexander Rapp	Writing of ImageJ macro for Data analysis and supervised the manuscript writing
M. Cristina Cardoso	Designed the project

chapter 3.3.:

Britta Muster	Carried out experiments, writing of the manuscript and figure preparation
Henry Herce	Carried out calculation of H_{coeff}
Barbara Kind and Min Ae Lee-Kisch	Providing of RNase H2 constructs
Alexander Rapp	Designed the project, writing of ImageJ macro for Data analysis and supervised the manuscript writing
M. Cristina Cardoso	Designed the project

6.3 Acknowledgements

First of all, I like to thank my 'Doktormutter' M. Cristina Cardoso for giving me the opportunity to carry out my PhD Thesis in her lab, for all the great discussions we had and for all the things I learned from her. I would also like to thank Prof. Paul Layer for agreeing to be my second examiner.

I am very thankful to my supervisor Dr. Alexander Rapp for all his support, help, patients and most of all his humor. For amazing technical support and for always having an 'open ear', I would like to thank Anne Lehmkuhl. For the great working atmosphere I would like to thank the whole Cardoso lab. Especially the lunch club and the great soccer matches made it a place to feel comfortable. I am very thankful that I did not only found great colleagues, but also good friends.
I am also very thankful to my fellow students at the graduate school who helped my to see thinks from another perspective, in particular Lucie Ilhoff and Adriana Längle. I would also like to thank Annabelle Becker, which whom it was fun to organize workshops in our role as woman representatives.
I would also like to thank my collaboration partners Dr. Barbara Kind, Dr. Henry Herce and Laurin Lengert for all their great ideas and motivation as well as Martin Thomas and Uwe Petzhold for letting my play around with lasers.
Many thanks also to the people form my diploma lab. You are the reason why I became fascinated by science!

Ein ganz großes Dankeschön an meine Freunde und Familie, ohne Euch wäre ich niemals so weit gekommen. Ganz besonders möchte ich meinen Eltern für ihre ständige Unterstützung danken und das sie immer an mich geglaubt haben.
Vor allem möchte ich auch meinen Korrektoren Alex, Marius und Laurence sowie Lena danken, die mir geholfen haben bis zum Ende durchzuhalten!

6.4 Declaration - Ehrenwörtliche Erklärung

Ich erkläre hiermit ehrenwörtlich, dass ich die vorliegende Arbeit entsprechend den Regeln guter wissenschaftlicher Praxis selbstständig und ohne unzulässige Hilfe Dritter angefertigt habe.

Sämtliche aus fremden Quellen direkt oder indirekt übernommenen Gedanken sowie sämtliche von Anderen direkt oder indirekt übernommenen Daten, Techniken und Materialien sind als solche kenntlich gemacht. Die Arbeit wurde bisher bei keiner anderen Hochschule zu Prüfungszwecken eingereicht.

Darmstadt, den 21.03.2014

(Britta Muster)

6.4 Curriculum vitæ

Personal Information

Name:	Britta Muster
Adress:	Technische Universität Darmstadt
	Schnittspahnstraße 10
	64387 Darmstadt, Germany
Date of birth:	25.09.1984
Place of birth:	Bad Homburg

Education

02/2011 - ongoing	**PhD thesis** at *TU Darmstadt*
	'DNA repair and chromatin'
	in the group of Prof. Cardoso 'cell biology and epigenetics',
	under supervision of Dr. Rapp
10/2004 - 10/2009	**Studies in biology** at *Goethe Universität Frankfurt am Main*
	majors: cell- and developmental biology, neurobiology, genetics
	degree/diploma (good)
	Diploma thesis at *Goethe Universität Frankfurt am Main*
	'Überexpression von autolyso-phagosomalen Proteinen in kultivierten Zellen'
	(Overexpression of Autolyso-phagosomal Proteins in cultured Cells)
	in the group of Prof. Bereiter-Hahn 'kinematic cell research group',
	under supervision of PD. Dr. Jendrach
06/2004	**Abitur** at *Philipp-Reis-Schule* Friedrichsdorf
	majors: biology, mathematics
	grade: 2,1

Teaching

2011 - 2013	supervision and planing of basic and advanced practical courses, TUD
2010	supervision of students during diploma work, University Hospital FFM
2008 - 2009	supervision of advanced practical courses, Goethe Universität FFM

in preparation	Discrimination of DNA repair pathways by laser microirradiation. Muster B, Rapp A, and Cardoso MC
in preparation	Altered spatio-temporal dynamics of RNaseH2 complex assembly at replication and repair sites in Aicardi-Goutières syndrome. Kind B*, Muster B*, Staroske W, Herce HD, Sachse R, Rapp A, Schmidt F, Schwillex P, Cardoso MC, Lee-Kirsch MA **equally contributing authors*
in preparation	Local heterochromatin decondensation is essential for processive DNA synthesis. Becker A., Chagin VO, Muster B, Mortusewicz O, Leonhardt H., Rapp A., Cardoso MC
2012	Autophagy proteins LC3B, ATG5 and ATG12 participate in quality control after mitochondrial damage and influence lifespan. Mai S, Muster B, Bereiter-Hahn J, Jendrach M. *Autophagy. 2012 Jan;8(1):47-62. doi: 10.4161/auto.8.1.18174. Epub 2012 Jan 1.*
2010	Respiratory chain complexes in dynamic mitochondria display a patchy distribution in life cells. Muster B, KohlW, Wittig I, Strecker V, Joos F, HaaseW, Bereiter-Hahn J, Busch K. *PLoS One. 2010 Jul 30;5(7):e11910. doi: 10.1371/journal.pone.0011910.*
2010	Do UCP2 and mild uncoupling improve longevity? Dikov D, Aulbach A, Muster B, Dröse S, Jendrach M, Bereiter-Hahn J. *Exp Gerontol. 2010 Aug;45(7-8):586-95. doi: 10.1016/j.exger.2010.03.011. Epub 2010 Mar 21.*
2010	Aging of different avian cultured cells: lack of ROS-induced damage and quality control mechanisms. Strecker V, Mai S, Muster B, Beneke S, Bürkle A, Bereiter-Hahn J, Jendrach M. *Mech Ageing Dev. 2010 Jan;131(1):48-59. doi: 10.1016/j.mad.2009.11.005. Epub 2009 Dec 3.*

Conference contributions

Poster:

Eukaryotic DNA replication and genome maintenance; Cold Spring Harbor, USA; September 2013

Titel: 'Microirradiation: see DNA damage and repair in a new light'

Talk:

Gesellschaft für Biologische Strahlenforschung; Darmstadt, Germany; September 2013

Titel: 'Microirradiation: see DNA damage and repair in a new light'

Talk and poster:

German Society for Cell Biology (DGZ) and the German Society for Developmental Biology (GfE); Heidelberg, Germany; March 2013

Titel: 'Discrimination of DNA repair pathways by laser miroirradiation'

Poster:

Biomarkers of ageing: from molecular biology to clinical perspectives; Halle, Germany; September 2009

Titel: 'Overexpression of the autophagosomal proteins LC3/ATG8 and ATG5 increases cellular fitness and life span'

Poster:

Joint Congress of the Swiss and the German Society for Cell Biology (ZMG and DGZ); Konstanz, Germany; March 2009

Titel: 'Impact of UCP2 over expression in different cell types on ROS production and ageing'